Polyfunctional Calcium Phosphate Nanoparticles as a Novel Vaccine Platform against HIV-1

Polyfunktionale Calciumphosphat-Nanopartikel als neuartige Impfstoff-Plattform gegen HIV-1

Der Naturwissenschaftlichen Fakultät
der Friedrich-Alexander-Universität Erlangen-Nürnberg
zur
Erlangung des Doktorgrades Dr. rer. nat.

Vorgelegt von
Dominik Damm
aus
Günzburg

Als Dissertation genehmigt von der Naturwissenschaftlichen Fakultät der Friedrich-Alexander-Universität Erlangen-Nürnberg

Tag der mündlichen Prüfung: 28.04.2023
Vorsitzender des Promotionsausschusses: Prof. Dr. Wolfgang Achtziger
Gutachter: Prof. Dr. Falk Nimmerjahn
PD Dr. Vladimir Temchura

Table of Content

Table of Content

I. Index of Abbreviations

%	percent
°C	degree celsius
× g	times gravity
µ	micro
AAS	atomic absorption spectroscopy
ADCC	antibody-dependent cellular cytotoxicity
AGHC	aminoguanidine hydrochloride
AIDS	Acquired Immunodeficiency Syndrome
Ald_6	aldehyde-tag (LCTPSR / L[Fgly]TPSR)
ANOVA	analysis of variance
AO	aminooxy
APC	antigen-presenting cell
APC	allophycocyanin
APS	ammonium persulfate
AUC	area under the curve
BCR	B cell receptor
bnAb	broadly neutralizing antibody
BSA	bovine serum albumin
BV	Brilliant Violet™
CaP	calcium phosphate nanoparticle
CCR5	C-C chemokine receptor type 5
CD	cluster of differentiation
CD	cytoplasmic domain
CD4bs	CD4 binding site
CDRH	complementarity determining region of antibody heavy chains
CHO	chinese hamster ovary
CHR	C-terminal helical region
CLSM	confocal laser scanning microscopy
CoV-2	coronavirus type 2
COVID-19	coronavirus disease 2019
CpG	cytosine/guanine-dinucleotide
CT	computer tomography

CTL	cytotoxic T-lymphocyte
CXCR4	C-X-C chemokine receptor type 4
Cy7	Sulfo-Cyanine 7
Da	dalton
DC	dendritic cell
DMEM	Dulbecco’s modified eagle medium
DMSO	dimethylsulfoxide
DNA	desoxyribonucleic acid
DPBS	Dulbecco’s phosphate-buffered saline
E. coli	*Escherichia coli*
ECL	enhanced chemiluminescence
EDC	1-ethyl-3-(3-dimethylaminopropyl)carbodiimide
EDTA	ethylenediaminetetraacetic acid
EGTA	ethylene glycol-bis(β-aminoethyl ether)-N,N,N′,N′-tetraacetic acid
ELISA	enzyme-linked immunosorbent assay
EM	electron microscopy
Env	envelope glycoprotein
et al.	and others (et alii)
EU	endotoxin units
FACS	fluorescence-activated cell sorting
Fc	fragment crystallizable
FCS	fetal calf serum
FcγR	Fc gamma receptor
FELASA	Federation of European Laboratory Animal Science Association
FGE	formylglycine-generating enzyme
Fgly	formylglycine
FITC	fluorescein isothiocyanate
FMe	Freestyle™ 293 Expression Medium
FRET	fluorescence resonance energy transfer
FV	friend virus
g	gram
Gag	group-specific antigen
GMP	good manufacturing practice
GNL	*Galanthus Nivalis* lectin

gp	glycoprotein
$gp41_{ecto}$	gp41 ectodomain
GSL	gel-shift linker
h	hour
H_2O	water
H_2O_2	hydrogen peroxide
HA	hemagglutinin
HAART	highly active antiretroviral therapy
hACE2	human angiotensin-converting enzyme 2
HBsAg	Hepatitis B virus surface antigen
HBV	Hepatitis B virus
hCMV	human cytomegalovirus
HEK	human embryonic kidney
HEL	hen egg lysozyme
HeLa	Henrietta Lacks
HEPES	4-(2-hydroxyethyl)-1-piperazineethanesulfonic acid
Hgpsyn	synthetic HIV-1 GagPol
His_8	8x poly-Histidin-tag
HIV	human immunodeficiency virus
HPV	human papilloma virus
HRP	horseradish peroxidase
i.m.	intramuscular
ICS	intracellular cytokine staining
IFN	interferon
Ig	immunoglobulin
IL	interleukin
ISH	intrastructural help
IAV	influenza A virus
JAK	janus kinase
k	kilo
kb	kilobase
KO	knockout
L	liter
LB	lysogeny broth

lnkr-Env	linker-bound Env trimer
log	logarithm
LPS	lipopolysaccharide
m	milli
m	meter
M	molar
MFI	median fluorescence intensity
MHC	major histocompatibility complex
MID	minimum infective dose
min	minute
MOPS	3-(N-morpholino)propanesulfonic acid
MPER	membrane proximal external region
MPLA	3-O-desacyl-4′-monophosphoryl lipid A
MPS	(3-mercaptopropyl)trimethoxysilane
mRNA	messenger ribonucleic acid
MS	mass spectrometry
m/z	mass-to-charge ratio
n	nano
NaOAc	sodium acetate
NaCl	sodium chloride
NaOH	sodium hydroxide
Nef	negative factor
NF-κB	nuclear factor kappa-light-chain-enhancer of activated B cells
NFL	native flexibly-linked
NHP	non-human primate
NHR	N-terminal helical region
Ni	nickel
NIR	near-infrared spectroscopy
NP	nanoparticle
NTA	nitrilotriacetic acid
oCaPs	orthogonally coupled calcium phosphate nanoparticles
OD	optical density
ORF	open reading frame
p30	Tetanus Toxoid-derived peptide 30

PAGE	polyacrylamide gel electrophoresis
PBS	phosphate-buffered saline
PBS/O	phosphate-buffered saline without bivalent cations
PCR	polymerase chain reaction
PdI	polydispersity index
PE	phycoerythrin
PEG	pegylation
PEI	polyethylenimine
PET	positron emission tomography
PFA	paraformaldehyde
PNGase F	Peptide:N-glycosidase F
Pol	polymerase
PrEP	pre-exposure prophylaxis
rCaP	randomly coupled calcium phosphate nanoparticle
Ref	reference
Rev	regulator of expression of virion proteins
RLU/s	relative light units per second
RNA	ribonucleic acid
rpm	revolutions per minute
RPMI	Roswell Park Memorial Institute
RSV	Respiratory syncytial virus
RT	room temperature
RT	reverse transcriptase
s	second
SARS	severe acute respiratory syndrome
SAsc	sodium ascorbate
SDS	sodium dodecyl sulfate
SEM	standard error of mean
SEM	scanning electron microscopy
SIV	simian immunodeficiency virus
SMCC	succinimidyl-trans-4-(N-maleimidomethyl)cyclohexane-1-carboxylate
SOS	sulphur-on-sulphur
SOSIP	sulphur-on-sulphur with I559P
STAT	signal transducers and activators of transcription

sulfo-NHS	N-Hydroxysulfosuccinimid
SUMF1	sulfatase modifying factor 1
Tat	trans-activator of transcription
TCR	T cell receptor
TEM	transmission electron microscopy
TEMED	N,N,N´,N´-Tetraacetylethylenediamine
TEOS	tetraethylorthosilicate
T_{FH}	T follicular helper
Th	T helper
THPTA	Tris(3-hydroxypropyltriazolylmethyl)amine
TLR	toll-like receptor
TM	transmembrane domain
TNF	tumor necrosis factor
TRES	Trianni-Erlangen anti-SARS-CoV-2 Spike
TRIS	Tris(hydroxymethyl)aminomethane
TT	Tetanus Toxoid
UFO	uncleaved pre-fusion optimized
UV-Vis	ultraviolet-visible
V	Volt
Vif	viral infectivity factor
Vpr	viral protein R
Vpu	viral protein U
VLP	virus-like particle
VSV	vesicular stomatitis virus
VSV-G	vesicular stomatitis virus G protein
wt	wild-type

II. Index of Tables

III. Index of Figures

IV. Summary

Synthetic nanoparticles functionalized with stabilized trimers of the HIV-1 envelope glycoprotein (Env) have become a major focus in AIDS vaccine research. The additional incorporation of T helper cell epitopes into such nanoparticles might recruit pre-existing CD4+ T cell responses induced by childhood vaccinations to provide intrastructural help (ISH) for Env-specific B cells upon immunization. In this study, calcium phosphate nanoparticles (CaPs), that encapsulate an immunodominant Tetanus Toxoid epitope (p30) and display Env trimers on the surface (T helper CaPs), were evaluated in preclinical vaccine trials. T helper CaPs induced the activation of Env-specific naïve B cells *in vitro*, which was not observed with soluble Env trimers. Immunization with T helper CaPs resulted in significantly stronger Env-specific humoral immune responses via ISH in mice that were immunized in advance with a licensed Tetanus vaccine. The magnitude of anti-Env antibody levels in ISH mice was comparable to a control group immunized with CpG-adjuvanted CaPs. In contrast to CpG, the induction of immune mechanisms suspected to increase the susceptibility for HIV infection was bypassed by harnessing ISH. Having provided evidence that the utilization of T helper CaPs resulted in versatile, immunomodulatory features, the nanoparticle design was improved by an orthogonal Env coupling mechanism (oCaPs). To this end, a genetically encoded aldehyde-tag (LCTPSR) was introduced at the C-terminus of native-like, soluble Env trimers. The tag-associated cysteine is post-translationally converted into a formylglycine harboring an aldehyde group, which was confirmed by mass spectrometry. This aldehyde was used for covalent bioconjugation with an aminooxy/alkyne-crosslinker. Linker-bound Env trimers (lnkr-Env) were then immobilized on the CaP surface via a Click reaction. Reporter assays based on fluorescent gel analysis and CLSM proved that the Env conjugation was highly aldehyde-specific and efficient. Most importantly, conformational ELISA and surface FACS analyses indicated that the pre-fusion conformation is preserved. oCaPs induced stronger B cell activation *in vitro* and higher Env-specific antibody levels *in vivo* than randomly coupled CaPs. Taken together, this study established a nanoparticle delivery platform for future immunomodulatory vaccine approaches and diagnostic applications in the context of various pathogens.

V. Zusammenfassung

Ein neuer Schwerpunkt der HIV Impfstoffforschung sind synthetische Nanopartikel, die mit optimierten Trimeren des Oberflächenproteins (Env) gekoppelt wurden. Der zusätzliche Einschluss von T-Helferzell-Epitopen aus humanen Impfstoffen in solche Nanopartikel macht es möglich, bestehende CD4+ T-Zellen zu rekrutieren, damit diese intrastrukturelle Hilfe (ISH) für Env-spezifische B-Zellen nach der Partikelimpfung leisten. In dieser Studie wurde die Eignung von T-Helfer-Calciumphosphat-Nanopartikeln (T-Helfer CaPs), die ein immunodominantes Tetanus-Toxoid-Epitop (p30) im Inneren und Env-Trimere auf der Oberfläche enthalten, funktionell und durch präklinische Immunisierungen untersucht. Verglichen mit löslichen Env-Trimeren konnten T-Helfer CaPs die Aktivierung Env-spezifischer, naiver B-Zellen *in vitro* induzieren. Immunisierungen mit T-Helfer CaPs führten zu signifikant erhöhten humoralen Immunantworten durch ISH in Mäusen, die zuvor mit einem lizensierten Tetanusimpfstoff immunisiert wurden. Die Env-Antikörperbildung in ISH-Mäusen war vergleichbar stark wie in Tieren, welche CpG-adjuvantierte CaPs erhielten. Im Gegensatz zu CpG wurden durch ISH keine Immunmechanismen induziert, die mit erhöhtem HIV-Infektionsrisiko in Verbindung gebracht werden. Infolge dieser vielversprechenden Ergebnisse wurde die Nanopartikelherstellung durch eine orthogonale Env-Kopplung optimiert (oCaPs). Dazu wurde ein Aldehyd-Tag (LCTPSR) an den C-Terminus eines Env-Proteins kloniert, das sich zu stabilen Trimeren zusammenlagert. Das Tag-interne Cystein wird nach der Translation in ein Formylglycin mit einer Aldehydgruppe konvertiert. Dies wurde mittels Massenspektrometrie bestätigt. Nach kovalenter Oxim-Ligation der Aldehydgruppe mit einem aminooxy/alkin-Linker, wurde Linker-gebundenes Env in Folge durch eine Click-Reaktion auf der Oberfläche von CaPs immobilisiert. SDS-PAGE-basierte Analysen und CLSM sowie konformationelle ELISAs und Oberflächen-FACS zeigten, dass der Vorgang spezifisch und effizient verläuft und die Env-Konformation erhalten bleibt. Verglichen mit unspezifisch gekoppelten CaPs, führten oCaPs zu besserer B-Zell-Aktivierung *in vitro* und erhöhten Env-Antikörperspiegeln *in vivo.* Zusammenfassend zeigt diese Studie die Etablierung einer Nanopartikelplattform für zukünftige Impfstoffstudien und diagnostische Anwendungen mit Bezug auf verschiedenste pathogene Erreger.

1. Introduction

1.1. HIV-1 / AIDS

1.1.1. The ongoing HIV-1 pandemic

The current social, economic and healthcare challenges caused by the worldwide spread of SARS-CoV-2 and related cases of COVID-19 overshadow the fact that the preceding HIV-1 pandemic has not been completely resolved yet [1,2]. In 1983, after years of alarmingly emerging cases of immunodeficiency in previously healthy people, the causative agent HIV-1, a lentivirus derived from the *Retroviridae* family, was isolated and identified [3–5]. Current data indicate, that HIV-1 originated from the simian immunodeficiency virus (SIV) of chimpanzees and adapted to humans via cross-species transmission in the first decades of the 20th century in central Africa [6,7]. The virus then became endemic in the sub-saharan African continent and caused an unrecognized epidemic on Haiti in the middle of the century. In the 1970s, HIV-1 finally spread to the American and European continent predominantly circulating among risk groups in larger cities [8]. The manifestation of HIV-1 prevalence in the former Soviet states and China after the fall of the Iron Curtain as well as in Southeast Asia, Australia and New Zealand in the 1990s ultimately sealed the worldwide spread of HIV-1 and AIDS-related deaths [9]. According to calculations by UNAIDS, approximately 38.4 million people are currently living with an HIV-1 infection. Another 40.1 million patients have already died of AIDS-related opportunistic diseases since the beginning of the pandemic [10]. At least, in contrast to respiratory pathogens (Influenza A, SARS-CoV-2) quickly spreading via aerosols, HIV-1 transmission via blood, breastmilk or sexual intercourse in combination with a high minimum infective dose (MID) are the main reasons for a moderate pandemic progression [11,12].

1.1.2. The HIV-1 envelope glycoprotein

HIV-1 is a lipid bilayer-enveloped virus with a single-stranded, positive-sense RNA genome that is encapsulated in a conical capsid [13]. Beside smaller open reading frames for several accessory proteins (Vif, Vpr, Tat, Vpu, Rev, Nef), the genome is largely comprised of three genes that encode for precursor proteins,

which are further processed during translation and form the major proteinaceous parts of the virion: *pol* (viral enzymes), *gag* ([nucleo]capsid) and *env* (surface glycoprotein) [14]. Whereas Gag-derived proteins are inducing cytotoxic (CD8+) and helper (CD4+) T cell responses upon infection, the envelope glycoprotein Env is the major target of humoral B cell-associated immune responses, since it is the sole protein present on the virion bilayer surface [15–17]. Env is a complex heterohexameric membrane protein based on the gp160 precursor protein, which is cleaved by the endogenous Furin protease at the REKR motif into gp120 and gp41 subunits [18]. It is comprised of three gp120-gp41 dimers that form a trimer. Notably, both the interactions between gp120 and gp41 as well as between the protomers are non-covalent [19]. 10 – 20 Env trimers are present on the surface of native HIV-1 virions [20]. gp41 and gp120 can be subdivided into various domains with distinct functions. gp41 consists of a C-terminal intracellular and transmembrane domain that embed the trimer complexes into the lipid bilayer and possibly interact with the viral matrix (p17) protein [21,22]. The ectodomain of gp41 consists of the membrane proximal external region (MPER) as well as two upstream-located alpha helices (CHR, NHR) and the N-terminal fusion peptide [23]. The gp120 subunit is subdivided into five alternating constant and variable domains (C1-C5, V1-V5 [24]) with the latter being the main loci of evolutionary selective pressure leading to quasispecies formation and immune evasion [25,26]. With exception of the co-receptor binding site, which is a linear amino acid sequence in the V3 region, most of the functional epitopes and domains within gp120 are non-linear and, thus, formed by the specific folding of the tertiary and quaternary structures. Two of these non-linear domains are the CD4 binding site (CD4bs) and the trimer apex [22]. Additionally, having more than twenty NXS/NXT motifs within the amino acid sequence, gp120 is heavily glycosylated with both N-linked oligosaccharide and high-mannose glycans [27]. The dense glycan shield is a major obstacle for proper antibody binding to Env and, therefore, another immune evasion mechanism [28,29].

CD4, expressed on T helper cells, monocytes, macrophages and dendritic cells, is the primary receptor of HIV [30–32]. The entry process of the virus is a complex synergy of conformational changes of both viral and cellular proteins [33]. The binding to CD4 via various amino acid residues of the non-linear CD4bs triggers the open trimer conformation, during which the gp120 subunits of the heterodimers fold back and expose formerly hidden epitopes from the trimer core, such as the co-receptor

binding site [34] [22]. A bond between this epitope and cellular CCR5 or CXCR4 finally forms the Env fusion complex [35] [36]. Here, the N-terminal fusion peptide of gp41 inserts into the host cell membrane and a six-helix bundle composed of the alpha-helices of the three gp41 subunits finally pulls the viral and cell membranes together resulting in the fusion of virus and cell as well as in the release of HIV-1 structural proteins, viral enzymes and genome into the host cell [37].

Recent FRET analyses propose that, even without receptor binding and cell fusion, native Env trimers on the HIV surface dynamically transition between three conformational states: low-FRET, intermediate and high-FRET. Hereby, the low-FRET state resembles the closed pre-fusion conformation [38,39]. The higher FRET states reflect a partially opened trimer, since these states can be stabilized by soluble CD4 and co-receptor mimetics [40].

1.1.2.1. Immune evasion mediated by Env

The incapability of a majority of HIV-infected patients to effectively control and neutralize the virus is based on an array of immune evasion features related to Env. i) The non-covalent association of Env subunits may result in a spontaneous shedding of gp120 domains resulting in dysfunctional “junk” Env on the virion surface. These gp41 stems with a reduced number of associated gp120 subunits may impede the binding of previously established humoral immune responses that are directed against conformational epitopes on functional trimers [41,42]. ii) The dense glycosylation of Env hinders antibody binding to proteinaceous epitopes below the glycan shield [28]. The length of the third complementarity-determining regions of the immunoglobulin heavy chains (CDRH3) plays a crucial role in the generation of neutralizing antibody responses against HIV. The CDRH3 lengths vary heavily within the B cell receptor repertoire of one individual and between different species (human average: 15.5 ± 3.2 aa / murine average: 11.5 ± 1.9 aa) [43]. Therefore, mice are not suitable for preclinical HIV neutralization studies, that are mainly performed in rabbits or non-human primates [44]. iii) The error-prone viral reverse transcriptase (RT) is responsible for the generation of HIV quasispecies in infected individuals [25]. The diversity of HIV species in single long-term patients can be much greater than the worldwide occurring influenza-A strains [45]. Especially mutations in the V1 – V5 regions of gp120 are under low selection pressure resulting in immune escape variants of Env [46]. iv) Lastly, the constant transitioning

of native Env trimers between different conformational states hinders the humoral immune response to focus on neutralizing epitopes of the closed pre-fusion state [47]. Especially the (partially) open conformation displays immunodominant epitopes that drive non-neutralizing antibody responses [46,48].

1.1.2.2. Native-like, soluble forms of Env trimers

Both live-attenuated vaccines as well as inactivated virus vaccines are unsuitable for application in the context of HIV due to safety concerns [49,50]. Another category are subunit vaccines containing soluble components of the viral surface antigen. For many years, an obstacle in the generation of proteinaceous Env vaccine candidates that may induce neutralization was the fragile conformational integrity of Env with truncated transmembrane domains (TMs) due to the non-covalent inter-subunit interactions resulting in quick dissociation of the soluble trimers [42]. Therefore, during the last two decades, much effort has been put into the generation of stabilized, soluble recombinant Env trimers that retain a native-like, pre-fusion conformation. The introduction of two recombinant cysteines (A501C, T605C) in gp120 and the gp41 ectodomain, respectively, induced the formation of recombinant disulfide bonds between these subunits (sulphur-on-sulphur, SOS) [51,52]. This covalent interaction highly reduced the likelihood of gp120 shedding under non-reducing environmental conditions. Additionally, another point mutation was inserted in the NHR helix of gp41 (I559P, IP) strengthening the inter-gp41 interactions about 1000-fold [53]. The truncation of Env constructs with these SOSIP mutations at amino acid position 664 directly upstream of MPER finally resulted in vectors coding for fully-cleaved, stabilized soluble gp140 Env trimers, which were proven to maintain a native-like conformation by staining with trimer-specific monoclonal antibodies (Fig. 1 A-C) [54,55]. This concept was established in Env derived from the Ghanaian transmitted/founder strain BG505.B1 (BG505 gp140 SOSIP.664) [56]. However, the SOSIP mutations can be applied to other Env proteins of multiple HIV-1 strains with comparable stabilization results [57]. One limiting factor of this recombinant design is the need for Furin protease overexpression during translation in order to guarantee thorough cleavage of the SOSIP gp140 proteins at the REKR cleavage site [18]. While one solution was to optimize the cleavage site itself (RRRRRR, R_6) [58], another approach persued the dispensability of cleavage by replacing the cleavage site with a flexible linker ($2xG_4S$), thus creating covalent

linkage between gp120 and $gp41_{ecto}$ (Fig. 1 D-E) without the need for the recombinant disulfide bridge. The production of these native-like, flexibly linked (NFL) SOSIP constructs does not require the presence of Furin at all [59,60]. Further optional modifications of the SOSIP design include the replacement of the NHR helix by a so-called UFO linker (uncleaved pre-fusion optimized) and the forced fixation of the closed conformation by connecting the gp120 subunits at the trimer apex with chemical crosslinkers [41,61].

Up to this date, several preclinical studies demonstrated the induction of tier-1 as well as tier-2 neutralizing antibody responses in guinea pigs, rabbits and non-human primates upon SOSIP protein immunization. However, despite adjuvantation, most of the stabilized Env constructs were poorly immunogenic and failed to induce long-lasting humoral immune responses [44,62,63]. In 2019, a phase-1 clinical study involving a consensus-M SOSIP (MSIP.528) and a consensus-S UFO gp140 (conSOSL.UFO.664) adjuvanted with MPLA-containing liposomes has started in London. This study had to be paused, however, due to the pandemic outbreak of SARS-CoV-2, so that the results remain largely elusive (EAVI2020_01; NCT03816137).

1.1.2.3. Recombinant, membrane-embedded forms of Env

As stated above, an average number of 14 Env spikes is present on the surface of native HIV virions [20]. Roughly 20 years ago, the production of lentiviral virus-like particles (VLPs) by co-transfection of producer cells with plasmids encoding for Env and a codon-optimized GagPol (Hgpsyn [64]) was one of the most promising vaccine design approaches [65–68]. However, using full-length gp160 for Env expression resulted in VLPs with a comparably low number of Env spikes on the surface [69–71]. Interestingly, truncation of the intracellular domain of Env (gp145) leads to a higher expression in producer cells and improved quantity of Env trimers on the surface of VLPs [71]. Recently, a membrane-embedded form of a stabilized, native-like conS trimer including a UFO linker was optimized for producer cell expression via truncation of the intracellular domain [61]. Another common way to improve the expression of antigens on the surface of VLPs is to fuse them with the transmembrane and intracellular domain of the surface protein G from Vesicular Stomatitis Virus (VSV-G) [72,73]. This modification has been done with surface proteins derived from multiple pathogens, such as hCMV and SARS-CoV-2 [74,75].

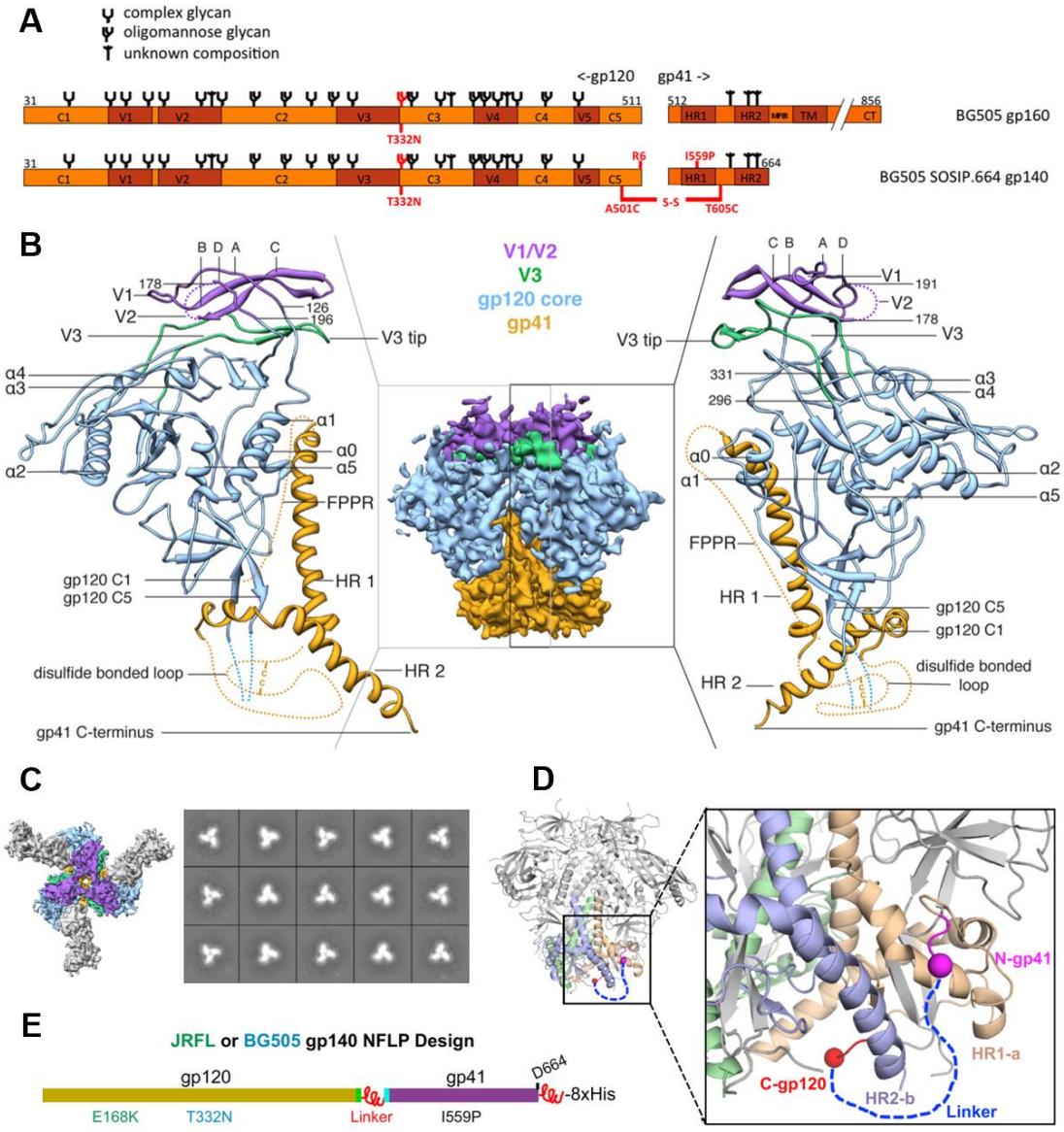

Figure 1) Native-like soluble Env trimers

(A) Introduction of SOSIP mutations. Based on a full-length gp160 ORF, i) the REKR cleavage site was replaced by R_6, ii) two recombinant cysteines were introduced (A501C, T605C), iii) a glycan site was added (T332N), iv) a stabilizing point mutation was introduced (I559P), and v) the construct was truncated at aa 664 (gp140). **(B)** Cryo-EM of BG505 SOSIP gp140 (side view). Apex (purple), co-receptor binding site (green), gp120 interface (light blue) and gp41 ectodomain (yellow) are outlined. **(C)** Cryo-EM (top view) and TEM of BG505 SOSIP gp140. Propeller-like structures in the top view indicate the pre-fusion conformation of Env trimers. **(D)** High-resolution crystal structure of BG505 SOSIP NFL gp140. A flexible glycine/serine linker ($2xG_4S$; blue) covalently connects the gp120 C-terminus (red) with the gp41 N-terminus (pink). **(E)** Design of BG505 NFL gp140 (Env-His_8). Based on a full-length gp160 ORF, i) the REKR cleavage site was replaced by a flexible linker ($2xG_4S$), ii) T332N was introduced for a recombinant glycan-site, iii) I559P was mutated for trimeric stabilization, iv) the construct was truncated at aa 664 and v) another linker ($1xG_4S$) as well as an 8x His-tag were introduced at the C-terminus. All images modified from Sharma *et al.* (2015), Lyumkis *et al.* (2013) and Sanders *et al.* (2013) [28,55,76].

For this study, the transmembrane and intracellular domain of the VSV-G protein (G/TMCD) were introduced to the C-terminus of a native-like, flexibly-linked BG505 trimer (pBG505-gp140-G/TMCD) to elicit lentiviral VLPs for control groups.

1.1.3. HIV-1 related treatment, prevention and vaccine trials

The main characteristic of untreated HIV-1 infections is the constant depletion of CD4+ cells, while the viral RNA in the patient's plasma is steadily increasing [77]. In order to counteract this progression, highly-active antiretroviral therapy (HAART) is commonly applied worldwide. This therapy includes a flexible combination of substances that block specific steps in the viral replication cycle (fusion inhibitors, integrase inhibitors, etc.). On a positive side note, the viral load in HAART-treated patients usually drops to a degree that renders the patient non-infectious for other persons, which may be beneficial for a containment of the HIV-1 pandemic in the future [78]. However, HAART still comes with high costs of therapy and, thus, is not fully available for the whole population in developing countries [4]. Beside conventional prevention strategies like the usage of condoms during sexual intercourse, a pre-exposure prophylaxis (PrEP) became available for daily oral administration in recent years [79]. This may further help to decrease the incidence in industrialized countries [80]. Nevertheless, constant administration is necessary to maintain protection. A prophylactic vaccine would yet be the most cost-effective way to prevent people worldwide, but especially in developing countries, from HIV-1 infection. A number of clinical HIV-1 vaccine trials have been performed in the course of the last 20 years. In short, all of these trials failed to induce sufficiently protective immune responses [81]. On the contrary, one trial even increased the probability for HIV-1 infection in the vaccine group compared to the placebo group [82]. However, so far, all of these phase-3 trials contained either soluble or vector-encoded, non-stabilized HIV-1 envelope glycoproteins [83,84]. Future clinical trials including conformation-optimized Env trimers, nanoparticle delivery platforms and/or immunomodulatory strategies may be more beneficial for the elicitation of a protective immune response.

1.2. Nanoparticles for clinical use

Synthetic nanoparticle delivery platforms have great potential for usage in clinical vaccine or therapeutic applications and received steadily increasing attention in biomedical research in the course of the last two decades [85]. While immunizations with conventional vaccines such as attenuated or inactivated viruses and viral protein subunits greatly diminished the spread of a multitude of pathogens and even contributed decisively to the eradication of some viruses (smallpox + poliovirus type 2 and 3) among the population, newly emerging viruses as well as pathogens with elaborate immune escape mechanisms and latency raise the need for modern, customizable and multifunctional vaccine candidates [86]. Early precursors and blueprints for synthetic nanoparticles are VLPs, particulate structures that mimic the parental viruses and are typically expressed by eukaryotic producer cells or bacteria upon transfection or transformation, respectively (Fig. 2 A-B) [87]. VLP-based vaccines that are based on proteinaceous capsids are already available for clinical use, i.e. as prophylactic vaccines against Hepatitis B (HBV) or human papilloma virus (HPV) [88]. However, VLPs derived from enveloped viruses, i.e. lentiviral VLPs, are difficult to meet the criteria for clinical administration due to the presence of producer cell-derived (self) antigens in the lipid bilayer membrane and the uncontrollable quantity of the antigen of interest displayed on the surface [89,90].

Synthetic nanoparticles are commonly characterized by a size smaller than 300 nm in diameter and a spherical morphology (Fig. 2 C-D) [91]. They usually have a customizable, rational design and can be organic (liposomes, lipid nanoparticles) or inorganic (gold, silica, iron oxide or calcium phosphate nanoparticles) [92–94]. Another class, polymer-based nanoparticles, is not covered in this study [95]. While the size of most types of nanoparticles ranges between 100 nm and 300 nm, iron oxide and gold nanoparticles in particular are scalable down to 5 nm in diameter [96]. Nevertheless, nanoparticles have sizes that are equal to viral pathogens and way smaller than immune cells such as macrophages, dendritic cells, B and T cells, which typically have diameters in the lower micrometer range. These proportions allow for an uptake by immune cells via endocytosis, phagocytosis or macropinocytosis [97,98]. The size, zetapotential and composition of nanoparticles may influence the rate of cellular uptake and the fate within the cells [99]. Regarding

in vivo immunization settings, nanoparticles smaller than 200 nm easily enter the lymphatic vessels and reach draining lymph nodes and/or the spleen [100].

Nanoparticles may have a solid (gold, iron oxide) or a hollow, aqueous core (liposomes). Particularly, the latter constitution enables the mimicking of viral structures. For some particulate platforms, i.e. calcium phosphate nanoparticles, it is even possible to generate multi-shell particles with the possibility to encapsulate biomolecules within each layer [101]. The encapsulation of bioactive substances in the core of nanoparticles is one of the most important features for customized and scalable delivery of drugs and bioactive substances [102]. While the distribution of free substances in tissue or blood after injection is unpredictable and uncontrolled, hollow nanoparticles are transporters of various biomolecules (i.e. adjuvants, peptides, DNAs) in a defined amount [103]. Moreover, biomolecules are protected from degradation by nucleases or proteases via incorporation into nanoparticles [102]. One way of compensating the generally low immunogenicity of synthetic nanoparticles is the encapsulation of adjuvants or immunostimulatory agents such as TLR ligands [104].

Another key feature of synthetic nanoparticles is the possibility to functionalize the surface with biomolecules. The two main objectives in this regard are i) targeting and ii) induction of immune responses [105]. i) The surface-immobilization of antibodies specific for membrane-embedded cell marker molecules enables the targeting of specific immune cells [101,106]. In the same way, functionalization of nanoparticles with ligand molecules may guide them to cells displaying the correspondent receptor molecules [107]. The nanoparticulate encapsulation of bioactive substances in combination with a targeting surface functionalization enables to transfer and introduce specific cargo to desired immune cell destinations [108]. ii) A multitude of studies gave the indication that the presentation of a dense array of repetitive antigens strongly increases the immunogenicity and humoral immune responses, probably via an improved recognition by the B cell receptors (BCRs) of antigen-specific B cells [109,110]. For inorganic nanoparticles it is rather easy to equip the nanoparticle surface with chemical groups that can be harnessed for chemical coupling with required antigens, antibodies, peptides or polysaccharides. Terminal thiol or carboxy groups in particular can be used for sulfo-SMCC- or EDC/Sulfo-NHS-mediated, unspecific

coupling via primary amines on the target molecule [101,111]. In order to introduce reactive groups on the surface of organic nanoparticles, phospholipids with specialized head groups need to be included in the nanoparticle composition [112]. The optimal coupling of nanoparticles with antigens is an ongoing subject of current research and a main feature of this study.

Synthetic nanoparticles are well-tolerated *in vivo*, since their composition is mainly based on physiological substances, that are naturally occurring in mammalian organisms. Organic nanoparticles are composed of cholesterol, phospho- and sphingolipids that are part of plasma cell membranes [94,113]. The majority of inorganic nanoparticles is biodegradable, which means that their structural components are sensitive for acidic environment (i.e. calcium phosphate) and dissolve in the cells' lysosomes [114]. Nevertheless, non-biodegradable nanoparticles, especially gold nanoparticles, are well-established for biomedical applications, especially in the fields of tumor thermotherapy and as a contrast agent [115,116]. In this regard, modern research approaches regarding iron oxide nanoparticles coupled with anti-tumor agents utilize their magnetic ability to steer them through the blood stream directly to the site of cancer after intravenous injection [117].

Taken together, the size, composition, charge, cargo and specificity of nanoparticles can be controlled in a customizable way. Nanoparticles are efficient in the induction of immune responses and the targeting of immune cells for immunomodulatory treatments. While conventional vaccines greatly contributed to the containment or eradication of a broad spectrum of pathogens in the 19th and 20th century, nanoparticle-based vaccines and therapeutics are highly promising to dominate and change biomedical applications in the 21th century. The best current example is the encapsulation of SARS-CoV-2 S-antigen-encoding mRNA into lipid nanoparticles as the main component of the first licensed vaccines administered in humans to contain the pandemic spread of SARS-CoV-2 [118].

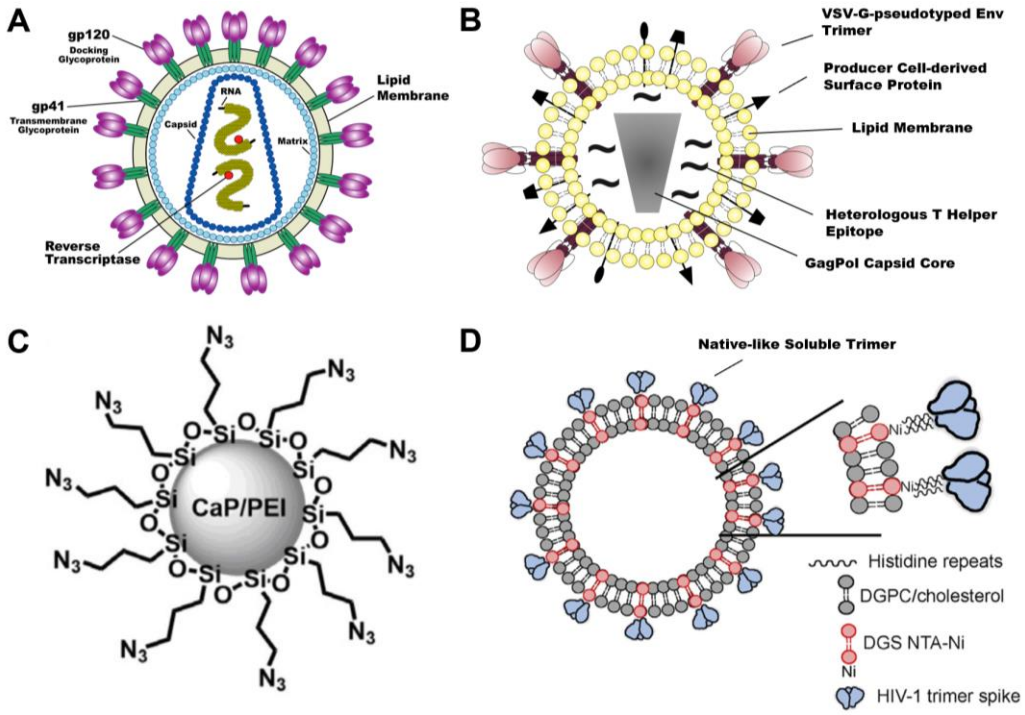

Figure 2) Schematic representation of different nanoparticles

(A) Native HIV-1 virion. Structural subunits are outlined and described. Importantly, the combination of both the presence of viral genomic RNA copies in the capsid core and fusion-competent Env trimers on the surface render these virions infectious. Unlike this image conveys, there is only an average of 14 Env trimers present on the viral surface. Adapted from niaid.nih.gov. **(B)** T helper VLP. The Env trimers are membrane-embedded and fusion-incompetent. No viral genome is present in the capsid. Due to expression in cells and budding, producer cell-derived proteins are included in the lipid membrane. Introduction of sequences coding for heterologous T helper epitopes in the GagPol ORF results in the incorporation of peptides for intrastructural help. **(C)** CaP. The inorganic nanoparticle is composed of calcium phosphate, polyethylenimine and silicon dioxide functionalized with terminal azide groups as prerequisite for site-specific coupling reactions (CaP/PEI/SiO_2-N_3). Adapted from Rojas-Sánchez *et al.* (2018) [119]. **(D)** Liposome. Fusion-incompetent native-like Env trimers with a C-terminal Histidin-tag are non-covalently conjugated to the liposomal surface via interactions with Ni-NTA-terminated phospholipids. Modified from Ingale *et al.* (2016) [120].

1.2.1. Composition and application of calcium phosphate nanoparticles

Inorganic CaPs are highly biodegradable and biocompatible, since their key component, calcium phosphate, is also part of human bone and teeth and dissolves in the presence of acidic environment i.e. in lysosomal compartments of target cells [121]. While the syntheses and applications of CaPs are versatile, the key features that are relevant for this study are predominantly listed in the following. The CaPs

used in this study have a spherical structure composed of calcium phosphate, polyethylenimine (PEI) and silicon dioxide (CaP/PEI/SiO_2) functionalized with terminal thiol or azide groups, which was established by Kozlova *et al.* and Rojas-Sánchez *et al.* [101,119]. They are produced by stepwise precipitation from aqueous solution with the possibility to incorporate biological compounds such as peptides or adjuvants in each step [122,123]. This method further enables to generate multi-shell nanoparticles that effectively protect the encapsulated cargo against degradation [124]. By incorporation of PEI, being a cationic polymer, the CaPs have a positive zetapotential, which stabilizes them in aqueous dispersions and prevents from aggregation via ionic repulsion. Furthermore, a positive zetapotential is favorable for the uptake by both the HeLa cell line and immune cells [99,114]. CaPs are well-characterized, effective tools for the induction and modulation of immune responses. Zilker *et al.* evaluated the effect of CaPs incorporating different TLR ligands and displaying the model antigen hen egg lysozyme (HEL) on the humoral immune response. As the main result, the intramuscular injection route as well as encapsulation of TLR9 ligand CpG induced the highest levels of anti-HEL antibodies in mice [104]. Furthermore, even non-adjuvanted HEL-CaPs were able to induce significantly higher antibody levels compared to a mixture of CaPs and soluble HEL, probably because antigen-specific B cells are more likely to be activated by BCR-crosslinking when the antigen is displayed in repetitive structures as shown by Temchura *et al. in vitro* [125]. CpG-CaPs that were coupled with the influenza A virus surface antigen hemagglutinin (HA) resulted in the activation of dendritic cells (DCs) and upregulation of co-stimulatory MHC-II molecules by DCs *in vitro* as well as a strong T cell-mediated protection against influenza by induction of high numbers of IFN-γ-producing CD4+ and CD8+ T cells [103,126,127]. In the context of retroviral infections, mice were immunized with CpG-CaPs that were functionalized with T cell epitopes of Friend virus (FV). These nanoparticles induced and reactivated FV-specific effector T cells that significantly reduced viral loads in the vaccinees [128]. Beside the induction of immune responses, CaPs were used in the past for targeting and transfection. A study combining both was conducted by Kozlova *et al.* [101]. Here, the incorporation of DNA molecules resulted in strong expression rates of the encoded fluorescent protein after CaP-transfection of HeLa cells. Furthermore, functionalization of these CaPs with CD11c antibodies resulted in the specific targeting of murine CD11c+ dendritic cells. The incorporation of

plasmids coding for the surface glycoprotein of Hepatitis B virus (pHBsAg) into CaPs and immunization of mice with these nanoparticles resulted in the expression of the protein *in vivo* as well as in the induction of T and B cell-mediated immune responses against Hepatitis B [129]. While the conjugation of biomolecules to the surface of CaPs was mainly done in an unspecific manner via electrostatic adsorption or covalently via terminal thiol groups in earlier publications, Rojas-Sánchez *et al.* established the quantitative functionalization with terminal azide groups that allow a site-specific coupling via Click chemistry (CaP/PEI/SiO_2-N_3) [119,130].

Endocytosis and phagocytosis are the most prominent uptake routes for CaPs into cells and are influenced by size and zetapotential [131]. The fate of CaPs within the cells was extensively studied via CLSM and FACS using fluorescent nanoparticles. Especially in HeLa cell models, co-localizations with the cells' endolysosomes indicate that the CaPs are dissolved in these compartments and the cargo is released within the cells [119,132,133]. NIR fluorescence imaging and PET-CT allow to trace fluorescent or isotope-labeled CaP distribution routes *in vivo.* Intravenously injected CaPs are mostly found in lung, liver and spleen, while intramuscularly or intratumorally administered CaPs largely remain at the site of injection [134,135]. In summary, CaPs are inorganic nanoparticles that fulfill all requirements for targeting and induction. They have defined uptake and degradation pathways and are well-tolerated by mammalian organisms. Thus, biomedical applications are versatile and extensively studied [136].

1.2.2. Nanoparticles conjugated with Env

The research and usage of Env-coupled, synthetic nanoparticles as vaccine delivery platforms steadily increased in the course of the last decades. Both organic (liposomal, proteinaceous) and inorganic (calcium phosphate, silica, gold) carriers have been evaluated for preclinical, clinical and *in vitro* applications [104,109,112,137]. In this regard, numerous coupling mechanisms were established that can be categorized in two major groups: i) Genetic fusion of Env with subunits of self-assembling nanoparticles or ii) chemical coupling after synthesis of the nanoparticle core.

One example of the first category are ferritin nanoparticles (Fig. 3 B). Here, the coding sequence for ferritin was recombinantly introduced at the C-terminus of gp140. Upon expression and release by the producer cells, the Env-ferritin complexes self-assemble in the conditioned supernatant to nanoparticles harbouring 24 heterodimers [138]. The general Env immunogenicity as well as neutralizing antibody (Nab) responses against the autologous virus were significantly enhanced in rabbits and macaques that have been immunized with these Env-ferritin nanoparticles [139]. In a similar context, Env was fused to one protein of two-component proteinaceous capsid nanoparticles, that were computationally designed and form an icosahedral shape (Fig. 3 A) [140]. These nanoparticles also self-assemble after cell secretion and induced autologous tier-2 neutralization in rabbits [141]. More recently, SARS-CoV-2 S-antigen-fused two-component nanoparticles elicited neutralizing anti-S responses in rhesus macaques [142].

The second category comprises both organic and inorganic nanoparticles that were chemically functionalized with Env trimers after synthesis. Ingale *et al.* produced liposomes including Ni-NTA-terminated phospholipids that were harnessed for non-covalent interaction with His-tagged Env trimers (Env-His_8), which resulted in a dense array of well-ordered spikes on the liposomal surface [113]. However, even though the non-covalent His/Ni-NTA interaction was stable in buffer, the Env trimers drastically dissociated from the liposomes in the presence of 10 % serum albumin [143]. This strongly limited the applicability in preclinical studies [144]. The non-covalent association was strengthened by incorporation of cobalt-porphyrin ring structures in the liposomal membrane that built multi-chelating complexes with the C-terminal His-tag of Env [145]. Nevertheless, emphasis was put on covalent coupling strategies. To this end, a recombinant cysteine was introduced at the C-terminus of Env to form covalent bonds with maleimide head groups on the liposomal surface (Fig. 3 C) [109,143]. Immunization of rabbits with such liposomes resulted in the focusing of B cell responses to conformational binding sites and the elicitation of neutralizing antibody responses, since immunodominant non-neutralizing epitopes at the trimer bases were masked by the conjugation [146]. Further studies harnessed the non-covalent interaction of chelating ions to bring Env trimers in position for covalent binding. Bi-functional liposomes harbouring both Ni-NTA and maleimide moieties were used to attract Env-His_8 quantitatively to the

liposomal surface, before the covalent disulfide bonds were induced [143,147]. A parallel approach was done with bi-functional (Ni-NTA, COOH) anionic liposomes. Here, during His-tag/Ni-NTA interaction, the Env trimers were immobilized by EDC/Sulfo-NHS chemistry (Fig. 3 E) [112,148]. A follow-up approach harnessed the negative zetapotential of tag-free Env trimers to bring them in proximity to the surface of cationic liposomes for EDC/Sulfo-NHS crosslinking [111]. However, despite the preservation of the pre-fusion conformation by this approach, the coupling efficiency was low [111].

A recent study with regard to inorganic nanoparticles evaluated the site-specific, maleimide-mediated coupling of Env trimers to the surface auf silica beads in comparison to unspecific coupling by physical adsorption (Fig. 3 D) [137]. Here, site-specifically coupled beads were significantly better recognized and taken up by antigen-presenting cells. Furthermore, immunization of mice with these nanoparticles induced potent humoral immune responses [149]. The unspecific, sulfo-SMCC-mediated coupling of non-Env model antigens to the surface of CaPs have been performed with high efficiency in various studies [101,104,125]. Recently, the quantitative surface functionalization of CaPs with azide groups was established to render site-specific, click reaction-based coupling mechanisms feasible [119].

Taken together, the majority of mechanisms to couple Env trimers to the surface of synthetic nanoparticles are based on His-tag interactions, cysteine-maleimide bonds or unspecific targeting of primary amines via EDC/Sulfo-NHS chemistry. All of these strategies have flaws. The prevalence of nickel and cobalt allergies in the human population are an obstacle for the application of nanoparticles coupled via chelating ions in clinical trials [150]. Maleimides easily hydrolyze in a temperature-, pH- and time-dependent manner. This impedes a straightforward upscaling of these protocols [151,152]. Lastly, the preservation of the pre-fusion Env trimer conformation after unspecific coupling targeting primary amines is hard to control and maintain. Thus, novel and versatile site-specific mechanisms for the surface functionalization of synthetic nanoparticles with Env trimers are needed to produce safe and effective delivery platforms for new HIV-1 vaccine candidates.

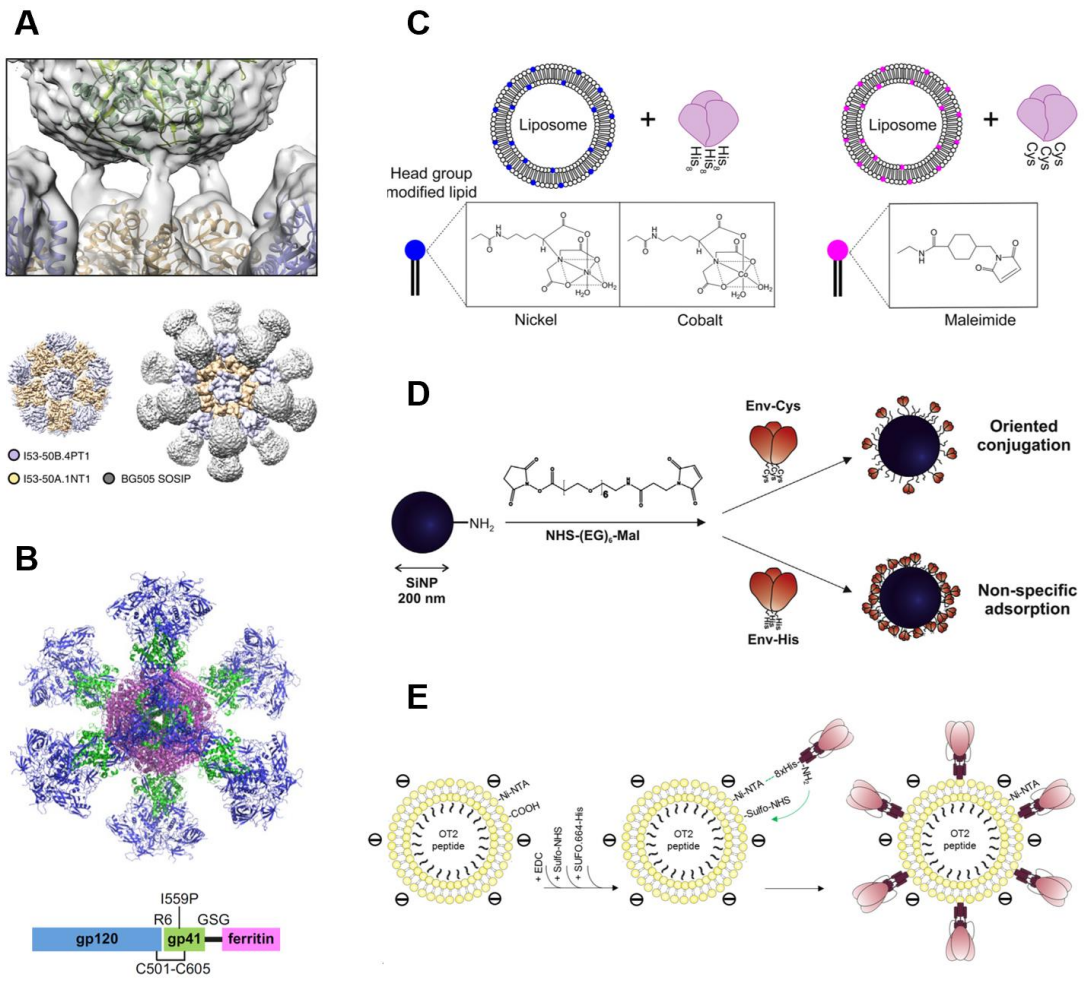

Figure 3) Strategies for nanoparticle functionalization with Env trimers

(A) Self-assembling two-component nanoparticles. BG505 SOSIP gp140 was genetically fused to component A (I53-50A). Upon purification, the subunits I53-50A-Env (trimeric) and I53-50B (pentameric) assemble to nanoparticulate capsids displaying 20 Env trimers on the surface. Modified from Brouwer *et al.* (2019) [140]. **(B)** Self-assembling ferritin nanoparticles. BG505 SOSIP gp140 genetically fused with ferritin is expressed in 293F cells and self-assembles to a nanoparticulate structure in the supernatant via ferritin interactions. Modified from Sliepen *et al.* (2015) [138]. **(C)** Site-specific, non-covalent and covalent Env coupling to liposomes. Env-His_8 was conjugated to the liposomal surface via interactions with phospholipids displaying Ni-NTA or cobalt (blue) head groups (left panel). Env-Cys was covalently conjugated with maleimide (pink) head groups (right panel). Modified from Bale *et al.* (2016) [109]. **(D)** Env coupling to inorganic silica nanoparticles. Env trimers were either physically adsorbed (unspecific conjugation) or covalently coupled via C-terminal cysteine residues and nanoparticle-associated maleimide groups (site-specific conjugation). Modified from Thalhauser *et al.* (2020) [137]. **(E)** Site-directed, unspecific coupling of Env trimers to liposomes. His-tagged Env trimers were attracted to the surface of anionic, bifunctional (Ni-NTA / COOH) liposomes via His/Ni-NTA interactions in a site-directed manner. Even though the subsequent EDC/Sulfo-NHS activation targets primary amines on Env in general, the reaction is likely to covalently bind residues in the proximity of the Env C-terminus. Modified from Damm *et al.* (2022) [112].

1.3. Bioorthogonal conjugation via genetically encoded aldehyde-tags

The underlying chemistry, that most of the coupling strategies mentioned above are based on, usually originates from the field of protein and/or tissue functionalization for bioengineering approaches. A site-specific, bioorthogonal and efficient conjugation is the crucial requirement for successful, promising efforts and applications [153–156]. Naturally occurring physiological or biological reactions may act as the blueprint for these bioengineering reactions.

One example is the discovery of a formylglycine (Fgly) residue in active, catalytic sites of sulfatases from various species across biological realms [157]. Formylglycine contains an aldehyde-group in its side chain and is post-translationally generated via cysteine oxidation mediated by the endogenous formylglycine-generating enzyme (FGE) [158,159]. The cysteine residue is located in a highly conserved 6-mer (xCxPxR, x = leucine, alanine, serine, glycine or threonine), which is part of a larger 13-mer sulfatase motif (Fig. 4 A). FGE is encoded in the *SUMF1* gene family which has – like the sulfatase motif – orthologs from prokaryotes to higher eukaryotes [160].

Carrico *et al.* have recognized the potential of this modification for recombinant bioengineering systems and termed the 6-mer sequence as “aldehyde-tag” (Ald_6) [161–164]. The aldehyde-tag sequence in human arylsulfatase E is LCTPSR, which is also the consensus sequence from various prokaryotic, archaean and eukaryotic species [161]. Carrico *et al.* performed proof-of-principle studies to evaluate Fgly conversion and site-specific bioconjugation efficiency. They genetically encoded the aldehyde-tag or the full 13-mer sequence at the N- and C-termini as well as within the open reading frames of three different proteins and had them expressed by *E. coli* (Fig. 4 B). As results, they found efficient Fgly conversion that was independent of the position of the tag. No significantly different conversion efficiency was seen between 6-mer and 13-mer sequences. The introduced aldehydes could be harnessed for bioconjugation with fluorescent reagents bearing terminal aminooxy groups, which preferably bind to aldehyde and ketone groups and form covalent bonds (oxime ligation) [165]. Likewise, efficient oxime formation was demonstrated via fluorescent gel and gel shift reporter assays [161]. Wu *et al.* transferred the mechanism in a mammalian CHO expression system

to generate aldehyde-tagged antibodies, thereby proving that FGE activity is present in the secretory pathways of eukaryotic cells. Additionally, overexpression of FGE, i.e. by co-transfection of cells with a FGE-encoding plasmid, resulted in increased Fgly conversion rates [166]. Rabuka *et al.* optimized the oxime ligation reaction for bioengineering approaches and provided detailed protocols for the whole mechanism including a mass spectrometry-based strategy to calculate the Fgly conversion rates [167]. Finally, Hudak *et al.* described the fusion of an aldehyde-tagged protein to another antigen via a bifunctional aminooxy/azide “click” linker in a two-step reaction (oxime ligation + click reaction) [168]. As a conclusion, the high specificity and efficiency of the aldehyde-tag-mediated bioconjugation mechanism renders this method a promising and competitive alternative for previously applied strategies to functionalize nanoparticles.

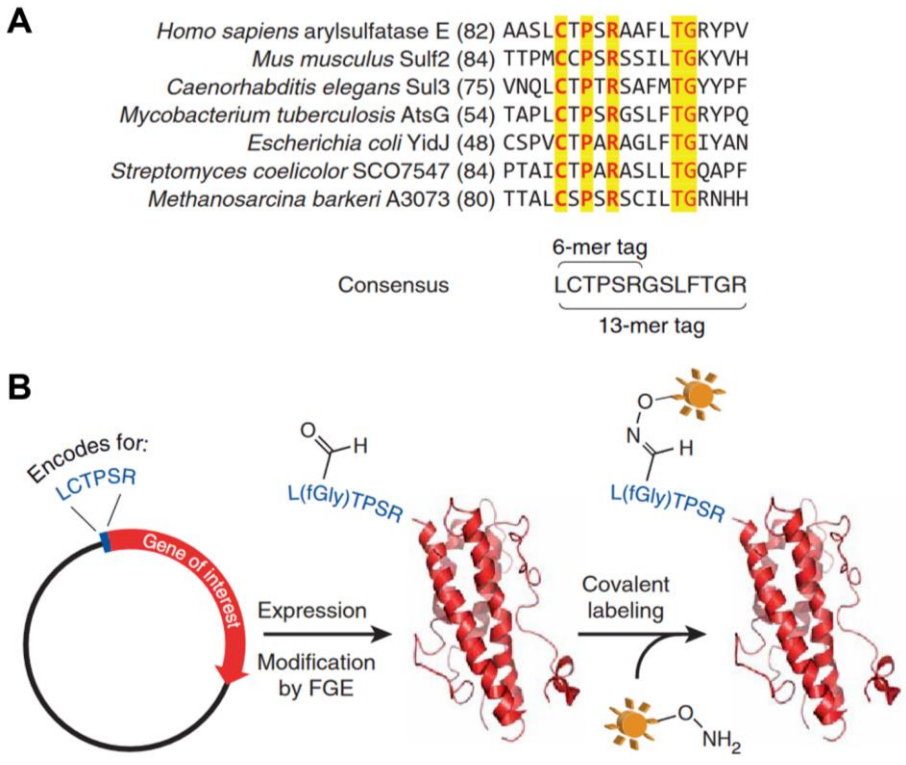

Figure 4) Aldehyde-tag mechanism

(A) The 13-mer sulfatase motif containing a highly conserved 6-mer aldehyde-tag has orthologs in various prokaryotic, archaean and eukaryotic species. The consensus aldehyde-tag sequence is LCTPSR. **(B)** The aldehyde-tag sequence can be genetically introduced at the N- or C-termini as well as within the ORFs of interest. Upon transfection of mammalian cells, the tag-associated cysteine is post-translationally converted into formylglycine by endogenous and/or co-expressed FGE. The Fgly residue can then be harnessed for covalent oxime ligations with aminooxy-terminated reaction partners. Adapted from Carrico *et al.* (2007) [161].

1.4. Modulation of the immune response

As outlined above, HIV-1 has a multitude of immune escape mechanisms that are mainly associated with the surface glycoprotein Env, which is the sole target for the humoral immune response. While the mentioned escape mechanisms primarily impede the formation of neutralizing immune responses, others affect the quality of the immune response in the context of antibody Fc effector functions. It has been reported that DNA immunizations of mice with plasmids coding for viral glycoproteins of HIV-1 (Env), influenza A (HA) and respiratory syncytial virus (RSV, F-antigen) resulted in predominant Th1-associated anti-HA and anti-F IgG2a responses. The Env response, on the contrary, was Th2 / IgG1-dominated [169]. A more recent study described the DNA immunization of hACE2 mice with a plasmid coding for the surface antigen S of the SARS-CoV-2 virus and here the anti-S humoral immune response was mainly Th1-based [170]. In fact, data indicated that N-glycosylation sites in the C2/V3 regions of Env are responsible for this IgG subtype bias [169].

Th1-type IgG2a/c murine antibodies bind the following Fcγ receptors (FcγR): FcγRI, FcγRIII and FcγRIV, all of which are correlated with strong antiviral effector functions like antibody-dependent cell cytotoxicity (ADCC) [171,172]. On the contrary, Th2-type IgG1 in the murine system, despite some low-affinity binding to FcγRIII, predominantly binds the inhibitory FcγRIIb [173]. Thus, modifying anti-Env IgG subtype responses in a Th1-like manner might be favorable for antiviral effector activity [174,175].

Initial studies have demonstrated that the fate of IgG subtype responses is largely defined by the cytokine profile that antigen-specific B cells receive from CD4+ T helper cells [176]. More recently, the communication of T follicular helper cells with germinal center B cells was identified to play a crucial role in immunoglobulin class switching after infection or vaccination [177–179]. IFN-γ is the key player of a Th1-polarized response. Being secreted by Th1-type CD4+ T cells, it actively stimulates an IgG2a/c class-switch in mice, whereas the expression of other IgG subtypes is suppressed [180]. Moreover, the secretion of TNF-α, IL-2 and IL-12 are correlated with a Th1 response [181,182]. Th2 polarization, on the contrary, is mediated and defined by IL-4 as the key cytokine [183]. IL-4 stimulates B cells to express IgG1

subtype antibodies and inhibits Th1 cell-specific factors [184]. Further Th2-type T helper cell-secreted cytokines are IL-5, IL-10, IL-13 and IL-25 [182,185].

In order to overcome the biased Th1-response against Env and to promote potent Fc effector functions, immunomodulatory vaccination regimens are needed. Strategies to modulate humoral immune responses are described as follows.

1.4.1. Cytokines

While the IgG subtype response is influenced by the cytokine profile provided by T helper cells, the Th-polarization itself depends on cytokine input from antigen-presenting cells (i.e. DCs) [186]. Upon binding to cytokine receptors on the T cell surface, signaling pathways are regulating the expression of transcription factors that ultimately mediate T cell differentiation into specific lineages [187]. IL-12 and IFN-γ induce the expression of Th1-defining transcription factor T-bet [188,189]. On the opposite, Th2-polarization is regulated by IL-4, which promotes the GATA-3 transcription factor [184,190]. Since CD4+ T cell lineage is decisive for the phenotype of the humoral immune response, it seems reasonable to influence the Th-polarization by induction of IL-12 or IL-4 overexpression via DNA immunization. DNA immunization leads to the long-term, endogenous expression of antigens and modulatory proteins [191]. Kim *et al.* were among the first in context of a retroviral vaccination setting that actively changed the Env-specific immune response in favor of a Th1-phenotype by co-administration of plasmids coding for Env and IL-12 [192]. In a follow-up study, the co-delivery of IL-10, IL-2, IL-4 or IL-12 DNA with a plasmid coding for SIV Gag/Pol drove the immune responses towards the respective Th phenotypes. In addition, cytokine overexpression resulted in dramatically enhanced antibody levels, Th proliferation and induction of CTL responses [193]. Thus, cytokine-encoding plasmids act as immunomodulatory molecular adjuvants upon DNA immunization and endogenous expression, that are capable of actively modifying the Th lineage and B cell stimulation [194].

1.4.2. Adjuvants

Conventional adjuvants are agents added to the vaccine antigen to stimulate innate and modify adaptive immune responses [195]. The usage of adjuvants and the corresponding effects are versatile and widespread and reach beyond the scope of this study. Thus, the following paragraph will summarize the key facts that are relevant for this study's findings.

Adjuvants may roughly be divided into two groups: i) Chemical substances like oil-in-water emulsions (MF59 [196], AS03 [197]), mineral compounds (aluminium hydroxide "Alum" [198,199]) or triterpene glycosides (QS21 [200]) and ii) TLR ligands like oligonucleotides (CpG [201,202]) as well as bacterial compounds (flagellin [203], MPLA [204,205]) or synthetic RNA (polyI:C [206]). While the first group mainly improves immune responses by causing irritations at the site of injection, the latter stimulates TLR-mediated immune responses, which further promote adaptive immunity. Nevertheless, in general, both cellular and humoral immune responses are improved by adjuvantation and some adjuvants clearly modify the quality of the response towards a Th1 or Th2 phenotype [207].

In the context of nanoparticles, Zilker *et al.* demonstrated that encapsulation of different TLR ligands in CaPs strongly improved and modulated the immune response to the surface-functionalized model antigen. Here, CpG adjuvantation resulted in the highest antibody levels with a prominent Th1 phenotype [104].

1.4.3. Intrastructural help

As previously outlined, immune escape related to Env both impedes the formation of neutralizing immune responses and drives the IgG subtype ratio in a Th2-dominated phenotype, which is associated with less potent antiviral Fc effector functions [208–210]. Another concern that was raised in the context of prophylactic HIV vaccine candidates including Env is the seemingly inevitable generation of Env-specific CD4+ T cell responses that provide help to stimulate Env-specific B cells after immunization with conventionally adjuvanted Env subunit or DNA vaccines [211]. Activated T helper cells with upregulated surface expression of CD4 are the main targets for HIV-1. Vaccine-induced, Env-specific CD4+ (memory) T cells resident in the genital mucosa may become activated in the course of an inoculum and provide

viral targets [212]. That situation may disrupt the steady-state of infection and protection in favor of HIV in this early stage of viral spread. In fact, studies have shown a correlation between the number of vaccine-induced HIV-specific CD4+ T cells and an increased risk of infection after challenge [213,214]. That was also true in the context of SIV-infection in previously immunized macaques [215]. This issue poses an unprecedented challenge to the field of experimental HIV-1 vaccine research, namely the induction of neutralizing antigen-specific B cell responses without the concomitant elicitation of cognate CD4+ T cell responses specific for antigen-derived peptides [216].

Studies of the late 1970s and 1980s have reported that CD4+ T helper cells specific for internal structural components of influenza A virus (IAV) and HBV are stimulated after immunization with VLPs or attenuated virus to provide help for surface antigen-specific B cells [217,218]. The observation was based on the BCR-dependent uptake of the particles into surface antigen-specific B cells and the subsequent presentation of particle-derived peptides on MHC-II molecules by the B cells which enables to recruit pre-existing CD4+ T cells specific for epitopes processed from internal components of the particles (Fig. 5). This heterologous T cell help, called intrastructural help (ISH), is a non-controlled loophole in the adaptive immune system that may be harnessed for immunomodulatory vaccination regimens [219,220]. In the last decade, the mechanism was widely applied to modify the Env-specific humoral immune response upon immunization. First attempts aimed at reproducing the core idea of the IAV- and HBV-related ISH studies in an HIV-1 context. Thus, mice were immunized with GagPol-encoding DNA and the elicited CD4+ T cell responses could provide intrastructural help for Env-specific B cells after a lentiviral VLP boost, which has been proven in adoptive transfer experiments [221]. Furthermore, ISH could significantly enhance antibody levels and rescue the Env-related Th2 bias towards a balanced IgG2a/IgG1 response [222]. Thus, ISH enables adjuvant-free immune modulation and might substitute the effects of conventional adjuvants. The phenotype of the prime response was imprinted on the Env immune response via ISH [223]. Follow-up studies demonstrated that CD4+ T cells specific for epitopes derived from licensed Tetanus- and Tuberculosis-vaccines can be recruited to provide ISH for Env-specific B cells *in vivo* [224,225]. While a prime immunization with Tetanol®pur induced a Th2-polarized T cell lineage and promotion of Env-specific IgG1 antibodies,

Klessing *et al* could generate a potent, long-lived Th1-dominated response associated with high levels of anti-Env IgG2b and IgG2c IgG subtype antibodies in mice using a Tuberculosis subunit vaccine (H1/CAF01 [226]) as a prime and lentiviral VLPs incorporating Tuberculosis epitopes (T helper VLPs) as boost [225]. In general, the utilization of pre-existing T cell responses specific for epitopes derived from childhood vaccines is a promising approach for a clinical HIV-1 vaccine trial in the context of ISH. However, due to a variety of concerns, lentiviral VLPs are unsuitable for “good manufacturing practice” (GMP) production and clinical applications. Upon expression and budding they are wrapped in a lipid bilayer containing producer cell-derived surface proteins in addition to Env, whereas HIV-derived capsid proteins serve no purpose for ISH. Moreover, the quantity of Env trimers on the VLP surface cannot be controlled and industrial upscaling of VLP batch production is critical [67,89]. Thus, synthetic nanoparticles with an aqueous cavity for peptide encapsulation (T helper nanoparticles) are a potential replacement for VLP-based vaccine candidates. Nevertheless, the requirements for synthetic T helper nanoparticles are a structural composition (size, charge) that allows entry to lymphatic vessels and secondary lymphoid organs, the recognition and BCR-dependent uptake by B cells specific for the antigen on the nanoparticle surface and the MHC-II-presentation of peptide epitopes previously encapsulated in the nanoparticles [220]. In fact, Hills *et al.* demonstrated ISH effects modulating the quality of the antibody response against the surface glycoprotein from Malaria using liposomes that were coupled with the Malaria antigen and encapsulated ovalbumine-derived OT2 peptides for the recruitment of pre-existing T cell responses [227]. More recently, the production of Env-coupled T helper liposomes has been optimized and critical requirements for ISH were evaluated in functional *in vitro* assays with these nanoparticles. In parallel, the internal and external functionalization of CaPs has been optimized and analyzed in recent years [101,104,106,119]. These nanoparticle delivery platforms are promising candidates for ISH vaccine applications in future preclinical and clinical trials.

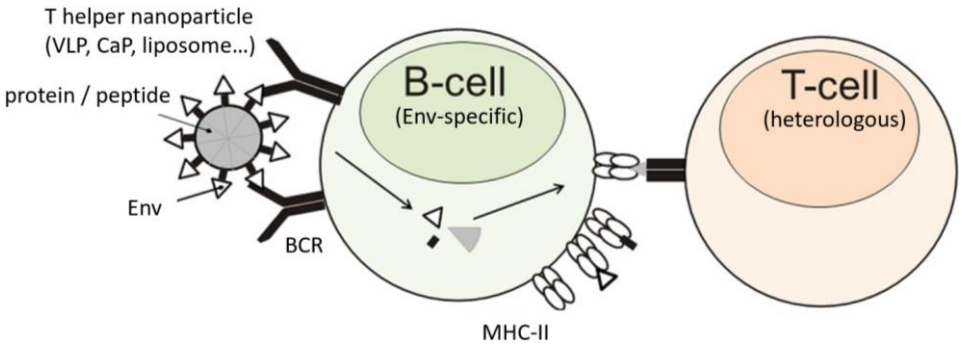

Figure 5) Concept of intrastructural help for Env-specific B cells

T helper nanoparticles conjugated with Env are recognized and taken up by Env-specific B cells in a BCR-dependent manner. The nanoparticles are processed within the B cells‘ endolysosomal compartments and epitopes derived from both Env and encapsulated peptides or proteins are presented on MHC-II molecules on the cell surface. Subsequently, pre-existing heterologous CD4+ T cells specific for the encapsulated components of the T helper nanoparticles can then recognize their target peptides and provide intrastructural help for the Env-specific B cells. Modified from Elsayed *et al.* (2018) [224].

1.5. Aims and Objectives

T helper VLPs have been used in previous studies to recruit heterologous T cell help for the modulation of Env-specific humoral immune responses with emphasis on Fc effector functions and long-term kinetics. However, the applicability of lentiviral VLPs in clinical studies that require GMP production is limited.

The first major objective of this thesis was to evaluate the utilization of synthetic T helper CaPs in comparison to VLPs in immunomodulatory ISH immunizations. The binding and inducibility of naïve Env-specific B cells by T helper CaPs was to be shown first as a crucial prerequisite for ISH. Afterwards, the phenotype of ISH effects mediated by T helper CaPs was compared with control groups comprising T helper VLPs or CpG-adjuvanted CaPs. In general, CaPs lack the self-adjuvanting character of VLPs that contain producer cell-derived proteins in the lipid membrane. Thus, it was of interest, whether i) the strength of ISH effects in terms of antibody levels and IgG subtype distribution was comparable between CaP and VLP groups, ii) the immunomodulatory features induced by ISH can compete with CpG adjuvantation, iii) ISH impedes the formation of vaccine-induced immune mechanisms that may increase the risk of HIV-1 infection.

The second major objective of this study was the optimization of the T helper CaP design by utilizing genetically encoded aldehyde-tags for orthogonal Env conjugation via a two-step mechanism. Here, the first aim was to evaluate the specificity and efficiency of the tag expression as well as of each bioconjugation step. Secondly, the preservation of the pre-fusion conformation of Env was evaluated throughout the coupling mechanism and on the finished nanoparticles. The last aim was to compare the optimized nanoparticles with the former ones in functional *in vitro* and *in vivo* assays with emphasis on improved BCR crosslinking and immunogenicity.

The approaches in this thesis helped to assess the applicability of synthetic nanoparticles for immunomodulatory vaccine trials. The orthogonal bioconjugation mechanism evaluated in this study can be used in the context of Env for further applications such as the site-specific labeling without conformational loss and to study the induction of neutralizing immune responses by the optimized nanoparticle design.

2. Results

The majority of results presented in this dissertation were published in the peer-reviewed scientific journals *Nanomaterials* (Damm *et al.*, “Calcium Phosphate Nanoparticle-Based Vaccines as a Platform for Improvement of HIV-1 Env Antibody Responses by Intrastructural Help”, 2019 [228]) and *Acta Biomaterialia* (Damm *et al*., “Covalent Coupling of HIV-1 Glycoprotein Trimers to Biodegradable Calcium Phosphate Nanoparticles via Genetically Encoded Aldehyde-Tags”, 2022 [229]).

2.1. Analysis of intrastructural help effects induced with T helper calcium phosphate nanoparticles

2.1.1. Production and characterization of Env trimers and nanoparticles

The induction of *in vivo* ISH effects is based on two major requirements. First, a nanoparticulate vaccine candidate that displays a dense array of the antigen of interest on the surface and encapsulates multiple copies of a heterologous peptide or protein. Secondly, the vaccinee must have pre-existing, heterologous T cell responses specific for the encapsulated peptide or protein. In order to modulate the HIV-specific humoral immune response by ISH, the antigen of interest is Env, since it is the only glycoprotein presented on the surface of native virions. Because the induction of neutralizing anti-Env responses in animal models was dependent on the Env conformation [44], faithful mimetics of the HIV-1 Env trimer representing the closed pre-fusion state were used for this study. The vector pBG505-NFL-gp140-His (provided by Prof. Richard T. Wyatt, The Scripps Research Institute, La Jolla, CA, USA) is encoding for a soluble, native-like gp140 Env trimer with a C-terminal 8x His-tag (Env-His_8). This SOSIP construct was further stabilized by two repeats of a flexible glycine/serine linker (GGGGSGGGGS, $2xG_4S$) that covalently links the C-terminus of gp120 with the N-terminus of $gp41_{ecto}$. An additional $1xG_4S$ linker is inserted directly upstream of the 8x His-tag. This soluble trimer is a recombinant form derived from a full-length gp160 Env of a subtype A isolate (BG505 gp160; Fig. 6 A,C). As a purification control, the $2xG_4S$ linker as well as the whole gp41 ectodomain were removed by mutagenesis PCR to elicit monomeric forms of Env-His_8 (Env-His_8-gp120). Furthermore, in order to generate BG505 VLPs, a

membrane-embedded version of BG505 gp140 (pBG505-NFL-gp140-G/TMCD) was cloned and provided by Dr. Ghulam Nabi (Ruhr-Universität, Bochum, Germany). Here, both the 1xG_4S linker and the His-tag were replaced by the transmembrane (TM) and intracellular domain (CD) of VSV-G (Fig. 6 A).

Env-His_8 was demonstrated to be thermostable up to 67.6°C and predominantly in trimeric state after affinity chromatography alone [76]. A 1 liter suspension culture of HEK293F cells was transiently transfected with plasmids encoding soluble forms of Env (Fig. 6 B) for protein expression. The supernatant was harvested after 3 days, filtered and run over a self-made affinity column filled with 5 mL of agarose-bound *Galanthus nivalis* lectin (GNL) by gravity flow. After elution and concentration, the purified Env proteins were analyzed by NativePAGE and silver stain. For trimeric Env-His_8, the trimer fraction was represented by a prominent band at approximately 700 kDa, while two minor bands at 480 kDa and 240 kDa indicated the presence of an expected low percentage of dissociated gp140 dimers and monomers. The purification of monomeric Env-His_8 resulted in two equally intensive bands on the native gel at approximately 420 kDa and 200 kDa representing gp120 dimers and monomers (Fig. 6 D). gp120 dimers were formed by aberrant intermolecular disulfide bridges despite the absence of the trimerization domain in $gp41_{ecto}$ [230]. Interestingly, no pronounced aggregate bands were detected in both samples.

In addition, T helper VLPs (Env-VLP-p30) were produced as control for *in vivo* ISH effects. The plasmid pHgpsyn-TTp30 (Fig. 6 A) coding for HIV-1 structural proteins (gag) and viral enzymes (pol) with an insertion of the coding sequence for the Tetanus Toxoid-derived peptide p30 in frame between the p17 matrix and the p24 capsid protein was provided by Dr. Vladimir Temchura (Universitätsklinikum Erlangen, Friedrich-Alexander Universität, Erlangen, Germany). HEK293T cells were co-transfected with pBG505-NFL-gp140-G/TMCD and pHgpsyn-TTp30 for VLP expression (Fig. 6 B). After 64 h, the supernatant was harvested and the VLPs were purified by ultracentrifugation. Subsequently, the amount of Env and Gag in the preparation was determined by VLP ELISA.

Both the purified proteins as well as the VLPs were further analyzed by reducing SDS-PAGE and Western Blot (Fig. 6 E). Env-His_8 and Env-His_8-gp120 were verified by two intensive bands at 140 kDa and 120 kDa, respectively, as

expected. Detection of VLP-derived proteins with an Env-specific anti-gp120 antibody resulted in a band at approximately 150 kDa, representing the membrane-embedded recombinant form (Env-G/TMCD). Gag-related bands were detected only in the VLP sample after incubation with an anti-p24 antibody at 55 kDa, 41 kDa and 24 kDa, representing different stages of the Gag p55 polyprotein processing (Fig 6E, lower panel).

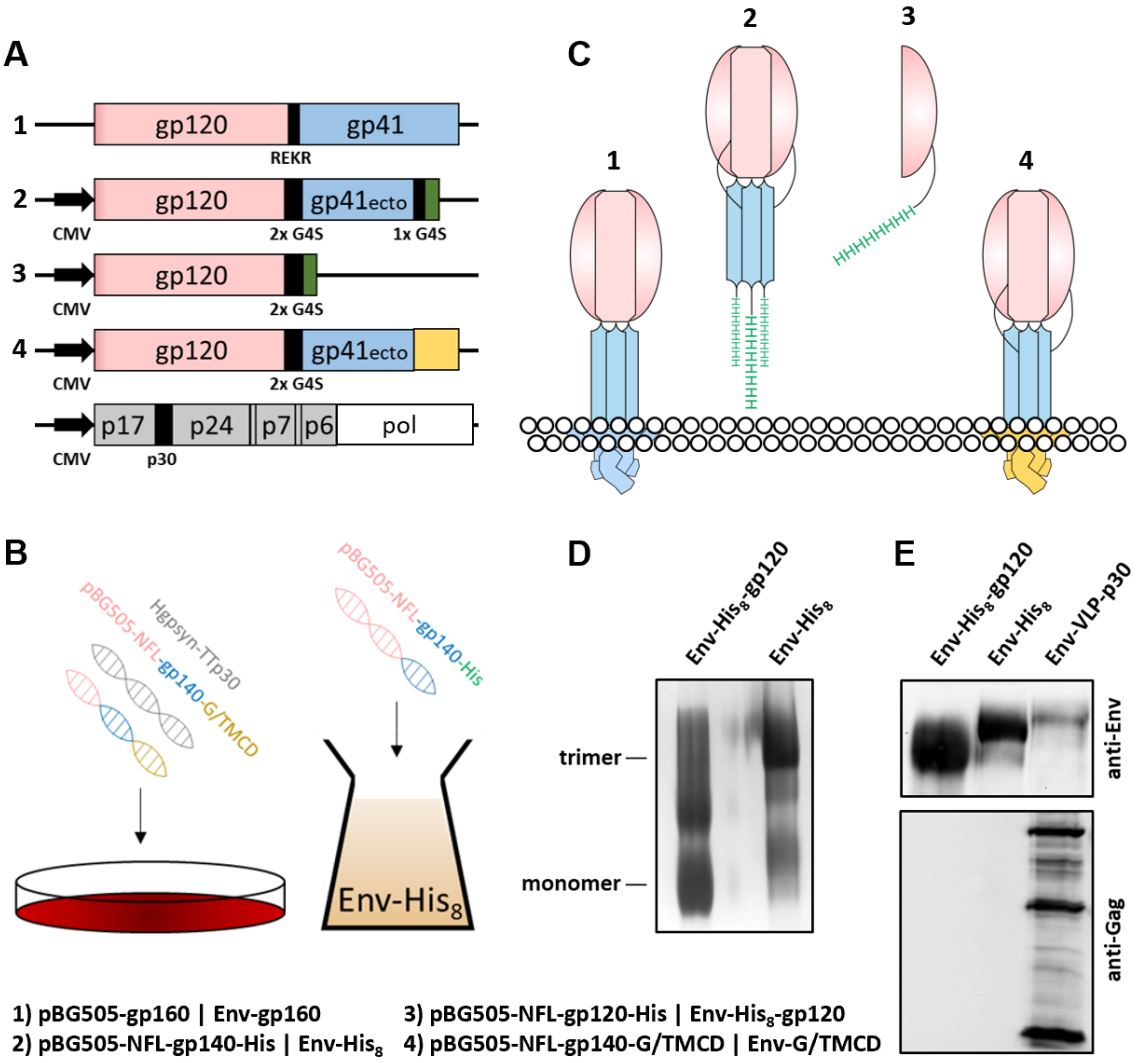

Figure 6) Production and characterization of Env trimers and Env-VLP-p30

(A) Open reading frames of various recombinant Env constructs and pHgpsyn-TTp30. The BG505 gp160 wildtype protein is composed of a gp120 sequence (light red) followed by full-length gp41 (blue) with a REKR motif inbetween for post-translational cleavage. The REKR motif is replaced in recombinant forms by a 2x G_4S linker. gp140 is composed of both gp120 and the gp41 ectodomain. Secreted Env constructs additionally contain a C-terminal G_4S linker and a His-tag (green). In order to express membrane-embedded trimers, the transmembrane and intracellular domains of VSV-G (yellow) are introduced downstream of $gp41_{ecto}$. pHgpsyn-TTp30 encodes the Gag p55 precursor protein (grey) and the viral enzymes (pol; white). The nucleotides coding for the Tetanus Toxoid-

derived peptide p30 are inserted between the p17 matrix and p24 capsid sequences. CMV promoters are indicated with black arrows. **(B)** Protein and VLP production. Adherent HEK293T cells (left) and suspension-adapted HEK293F cells (right) were (co)-transfected with the vectors pHgpsyn-TTp30 + pBG505-NFL-gp140-G/TMCD and pBG505-NFL-gp140-His to express virus-like T helper particles (Env-VLP-p30) and soluble trimers (Env-His_8), respectively. Soluble monomers were additionally produced in HEK293F cells as purification controls. **(C)** Overview of different Env proteins. Color codes and protein domains match with the respective ORFs in **(A)**. In general, trimers are composed of three non-covalently linked gp120-gp41 heterodimers. **(D)** NativePAGE and silver stain of Lectin-purified trimers and monomers. The most prominent gp140 trimers and gp120 monomer bands are indicated. Band sizes inbetween represent both gp140 and gp120 dimers as well as gp140 monomers. **(E)** Reducing SDS-PAGE and Western Blot of soluble Env proteins and Env-VLP-p30. The membranes were detected with both a polyclonal anti-gp120 Env antibody (upper panel) and a hybridoma anti-p24 Gag antibody (lower panel). A legend summarizing the Env ORFs and the corresponding proteins is located at the bottom of the figure. Modified from Damm *et al.*, (2019).

The purified Env trimers were used for the surface functionalization of CaPs. CaPs stabilized with a PEI and silica shell were synthesized by Dr. Leonardo Rojas-Sánchez (Institut für Anorganische Chemie, Universität Duisburg-Essen, Essen, Germany) for subsequent ISH immunizations. Thiol groups on the CaP surface as well as primary amines on the Env molecules were targeted via sulfo-SMCC crosslinkers to couple the trimers to the nanoparticle surface in a random manner (rCaPs, Fig. 7 A). In detail, Env-His_8 was activated with sulfo-SMCC by reaction of the primary amines on the protein with the linkers' N-hydroxysuccimide groups. Then, after addition of CaPs (CaP/PEI/SiO_2-SH), the maleimide groups of sulfo-SMCC can form covalent bonds with the thiol groups on the nanoparticle surface. For ISH immunizations and controls, rCaPs encapsulating p30 (rCaP-p30; T helper rCaPs) or CpG (rCaP-CpG) were further produced. Here, the peptide or adjuvant was adsorbed onto the CaP/PEI core before the stabilizing silica shell was layered around it as previously described for encapsulating DNA [101]. All produced batches of nanoparticles were analyzed by SEM and DLS (Fig. 7 B-D).

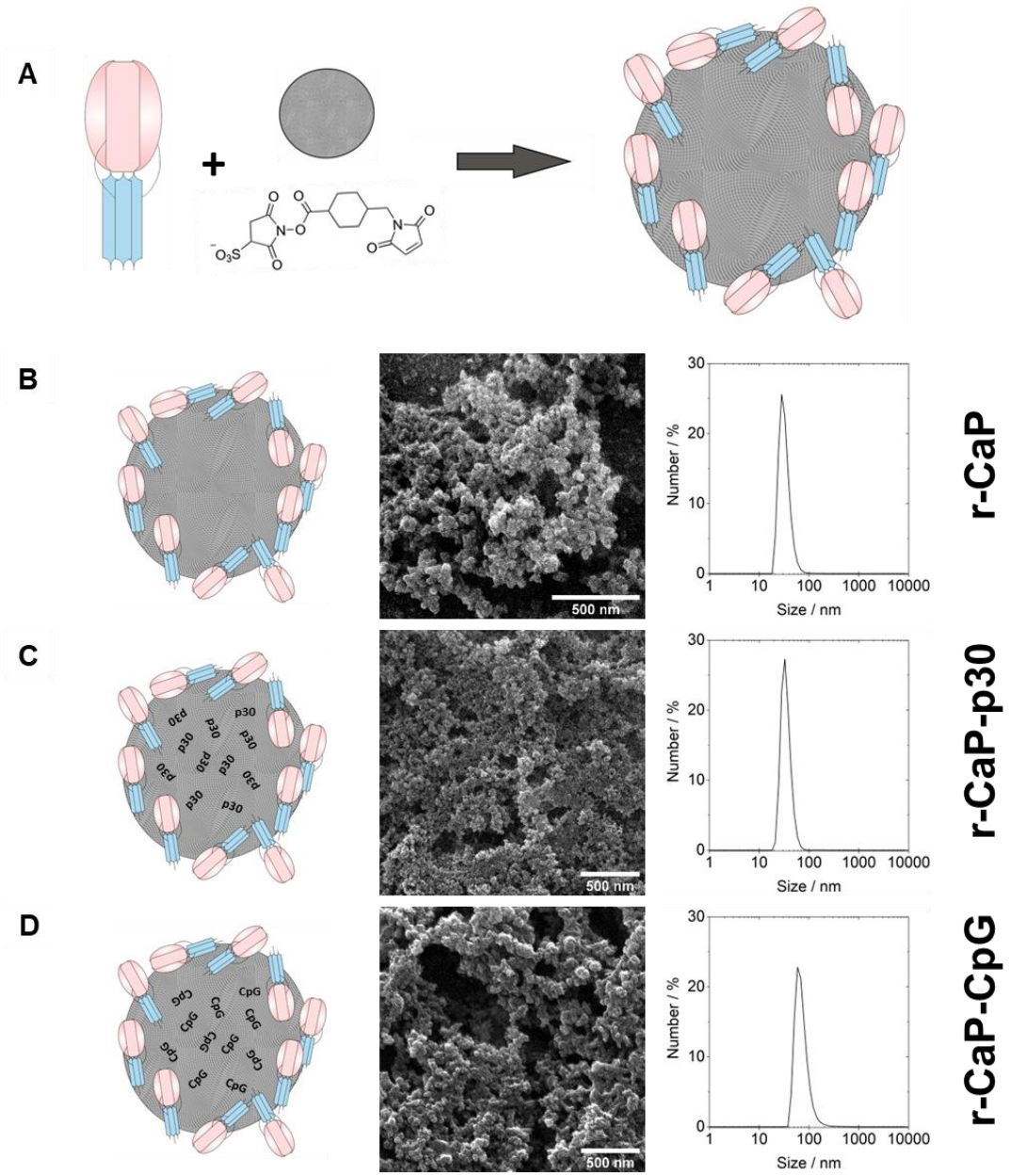

Figure 7) Physicochemical characterization of functionalized rCaPs

(A) Schematic presentation of rCaP formation. Env trimers were activated by sulfo-SMCC crosslinkers and covalently linked with thiol groups on the CaP surface in a randomly oriented manner. This procedure can be further done with CaPs encapsulating p30 peptides or CpG molecules. **(B-D)** Design, scanning electron microscopy (SEM) and dynamic light scattering (DLS) of rCaP **(B)**, rCaP-p30 **(C)** and rCaP-CpG **(D)** nanoparticles. The syntheses and experiments were performed by Dr. Leonardo Rojas-Sánchez. Modified from Damm *et al.*, (2019).

The physicochemical characterization data of rCaPs collected by Dr. Leonardo Rojas-Sánchez is listed in Table 1. The solid core diameters and zetapotentials of functionalized rCaPs ranged from 45 – 57 nm and +20 - +27 mV. Endotoxin levels in the preparations were below detection range. Average numbers

of coupled Env-His_8 molecules per particle were 942 for rCaP, 655 for rCaP-p30 and 1965 for rCaP-CpG. Furthermore, an average of 3.2 x 10^4 p30 peptides and 2.0 x 10^4 CpG molecules were encapsulated per nanoparticle. The polydispersity indices (PdIs) of all nanoparticle batches ranged from 0.38 - 0.43 assuming a homogenous particle population. The hydrodynamic diameters ranged from 312 nm - 411 nm. The coupling efficiency was defined by using an AlexaFluor®-488-labeled Env-His_8 for functionalization via sulfo-SMCC. Here, the reaction yield was determined to be 85 % according to UV-Vis-spectroscopy. This factor was then assumed for the calculation of successfully coupled Env trimers in further reactions under equivalent conditions with unlabeled protein. Moreover, the Env concentration in the coupling reaction vessel was measured by NanoDrop before the addition and after the pelletizing of the nanoparticles and the differences were used to calculate the coupling efficiency.

Table 1) Physicochemical characterization data of rCaPs

Sample	CaP	rCaP	rCaP-p30	rCaP-CpG
Solid core diameter / nm	38	45	45	57
N (Env-His_8) per NP	−	865	710	1950
N (Env-His_8) per NP (Nanodrop)		1020	600	1980
N (adjuvant) per NP	−	−	p30: 3.2×10^4	CpG: 2.0×10^4
Hydrodynamic diameter by DLS / nm (*z*-average)	312	411	386	362
PdI by DLS	0.31	0.43	0.41	0.38
Zeta potential / mV	+27	+20	+23	+27
Endotoxins / EU mL^{-1}	<0.1	<0.1	<0.1	<0.1

2.1.2. Functional characterization of T helper calcium phosphate nanoparticles

A previous study has shown that CaPs functionalized with HEL as a model antigen were superior over soluble HEL proteins in the dose-dependent activation of antigen-specific B cells *in vitro* [125]. The recent generation of B cell-receptor transgenic mouse strains expressing broadly-neutralizing Env antibodies as IgMs on the majority of the naïve B cell repertoire paved the way to do such functional experiments in the context of Env-coupled nanoparticles [113,231–233]. Splenic B cells from wildtype (*wt* B cells) and PGT121 B cell receptor-transgenic mice (PGT121 B cells) were purified and incubated overnight in the presence of rCaP or Env-His_8 dilutions (200 – 8 ng/mL bulk Env). Additional cells were mock-treated as a negative control or incubated in the presence of either Env-VLPs or LPS as positive controls for BCR-specific or polyclonal B cell activation, respectively. The cells were then stained with both B cell and early activation markers for subsequent FACS analysis (Fig. 8). rCaPs presenting an array of Env trimers on the surface were able to induce PGT121 B cell activation more efficiently in a dose-dependent manner than soluble Env-His_8 alone as judged by the upregulation of early activation marker CD69. B cell activation rates with the lowest particle concentration (8 ng/mL Env) were in the same range as those with the highest concentration (200 ng/mL) of soluble trimer (18 % vs. 21 %). At 200 ng/mL bulk Env concentration, the percentage of activated PGT121 B cells incubated with rCaPs were in a comparable range to those incubated with Env-VLPs (70 % vs. 84 %). Notably, as expected, neither rCaPs nor Env-His_8 could induce activation of *wt* B cells, which were always at the background level of the unstimulated negative controls. Nevertheless, the functional activity of the *wt* B cells was proven by polyclonal LPS stimulation.

This experiment demonstrated that Env-specific BCRs can recognize Env trimers that were randomly coupled to the surface of CaPs and that these rCaP nanoparticles were capable to induce the BCR-dependent activation of naïve B cells at a high rate in contrast to soluble HIV-1 Env trimers.

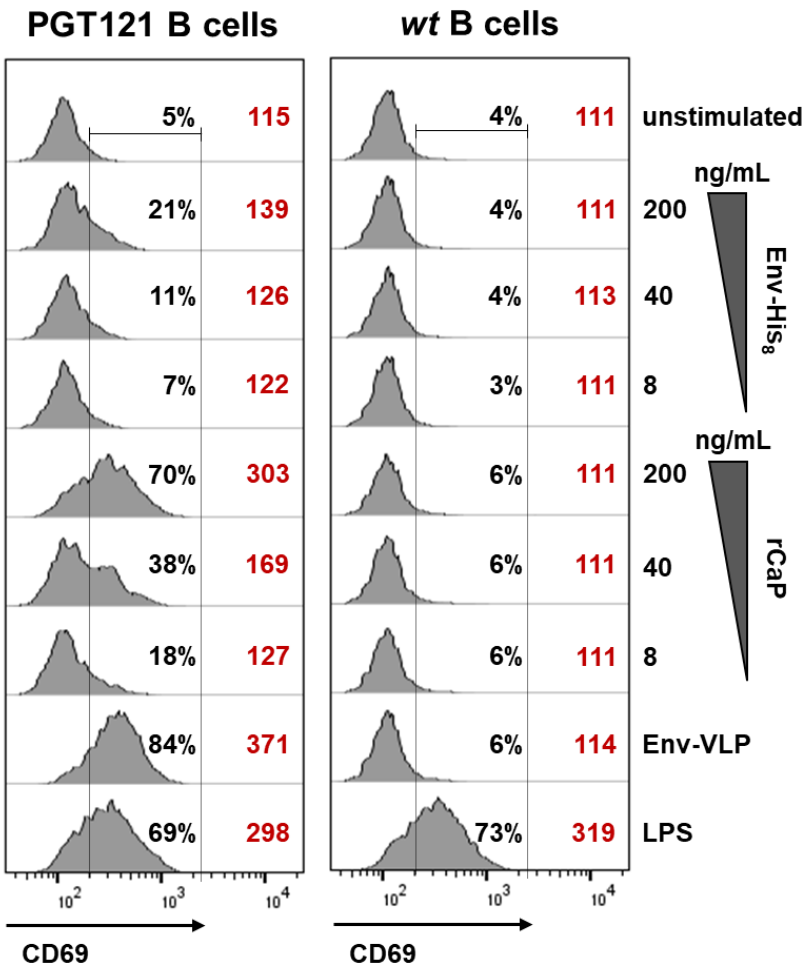

Figure 8) *In vitro* activation of naïve B cells by rCaPs

Naïve B cells were isolated from the spleens of *wt* and PGT121 B cell receptor-transgenic mice (*wt* / PGT121 B cells) and incubated overnight with dilutions of rCaPs or soluble Env-His_8 proteins normalized to the bulk concentration of Env (200 – 8 ng/mL). Controls were either unstimulated or incubated in the presence of Env-VLPs (200 ng/mL bulk Env) or LPS (2 µg/mL). After 18 h, the cells were stained with both a B cell (anti-CD19) and an early activation marker (anti-CD69) as well as with a viability dye and analyzed by flow cytometry. Shown are the histograms for CD69 expression on the surface of living, CD19+ cells. The percentage of gated CD69-expressing cells and the CD69 median fluorescence intensity (dark red) are given in numbers beside the histograms. The experiment was independently conducted four times with similar results. Modified from Damm *et al.*, (2019).

2.1.3. Modulation of the immune response against HIV-1 with T helper calcium phosphate nanoparticles

The induction of ISH with lentiviral VLPs that incorporated heterologous T helper cell epitopes has been thoroughly evaluated in the past [224,225]. VLPs are an optimal model for preclinical trials due to their self-adjuvanting character and mimicking of the viral pathogen. T helper VLPs, however, are not quite suitable for clinical application in terms of scalability and purification costs [89]. Synthetic nanoparticles represent a possible alternative. The *in vivo* induction of ISH with synthetic T helper liposomes has been demonstrated lately [227]. As a *proof-of-principle* trial with inorganic CaPs, mice were intramuscularly immunized with the licensed Tetanus vaccine Tetanol®pur in week 0 and week 4 and then boosted thrice with rCaP-p30 in week 8, 12 and 16. Control groups were either mock-primed or boosted with rCaPs lacking p30 epitopes or Env-VLP-p30 (Fig. 9 A). The immunization doses were normalized to a total of 10 µg Env per mouse. The humoral immune response was analyzed in week 18. Immunizations with rCaPs alone induced a weak anti-Env IgG1 humoral immune response that was not significantly different from the naïve group (Fig. 9 B, naïve vs. rCaP). In contrast, immunization of mice with T helper CaPs alone significantly increased the magnitude of the Env-specific IgG1 response (Fig 9 B, rCaP-p30 vs. rCaP). However, the IgG2c response in this group was unaffected (Fig 9 C, rCaP-p30 vs. rCaP). The induction of ISH by harnessing previously induced p30-specific T cell responses to provide help for Env-specific B cells upon nanoparticle application further improved the anti-Env IgG1 response more than a ten-fold (Fig 9 B, rCaP-p30 (ISH) vs. rCaP-p30). This group also demonstrated significantly elevated anti-Env IgG2c levels compared to the naïve group (Fig 9 C, rCaP-p30 (ISH) vs. naïve). Tetanus-mediated ISH was further induced using lentiviral T helper VLPs as a positive control (Fig. 9 B-C, Env-VLP-p30 (ISH) vs. Env-VLP-p30), which resulted in significantly elevated anti-Env IgG subtype levels and reproduced previously published results [224]. Importantly, the strength of the ISH effects was comparably high between T helper CaPs and VLPs (Fig. 9 B-C, rCaP-p30 (ISH) vs. Env-VLP-p30 (ISH)). In general, the Env-specific subtype responses were strongly IgG1-dominated throughout all groups in this experiment and correlated with the results of the p30-specific CD4+ T cell cytokine profiling. For this, isolated splenocytes from immunized mice were stimulated with soluble p30 peptide *in vitro* for the

reactivation of p30-specific CD4+ T cells. The cytokine profile was evaluated by intracellular cytokine staining (ICS) of cells as well as ELISA with conditioned cell supernatants. Even though the CaP-related ISH group had the highest levels of Th1 cytokines IFN-γ and TNF-α, those were not significantly different from the control groups (Fig. 9 D-E). On the contrary, the Th2 cytokine IL-5 was strongly expressed only in the ISH group (Fig. 9 F).

Taken together, based on these results, T helper CaPs elicited the modulation of Env-specific humoral immune responses in a comparably effective and phenotypic manner than previously utilized T helper VLPs.

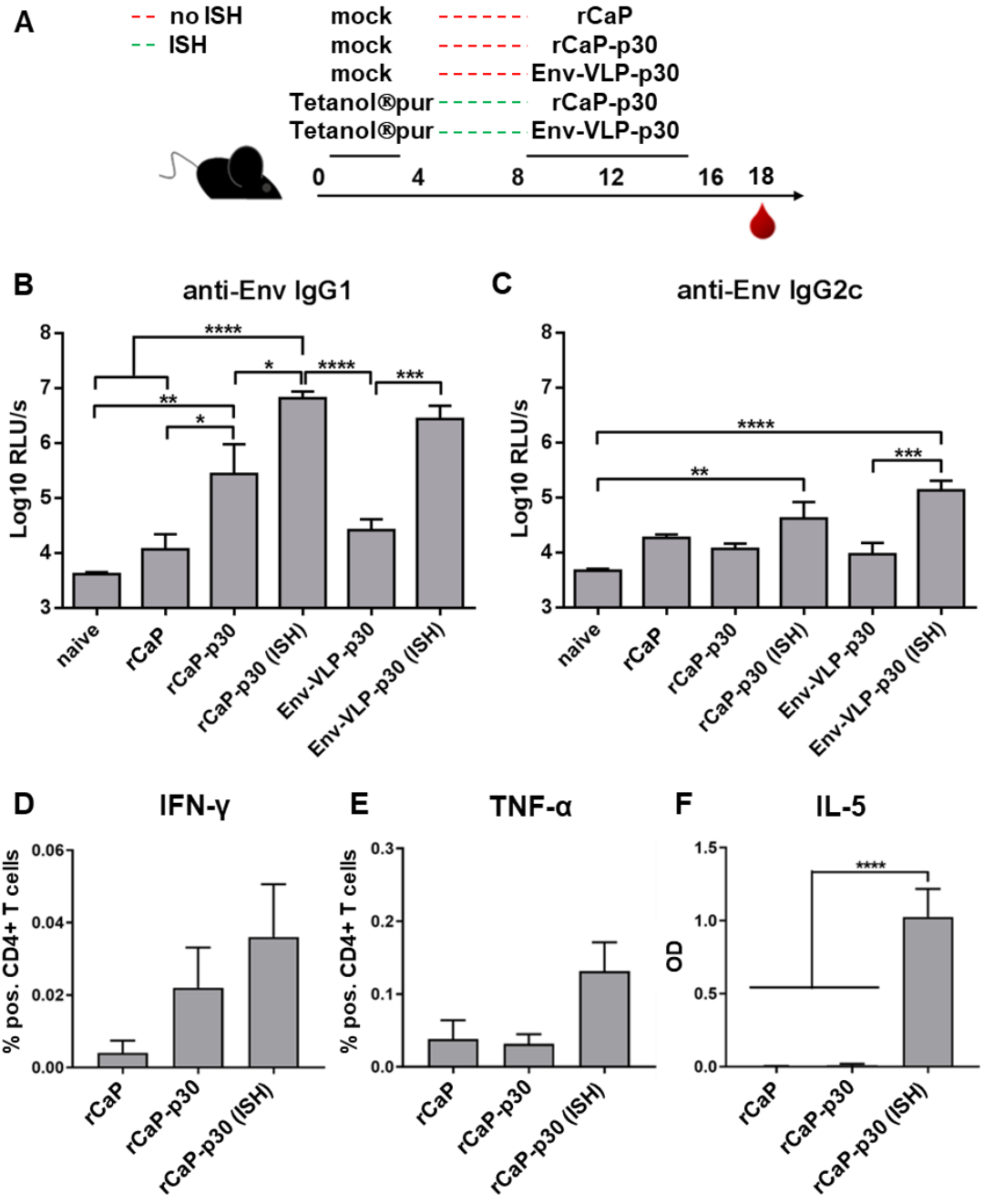

Figure 9) Induction of intrastructural help with T helper CaPs

(A) Immunization schedule. C57bl/6NRj mice were immunized with either PBS/O (mock) or a 1:10 dilution of the licensed Tetanus vaccine Tetanol®pur in week 0 and week 4. The animals were boosted three times in week 8, 12 and 16 with rCaP, rCaP-p30 or Env-VLP-p30. Blood was taken in week 18 for the analysis of humoral immune responses. Prime/boost combinations resulting in the induction of ISH or no ISH are indicated with green or red dashed lines, respectively. **(B-C)** Anti-Env IgG1 **(B)** and IgG2c **(C)** humoral immune responses analyzed in week 18 from the sera of immunized mice. Shown are the logarithmic values of the relative light units per second (Log10 RLU/s). The x-axes outline the prime/boost combinations of the different groups. **(D-E)** Percentage of p30-restimulated CD4+ T helper cells with intracellular secretion of Th1 cytokines IFN-γ **(D)** and TNF-α **(E)** from the spleens of immunized mice. **(F)** Optical density (OD) values of Th2 cytokine IL-5 secretion in the conditioned supernatants from p30-restimulated splenocytes as determined by ELISA. The values of the unstimulated control cultures were subtracted. The columns in all experiments represent the mean values of six mice ± SEM. * $p < 0.05$; ** $p < 0.001$; *** $p < 0.0005$; **** $p < 0.0001$; one-way ANOVA with Tukey's multiple comparison post-hoc test. Modified from Damm *et al.*, (2019).

2.1.4. Substitution of adjuvant effects by intrastructural help

The aim of harnessing ISH in experimental vaccine settings is to increase immunoglobulin levels specific for the target antigen and to influence the IgG subtype distribution [221,222,224,225]. Since these are characteristics of common adjuvants, ISH might enable adjuvant-free vaccination regimens without the loss of immunomodulatory effects. In order to test this hypothesis, the CaP-related ISH group was compared with an additional group of mice immunized with rCaPs that incorporated clinically approved CpG 1018 [234] molecules after two Tetanol®pur primes (rCaP-CpG; Fig10 A). In fact, both groups demonstrated equally high anti-Env total IgG levels (Fig.10 B). Nevertheless, the IgG subtype distribution was different. Tetanus-mediated ISH induced an IgG1-dominated response, whereas CpG is a well-characterized driver of IgG2c (Fig. 10 C) [104,235,236]. In summary, this experiment demonstrated that ISH-related immunization without additional adjuvants can increase the magnitude of the total humoral immune response in the same range as comparable, adjuvanted immunizations.

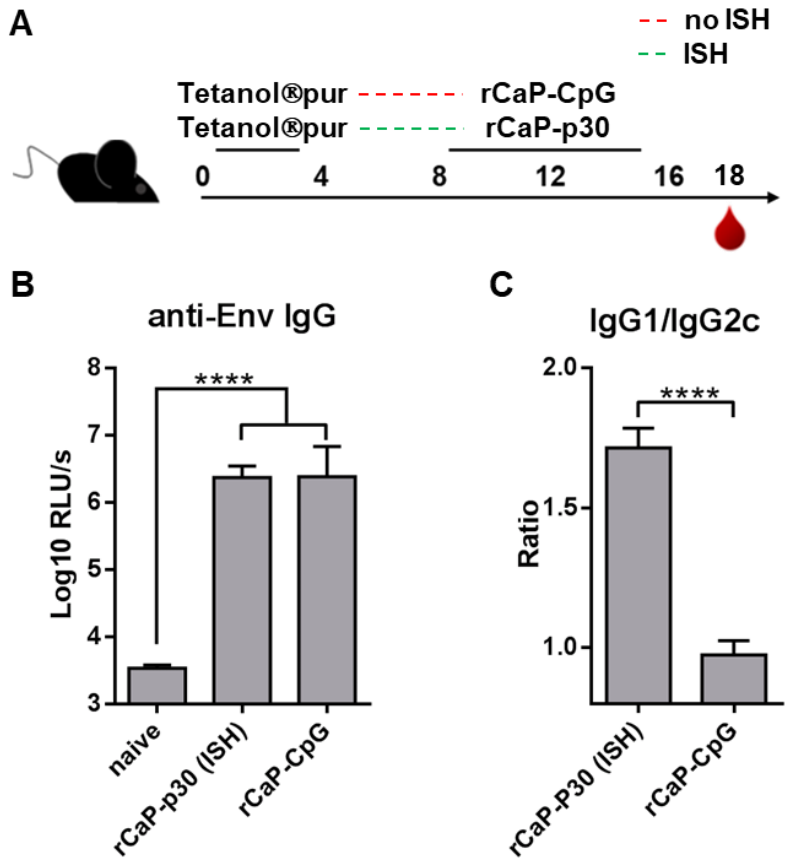

Figure 10) Substitution of adjuvant effects by intrastructural help

(A) An additional group of C57bl/6NRj mice was primed twice with Tetanol®pur and boosted with CpG-adjuvanted CaPs (rCaP-CpG) to compare heterologous ISH and CpG adjuvantation. **(B)** Total anti-Env IgG levels of ISH- and CpG-adjuvanted groups as measured by serum ELISA. The columns depict the mean Log10 RLU/s values of six animals ± SEM. **** $p < 0.0001$; one-way ANOVA with Tukey's multiple comparison post-hoc test. **(C)** Anti-Env IgG1/IgG2c ratio in individual mice from the same groups. The columns represent the mean values of six mice ± SEM. **** $p < 0.0001$; unpaired student t-test. Modified from Damm *et al.*, (2019).

2.1.5. Avoidance of the induction of HIV-specific CD4+ T cell responses by intrastructural help

Previously, it was reported that vaccine-induced HIV-specific T cells correlate with an increased risk of infection [213,214,216]. Since Env-specific B cells receive rapid help from heterologous, non-HIV T cells in an ISH setting (Elsayed *et al.*, Fig. 4 [224]), the formation of HIV-specific T cells might be impeded in this immunization context. In order to test this hypothesis, the splenocytes from immunized mice were additionally restimulated with Env epitopes. Since no

ubiquitous MHC-II-restricted Env peptide is described in the literature, a CD4+ T cell restimulation protocol based on the unique capacities of naïve B cells to process proteins from cognate VLPs and present them on MHC-II molecules (Kolenbrander *et al.*, Fig. 2 [237]) was designed and applied within this thesis. Instead of incubating cells with soluble peptides, Env-specific PGT121 B cells were incubated with lentiviral Env-VLPs in a first step. Once the B cells have taken up the VLPs in a BCR-dependent manner and have presented a complete repertoire of naturally processed Env peptides on MHC-II molecules, they were co-cultured overnight with Brefeldin-treated splenocytes from immunized mice in week 18 (Fig. 11 A). The cells were stained for CD4 surface marker and intracellularly for Th1 pro-inflammatory cytokines TNF-α, IL-2 and IFN-γ (Fig. 11 B-D). Despite the equally strong induction of anti-Env total IgG levels in both ISH- and CpG-adjuvanted groups (Fig. 10 B), a highly significant induction of Env-specific, Th1 cytokine-secreting CD4+ T cells was only detectable in the rCaP-CpG group. The ISH mice as well as the mice that received rCaP and rCaP-p30 without ISH showed a background level of such T cells, even though these groups had significantly different Env-specific IgG1 levels. Thus, ISH has increased Env-specific antibody response without the induction of Env-specific T helper cells.

Taken together, this data clearly indicated that rCaP-mediated ISH i) can act as a substitute for adjuvant reagents by induction of comparable humoral immune response levels whereas it ii) avoids the induction of HIV-specific CD4+ T cells, which are suspected to increase the susceptibility for HIV infection.

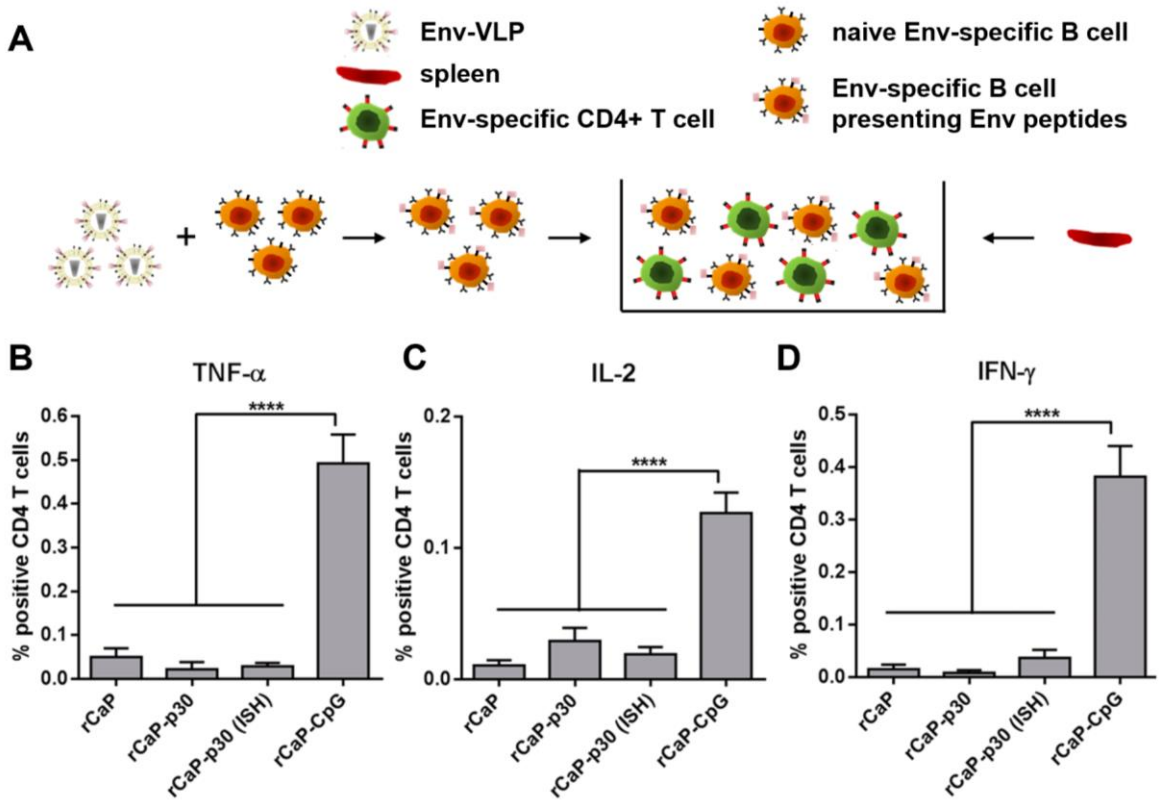

Figure 11) Impeded induction of HIV-specific T cells in ISH mice

(A) Restimulation of splenocytes from immunized mice with VLP-activated cognate B cells displaying naturally processed Env peptides on MHC-II molecules. PGT121 B cells (orange) were incubated with lentiviral Env-VLPs (left). In parallel, spleens were isolated from mice immunized with different immunization schedules. The purified splenocytes represented by the target CD4+ T cells (green) were then incubated with the Env peptide-presenting B cells. **(B-D)** Intracellular cytokine staining of restimulated Env-specific CD4+ T cells. Restimulated splenocytes were stained for CD4 surface marker as well as for intracellular Th1 cytokines TNF-α **(B)**, IL-2 **(C)** and IFN-γ **(D)**. The percentage of cytokine-producing CD4+ T cells among immunization groups is shown in columns representing the mean values of six mice ± SEM. The values of the unstimulated control cultures were subtracted. **** $p < 0.0001$; one-way ANOVA with Tukey's multiple comparison post-hoc test. Modified from Damm *et al.*, (2019).

In total, inorganic T helper CaPs functionalized with Env trimers and incorporating non-HIV epitopes represent a suitable replacement for lentiviral T helper VLPs used in former ISH immunization approaches established for preclinical HIV vaccine trials. In mice, CaP-mediated ISH improved Env-specific antibody levels without additional induction of HIV-specific T helper cells. Therefore, these synthetic nanoparticles are an advantageous delivery platform that may be further modified for future clinical, immunomodulatory vaccine trials.

2.2. Improvement of vaccine design by orthogonal Env conjugation via genetically encoded aldehyde-tags

Native-like, soluble Env trimers are covered by a dense glycan shield except for the C-terminal domains of the gp41 ectodomain. This non-glycosylated trimer base contains immunodominant epitopes that drive non-neutralizing humoral immune responses [48]. In theory, the random coupling of Env trimers by sulfo-SMCC crosslinkers does not occlude these epitopes on the nanoparticle surface [109,113,137,149]. Furthermore, the unspecific targeting and binding of primary amines may degrade the conformational state of the trimer [238]. Thus, the immune response is likely to be biased by the non-neutralizing base epitopes and broadly neutralizing responses against conformational epitopes may be diminished. Current state-of-the-art coupling mechanisms for nanoparticle functionalization comprise orthogonal, site-directed binding strategies to mask the trimer base. In the course of this study, a previously described, post-translationally modified tag (aldehyde-tag, LCTPSR) was introduced at the C-terminus of Env (Env-Ald_6) and used for the covalent oxime ligation with an aminooxy- and alkyne-terminated crosslinker (Step-one; Fig. 12). The resulting linker-bound Env trimers (lnkr-Env) were then conjugated with azide-functionalized CaPs by azide-alkyne cycloaddition (Step-two; click reaction) to ultimately obtain orthogonally coupled CaPs (oCaPs; Fig 12). The mechanistical and functional characterization of the coupling mechanism and the oCaPs in comparison to rCaPs was a main part of this thesis and is described below.

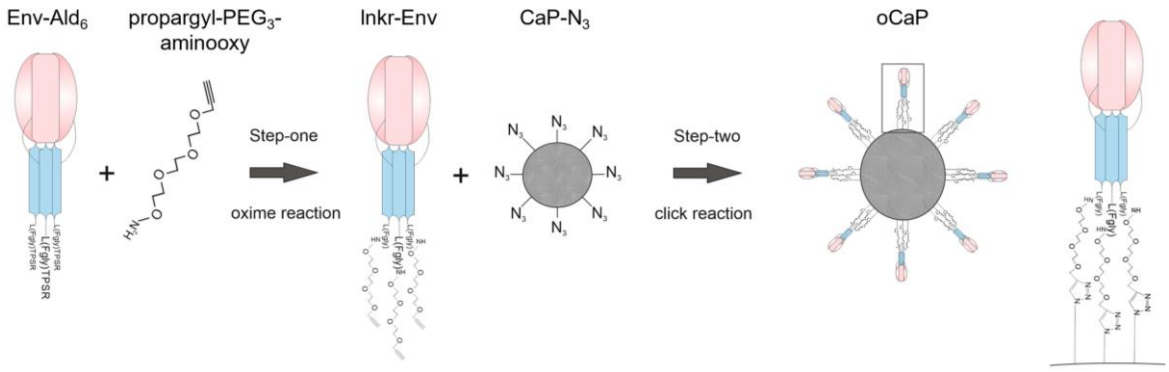

Figure 12) Overview of the orthogonal coupling mechanism

The site-directed coupling of Env trimers to the surface of CaPs comprises two major reaction steps. An oxime ligation (Step-one) of aldehyde-tagged Env trimers (Env-Ald$_6$) with propargyl-PEG$_3$-aminooxy linkers results in linker-bound Env (lnkr-Env). A subsequent click reaction (Step-two) with azide-functionalized CaPs (CaP-N$_3$) finally leads to the generation of CaPs orthogonally conjugated with Env (oCaPs). Modified from Damm *et al.*, (2022).

2.2.1. Expression of Env trimers with a C-terminal aldehyde-tag

In a first step, the C-terminal 8x His-tag in Env-His$_8$ was replaced by the aldehyde-tag 6-mer sequence (Ald$_6$; LCTPSR [166]) derived from *Homo Sapiens* arylsulfatase E via mutagenesis PCR [161]. The cysteine in this amino acid motif is post-translationally converted into aldehyde-bearing formylglycine (Fgly) by formylglycine-generating enzyme (FGE). The nucleotide triplets in the corresponding plasmid pBG505-NFL-gp140-Ald$_6$ were optimized for human codon usage (Fig. 13 A) to improve the expression in the human HEK293F producer cell line. The cells were then either transfected with pBG505-NFL-gp140-Ald$_6$ alone or co-transfected with pBG505-NFL-gp140-Ald$_6$ and pcDNA3.1-hFGE to have the formylglycine conversion done by endogenous FGE only (Env-Ald$_6$) or by additional overexpression of the enzyme (Env-Ald$_6$/FGE; Fig. 13 B), respectively. As a negative control, Env-His$_8$ was expressed in parallel by transfection of HEK293F cells with pBG505-NFL-gp140-His. The secreted Env trimers were purified from the cell supernatants by Lectin affinity chromatography and subsequently concentrated by ultrafiltration. Based on the transfection regimen, Env trimers with i) three His-tags (Env-His$_8$), or ii) endogenously converted aldehyde-tags (Env-Ald$_6$) and iii) pro-actively converted aldehyde-tags (Env-Ald$_6$/FGE) with unknown ratios of converted (L[Fgly]TPSR) and unconverted (LCTPSR) cysteine/Fgly residues were produced for further experimental steps (Fig. 13 C). A reducing SDS-PAGE and Western Blot

of all proteins in comparison to a size-exclusion purified reference BG505 trimer (Ref.) using polyclonal anti-Env antibodies for detection was performed to explore, whether the presence of the aldehyde-tag alters the antigenicity of Env (Fig. 13 D). Furthermore, NativePAGE with subsequent silver stain revealed that, despite the purification by affinity chromatography only, the majority of proteins were in a trimeric conformation with minimal dimer, monomer and aggregate side products (Fig. 13 E). However, the percentage of aggregates varied strongly between different production batches.

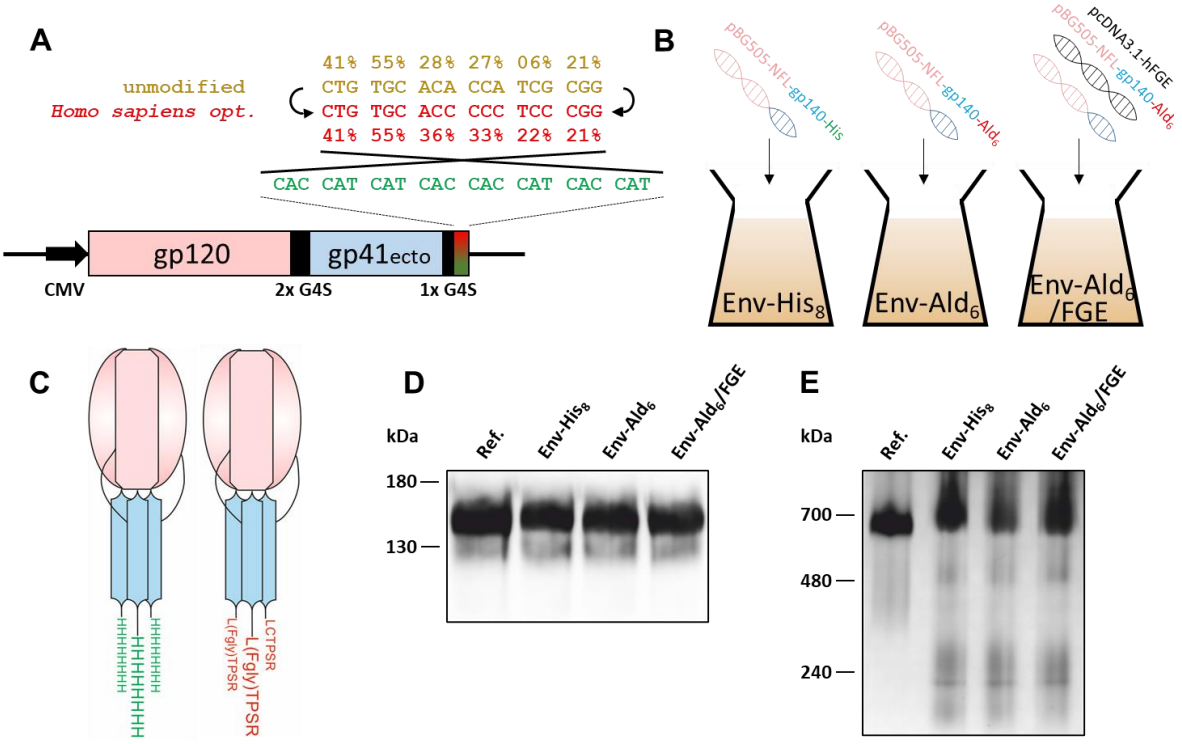

Figure 13) Aldehyde-tag introduction and protein analysis

(A) Introduction of a codon-optimized aldehyde-tag sequence at the C-terminus of Env. The 8x His-tag (green) was replaced by the aldehyde-tag via mutagenesis PCR. The nucleotide sequence derived from human arylsulfatase E (yellow) was modified according to the human codon usage (red). The frequency for each amino acid-coding triplet in humans is given in %. **(B)** Three different transfections of HEK293F producer cells were performed: i) With pBG505-NFL-gp140-His for the expression of Env-His_8, ii) with pBG505-NFL-gp140-Ald_6 alone or iii) in combination with pcDNA3.1-hFGE for the production of aldehyde-tagged trimers Env-Ald_6 and Env-Ald_6/FGE, respectively. **(C)** Purified His-tagged (left) and aldehyde-tagged (right) Env trimers. A 2x G_4S linker covalently connects the globular gp120 subunits (pink) with the gp41 ectodomains (blue) and another 1x G_4S linker is located between $gp41_{ecto}$ and the respective C-terminal tag. **(D)** SDS-PAGE / Western Blot and **(E)** NativePAGE / silver stain of purified Env trimers in comparison to a size-exclusion purified BG505 reference trimer (Ref.). Modified from Damm *et al.*, (2022).

2.2.2. Mass spectrometry analysis of the formylglycine conversion rate

In order to define the percentage of Fgly conversion in Env-Ald$_6$ and Env-Ald$_6$/FGE, both proteins were analyzed by mass spectrometry. Samples were measured and data was evaluated by PD Dr. Sabrina Gensberger-Reigl (Institut für Chemie und Pharmazie, Friedrich-Alexander-Universität Erlangen-Nürnberg, Erlangen, Germany). Since Env consists of approximately 50 % glycosylation by weight [24], the proteins were initially deglycosylated with glycerol-free PNGase F. However, the enzyme could not be quantitatively removed from the deglycosylated Env proteins by ultrafiltration and, thus, caused high background and signal distraction during mass spectrometry (data not shown). Since the amino acid sequence of interest is at the naturally non-glycosylated C-terminus of the protein, mass spectrometry analysis was performed with untreated Env-Ald$_6$ and Env-Ald$_6$/FGE. Following Glu-C digestion, the unconverted aldehyde-tag sequence E.QDLLALDGGGGSLC(+57.02)TPSR (theoretical m/z: 908.9466; measured m/z: 908.9463) was detected in both samples indicating the successful replacement of the 8x His-tag (Fig. 14 A). Importantly, the converted sequence E.QDLLALDGGGGSL(Fgly)TPSR was also verified in both Env-Ald$_6$ (theoretical m/z: 871.4394; measured m/z: 871.4370) and Env-Ald$_6$/FGE (theoretical m/z: 871.4394; measured m/z: 871.4379), which proved the post-translational conversion (Fig. 14 B-C). Furthermore, as expected, the Fgly residue was observed to be partly hydrated and, thus, formed a geminal diol (theoretical m/z: 880.4447; measured m/z: 880.4432). The product ion spectra included almost the complete b- and y-ion series of the peptide sequences of interest (Fig. 14 D-F).

Based on data calculations using a formula described by Rabuka *et al.* [167], the Fgly conversion by endogenous FGE alone (Env-Ald$_6$) was 7 %, whereas 42 % of former cysteine residues were converted in the FGE overexpression system (Env-Ald$_6$/FGE). This data unequivocally proved the presence of recombinantly introduced aldehydes in Env-Ald$_6$ and Env-Ald$_6$/FGE and indicated that FGE overexpression is recommendable for a quantitative Fgly conversion.

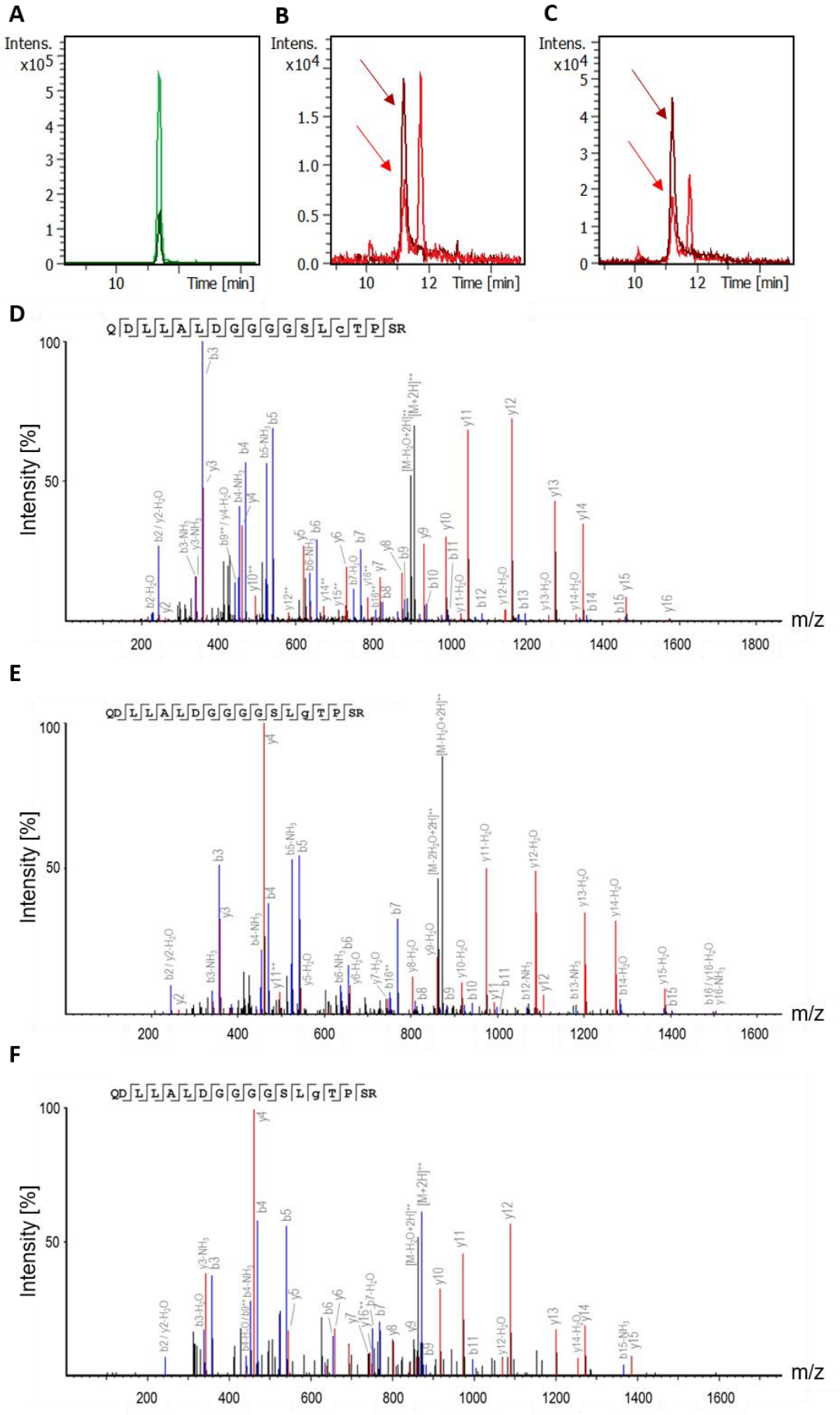
A
B
C
Intens.
x10^5
x10^4
Time [min]
D
E
F
Intensity [%]
m/z
Q[D][L][L][A][L][D][G][G][G][G][S][L][c][T][P][SR]
Q[D][L][L][A][L][D][G][G][G][G][S][L][q][T][P][SR]

Figure 14) Mass spectrometry analysis of the formylglycine conversion rate

All data was measured and evaluated by PD Dr. Sabrina Gensberger-Reigl. **(A)** Extracted ion chromatograms of the unconverted aldehyde-tag (m/z 908.947 ± 0.015; LC(+57.02)TPSR) in Env-Ald_6 (light green) and Env-Ald_6/FGE (dark green). **(B-C)** Extracted ion chromatograms of the converted aldehyde-tag in the $Fgly_{aldehyde}$ state (light red; m/z 871.439 ± 0.015) and the $Fgly_{diol}$ state (dark red; m/z 880.445 ± 0.015) in Env-Ald_6 **(B)** and Env-Ald_6/FGE **(C)**. **(D-F)** Identification of the respective peptide sequences via their precursor product ion spectra: m/z 908.9 for LC(+57.02)TPSR **(D)**, m/z 880.4 for $Fgly_{diol}$ **(E)** and m/z 871.4 for $Fgly_{aldehyde}$ **(F)**. The characteristic b- and y-ions are indicated in blue (b-ions) and red (y-ions). Modifications of cysteine (carbamidomethylation) or formylglycine ($Fgly_{aldehyde}$, $Fgly_{diol}$) are notificated with small letters in the fragmentation pattern. Adapted from Damm *et al.*, (2022).

2.2.3. Specificity and efficiency of oxime ligations with aldehyde-tagged Env

Reporter assays were performed to evaluate the specificity of the oxime ligation for the genetically introduced C-terminal aldehyde-tag as well as the efficiency of the reaction. For specificity evaluation, purified His- and aldehyde-tagged Env trimers were incubated with an aminooxy-dye (AlexaFluor®-647-hydroxylamine) under previously published optimized oxime ligation conditions (6 h, 37°C, pH 4.5) [166]. The reactions were loaded on a 10 % acrylamide gel and separated by SDS-PAGE. Fluorescent bands were detected via gel imaging under red light exposure (Fig. 15 A). As expected, the reporter dye reacted in a highly specific manner with aldehyde-tagged Env trimers as seen by fluorescent signals at 140 kDa. Furthermore, the signal intensity was stronger with Env-Ald_6/FGE indicating an improved binding, when the Fgly conversion rate was increased by FGE overexpression. Nevertheless, a weak fluorescent signal with Env-His_8 hinted at a neglectable binding of aminooxy-dye to other potentially reactive moieties on Env. As a control, no signal was detected in the reaction without aminooxy-dye.

Even though this reporter assay has proven that aldehyde-tagged Env trimers were specific targets for aminooxy reagents, it did not allow to evaluate the percentage of Env-Ald_6 and Env-Ald_6/FGE that successfully reacted with the dye. Thus, in order to address the efficiency of the oxime ligation, Env-His_8, Env-Ald_6 and Env-Ald_6/FGE were incubated with a 40 kDa aminooxy-$PEG_{[n]}$ gel shift linker (GSL) under above mentioned conditions. Reactions without GSL were performed as control. The different samples were slowly separated by SDS-PAGE using 8 %

acrylamide gels to avoid any disturbances of the gel matrix by an excess of the rigid GSL. Western Blot was performed subsequently. Notably, only aldehyde-tagged Env trimers strongly reacted with the GSL resulting in prominently shifted Western Blot bands (Fig. 15 B). This shift was not seen with Env-His_8 or when no GSL was included in the reaction. AIDA signal quantification analysis of the shifted and non-shifted bands revealed that 71.8 % of Env-Ald_6 and 92.2 % of Env-Ald_6/FGE bound to the GSL, whereas only 0.5 % of Env-His_8 has successfully reacted, which is in line with the weak background signal in the fluorescent reporter assay (Fig. 15 A). Thus, in summary, these data have shown that the oxime ligation with aldehyde-tagged Env trimers was specific and highly efficient. Importantly, as expected, the improved Fgly conversion by FGE overexpression (Env-Ald_6/FGE) resulted in stronger binding signals compared to Env-Ald_6.

Recombinant native-like Env trimers were repeatedly shown to be conformationally stable up to 62.5°C as well as after numerous freeze/thaw cycles [53,76]. However, detailed studies about pH sensitivity are rare. The maintenance of the native-like trimer conformation during and after the coupling procedure is most crucial for the qualitative competition with other state-of-the-art coupling mechanisms. Thus, any negative effects of low acidic oxime reaction environment on the Env conformation had to be excluded, before the project could be continued. To this end, Env-His_8 was incubated under oxime ligation conditions with binding buffers adjusted to pH 4.5 or pH 3.0. As a control, one sample remained in PBS/O at pH 7.0. In the following, all samples were adjusted to pH 7.0 using PBS/O and immobilized on anti-His antibody-coated ELISA plates, which were then stained with serial dilutions of trimer-specific apex antibodies PG9, PG16 and PGT145 as well as glycan-specific antibody 2G12 (Fig. 15 C). Binding curves for all antibodies were in a comparable range for pH 4.5- and pH 7.0-treated Env trimers. In contrast, pH 3.0 treatment resulted in a significant loss of antibody binding. Moreover, the conformational ELISA assay was used to evaluate, whether lyophilization and reconstitution have negative effects on the Env trimer conformation. Here, binding of PG16, PGT145 and 2G12 were unaffected, whereas PG9 binding was reduced about half (data not shown). In summary, these experiments have proven that the native-like conformation of stabilized Env trimers is negatively affected by a highly acidic environment, but not under oxime ligation conditions at pH 4.5. This finding was decisive for the whole aldehyde-mediated coupling mechanism.

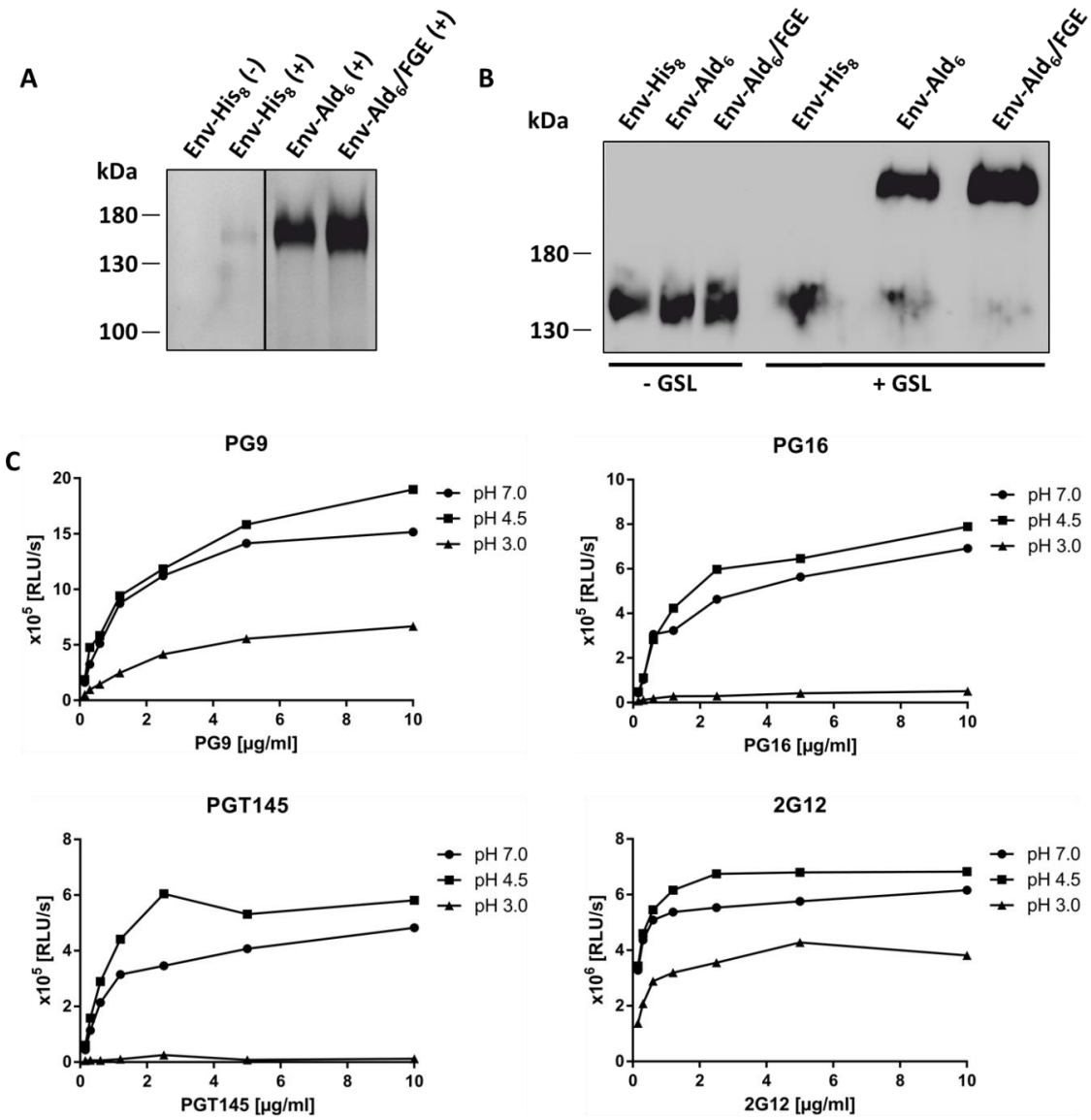

Figure 15) Oxime ligation reporter assays

(A) Oxime reaction with an aminooxy-dye. Env-His_8, Env-Ald_6 and Env-Ald_6/FGE were incubated for 6 h at 37°C and pH 4.5 in the presence (+) or absence (-) of AlexaFluor®-647-hydroxylamine. The covalent reaction was analyzed by reducing SDS-PAGE and fluorescent gel imaging. **(B)** Gel shift. Aldehyde- and His-tagged Env trimers were incubated in the presence (+ GSL) or absence (- GSL) of a 40 kDa aminooxy-$PEG_{[n]}$ gel shift linker under oxime ligation conditions. The reactions were separated on an 8 % SDS gel at low voltage. Western Blot was performed afterwards. **(C)** Conformational ELISA. His-tagged Env trimers were incubated overnight in low acidic (pH 4.5), highly acidic (pH 3.0) or neutral (pH 7.0) environment. All samples were adjusted to pH 7.0 afterwards. A conformational sandwich ELISA was then performed on opaque high-binding plates coated with anti-His antibody and detected with trimer-specific antibodies (PG9, PG16, PGT145) and glycan antibody 2G12 in serial dilutions as well as anti-human-HRP secondary antibody. The ECL-induced relative light units per second (RLU/s) were measured with a photometer. One representative ELISA out of three independent experiments with comparable results is shown. Modified from Damm *et al.*, (2022).

2.2.4. Evaluation of a two-step conjugation mechanism

Despite the stability of native-like Env in a low acidic environment, calcium phosphate nanoparticles would dissociate at pH 4.5. As a consequence, oxime ligations of aldehyde-tagged Env with aminooxy-functionalized CaPs were not feasible and, thus, this circumstance had to be bypassed via a two-step coupling mechanism (Fig. 12; Fig. 16 A).

As a first reaction, purified Env trimers were conjugated with a bi-specific linker molecule, propargyl-PEG_3-aminooxy, to generate linker-bound Env (Step-one; oxime ligation). These modified proteins (lnkr-Env) with linker-associated terminal alkyne groups at the C-termini could then be used for copper-catalyzed azide-alkyne cycloadditions with azide-functionalized CaPs (Step-two; click reaction) or an azide-conjugated dye in terms of a click reaction reporter assay (Fig. 16 A). For the latter, oxime ligations with all purified Env trimers in the presence of different concentrations (125 µM, 250 µM, 500 µM) of propargyl-PEG_3-aminooxy linker were performed as a first step. The ligation mixtures were then directly put into click reactions with AlexaFluor®-488-azide. This reporter assay was done to evaluate the efficiency of the click reaction and to define the optimal stoichiometry between linker molecules and Env trimers. Since oxime ligations were performed in lab scale for this study, lnkr-Env could not be properly purified afterwards and, thus, excessive propargyl-PEG_3-aminooxy molecules would compete with lnkr-Env for the click reaction with terminal azide groups. As a consequence, a linker concentration that allowed maximal efficiency and minimal binding competition would be the best compromise. The completed click reactions with AlexaFluor®-488-azide were analyzed via fluorescent SDS-PAGE. To this end, after protein separation, the gels were evaluated under blue light exposure (Fig. 16 B). Click reactions with lnkr-(Env-Ald_6) resulted in strong fluorescent signals. In comparison, the signal intensity was clearly increased with lnkr-(Env-Ald_6/FGE) as expected. Interestingly, two-step coupling reactions of aldehyde-tagged Env with 125 µM propargyl-PEG_3-aminooxy linker showed the strongest binding signals indicating the most favorable stoichiometry between the oxime ligation binding partners. Reactions with 250 µM linker already resulted in severely diminished binding signals (Fig. 16 B), whereas reactions with 500 µM linker did not result in fluorescent gel bands at all (data not shown). Thus, a linker concentration of 125 µM was

chosen for the subsequent nanoparticle coupling reactions. The absence of fluorescent signals in reactions including Env-His_8 in the presence of propargyl-PEG_3-aminooxy linker or Env-Ald_6/FGE in the absence of linker proves the high specificity of the click reaction for linker-bound, aldehyde-tagged Env trimers. On another note, this reporter assay was not only done for evaluation of the click reaction efficiency alone, but additionally prove a conducted Fgly conversion and oxime ligation, since successful click reactions were dependent on these two requirements.

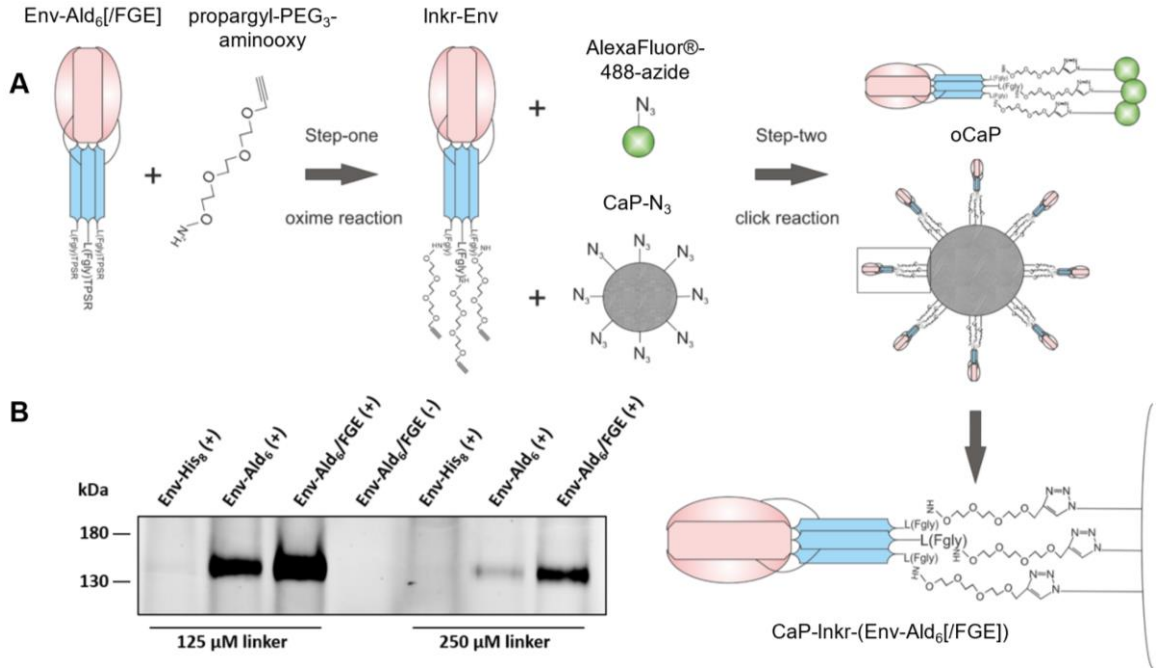

Figure 16) Concept and evaluation of a two-step coupling mechanism

(A) Details of the two-step coupling mechanism. Aldeyhde-tagged Env trimers (Env-Ald_6[/FGE]) with converted Fgly residues at the C-terminus were conjugated to bispecific linker molecules with terminal alkyne and aminooxy groups connected by short PEG spacers (propargyl-PEG_3-aminooxy) via an oxime ligation reaction (Step-one). The alkyne groups of linker-bound Env (lnkr-Env) were harnessed for click reactions with azide-terminated reagents (AlexaFluor®-488-azide or azide-functionalized CaP-N_3; Step-two). The chemical structure of Env trimers orthogonally coupled to the surface of CaPs (oCaP) is shown in detail (CaP-lnkr-(Env-Ald_6[/FGE]). **(B)** Fluorescent reporter gel assay to evaluate the click reaction. Step-one was conducted with Env-His_8, Env-Ald_6 and Env-Ald_6/FGE in the presence of either 125 µM or 250 µM linker (+) or in the absence of linker (-). The unpurified, lab-scale oxime ligation mixtures were then used for click reactions with AlexaFluor®-488-azide. The conjugates were separated by SDS-PAGE and analyzed under blue light exposure. Modified from Damm *et al.*, (2022).

2.2.5. Synthesis and chemical characterization of orthogonally conjugated calcium phosphate nanoparticles

Rojas-Sanchez *et al.* previously optimized the quantity of terminal azide-groups on the surface of CaPs (CaP-N_3) [119]. These particles were the basis for the generation of orthogonally coupled CaPs. oCaPs were synthesized and chemically characterized by Kathrin Kostka (Institut für Anorganische Chemie, Universität Duisburg-Essen, Essen, Germany).

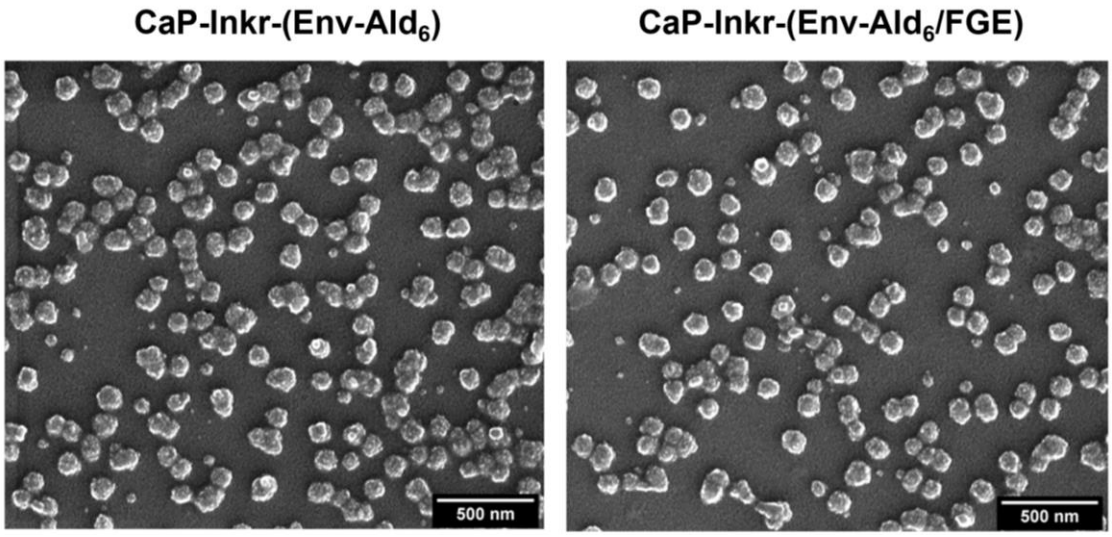

Figure 17) SEM analysis of oCaPs

Scanning electron microscopy of CaP-lnkr-(Env-Ald_6) (left panel) and CaP-lnkr-(Env-Ald_6/FGE) (right panel). Scale bar = 500 nm. Modified from Damm *et al.*, (2022).

After performing the orthogonal two-step coupling mechanism using purified aldehyde-tagged Env trimers and CaP-N_3 (Fig. 16 A), the resulting oCaPs were analyzed via SEM (Fig. 17) and ZetaSizer measurement (Table 2). Additional reactions were done either with Env-His_8 in the presence of linker (CaP//lnkr//(Env-His_8)) or with Env-Ald_6/FGE in the absence of linker (CaP//(Env-Ald_6/FGE)) to control the specificity of the oxime ligation and click reaction, respectively. SEM imaging of Env-coupled oCaPs demonstrated a spherical morphology of the nanoparticles (Fig. 17). While the solid core diameters of CaP-lnkr-(Env-Ald_6) and CaP-lnkr-(Env-Ald_6/FGE) were hardly different than that of the CaP//lnkr//(Env-His_8) control (49 ± 6 nm and 57 ± 6 nm vs. 47 ± 5 nm), the hydrodynamic diameters of the coupled CaPs were clearly larger than the ones of all control particles (104 nm and 120 nm vs. 52 nm and 44 nm; Table 2). Interestingly, the CaP-lnkr-(Env-

Ald_6/FGE) particle preparation was more homogeneous as judged by the polydispersity index than the other preparations (0.34 vs. 0.42 and 0.41). An average of 722 (488 – 1020) and 1540 (1100 – 2080) Env trimers were coupled to the surface of CaP-lnkr-(Env-Ald_6) and CaP-lnkr-(Env-Ald_6/FGE), respectively. No Env trimers were detected by UV-Vis spectroscopy on the surface of control particles.

Table 2) Physicochemical characterization data of oCaPs

Sample	CaP-N_3	CaP-Inkr-(Env-Ald_6)	CaP-Inkr-(Env-Ald_6/FGE)	CaP//Inkr//(Env-His_8)	CaP//(Env-Ald_6/FGE)
Solid core particle diameter by SEM / nm	34 ± 4*	49 ± 6*	57 ± 6*	47 ± 5*	56 ± 6*
Hydrodynamic particle diameter by DLS / nm	38	104	120	52	44
Polydispersity index (PdI) by DLS	0.39	0.42	0.34	0.41	0.31
Zeta potential by DLS / mV	+26	+25	+20	+19	+15
N(Env) molecules per nanoparticle	-	722 (488-1020)**	1540 (1100-2080)**	-	-

* mean ± standard deviation; ** mean (% 95)

A microscopy-based reporter assay was established to monitor the specific coupling of aldehyde-tagged lnkr-Env to the surface of CaP-N_3. To this end, aldehyde-tagged Env trimers were labelled with a red dye (AlexaFluor®-647) by using a primary amine-targeting protein labeling kit (Fig. 18 A). Both oCaPs and control nanoparticles as stated above were synthesized using these fluorescent Env trimers. A cell uptake reporter assay that was previously established to monitor the internalization and cell fate of fluorescently labelled CaPs was performed by Kathrin Kostka. HeLa cells were incubated for 24 h in the presence of different CaP preparations. This reporter assay was not done to address the question whether oCaPs are taken up by HeLa cells, since this has been extensively shown before [119,129]. In contrast, it was conducted to prove the presence of AlexaFluor®-647 signals inside the cells after incubation with oCaPs, but not with control CaPs, by fluorescence light and confocal laser scanning microscopy. This would strongly indicate the specific and efficient functionalization of CaP-N_3 with lnkr-(Env-Ald_6) and lnkr-(Env-Ald_6/FGE) via click reactions.

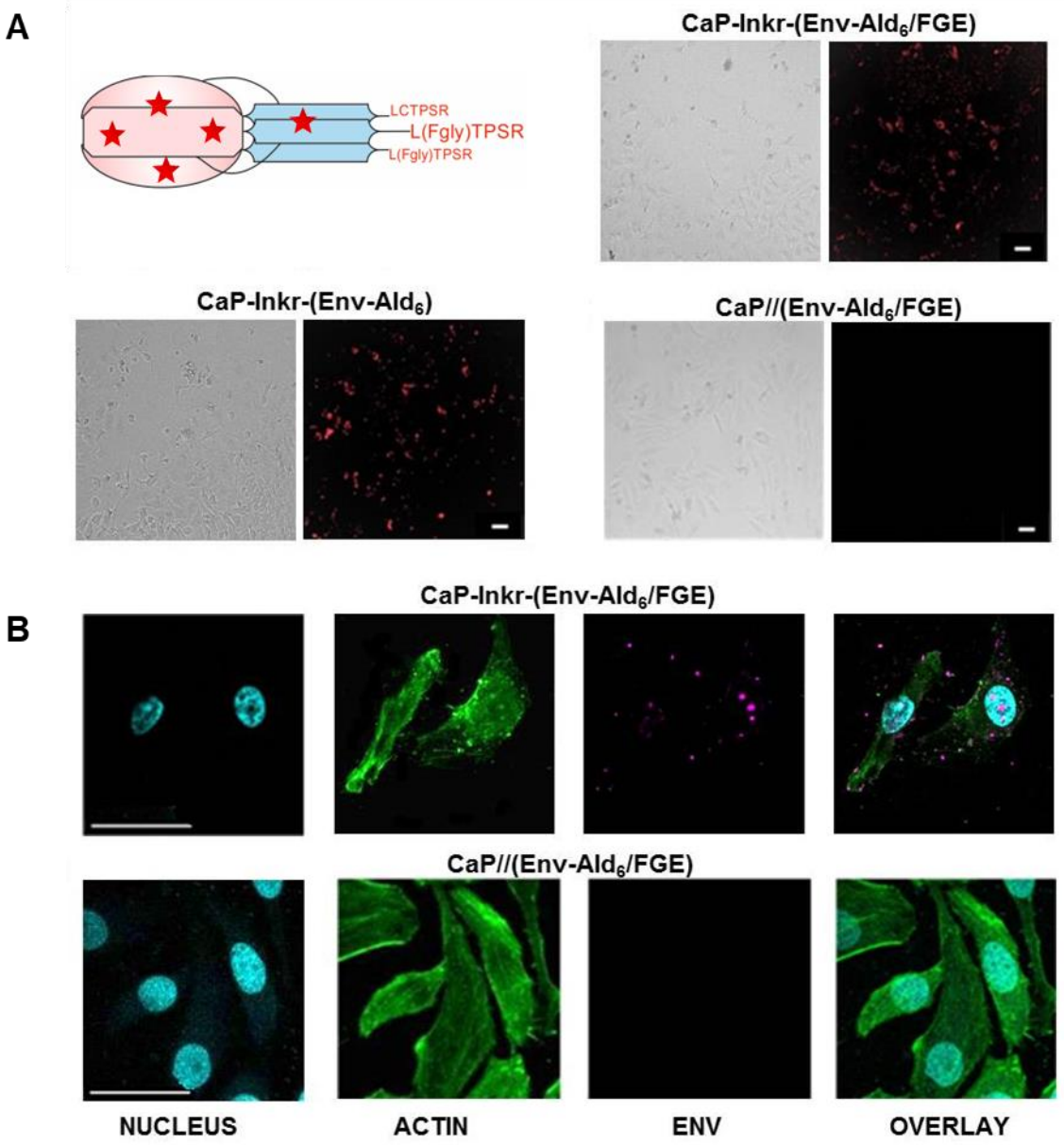

Figure 18) Nanoparticle uptake by HeLa cells

All practical steps were performed and measured by Kathrin Kostka. **(A)** Fluorescence microscopy. Aldehyde-tagged Env trimers were conjugated with AlexaFluor®-647 using a protein labeling kit that targets primary amines on Env. The fluorescent Env molecules were further used for the aldehyde-mediated two-step coupling mechanism. HeLa cells were analyzed after 24 hours incubation in the presence of fluorescent oCaPs (CaP-lnkr-(Env-Ald$_6$) and CaP-lnkr-(Env-Ald$_6$/FGE)) or mock-coupled CaPs controlling the oxime ligation specificity (CaP-lnkr-(Env-His$_8$)) or the click reaction specificity (CaP//(Env-Ald$_6$/FGE)). Bright field (left panels), nanoparticle fluorescence channel (right panels). Scale bar = 50 µm. **(B)** Confocal laser scanning microscopy of HeLa cells after 24 h incubation with CaP-lnkr-(Env-Ald$_6$/FGE) or CaP//(Env-Ald$_6$/FGE). The cells were stained with HOECHST 3342 (NUCLEUS) and AlexaFluor®-488 phalloidin (ACTIN) to localize the fluorescent signatures of the nanoparticles coupled with fluorescent Env trimers (ENV) in overlay images. Scale bar = 20 µm. Modified from Damm *et al.*, (2022).

After nanoparticle incubation, fluorescent light microscopy revealed HeLa cells with red signals in samples that were incubated with CaP-lnkr-(Env-Ald_6) and CaP-lnkr-(Env-Ald_6/FGE), as expected (Fig 18 A). Notably, no signals were detected in samples treated with the linker control CaP//(Env-Ald_6/FGE).

The HeLa cells that were incubated in the presence of CaP-lnkr-(Env-Ald_6/FGE) and CaP//(Env-Ald_6/FGE) have been analyzed in detail on cell organelle level by CLSM (Fig 18 B). To this end, the nuclei and actin filaments were stained with HOECHST and AlexaFluor®-488, respectively. Importantly, red signal dots derived from fluorescently labelled Env-Ald_6/FGE on oCaPs appeared in HeLa cells incubated with CaP-lnkr-(Env-Ald_6/FGE), but not in those samples treated with the control particles coupled in the absence of linker. Besides the click reaction reporter assay (Fig 16 B), these data have proven on nanoparticle level that the two-step coupling mechanism resulted in the generation of oCaPs and that both reactions (Step-one and Step-two) were specific and efficient.

2.2.6. Biological, functional and immunological characterization of the improved nanoparticle design

To this point, it was shown that the low acidic environment of the oxime ligation is not harmful for the stabilized Env trimer conformation and that oCaPs were orthogonally functionalized with a high number of Env spikes via the two-step coupling mechanism. However, there has been no evaluation yet, whether the Env trimer conformation on the surface of the final oCaPs was still intact after the coupling procedure. Thus, the preservation of the closed trimeric conformation after orthogonal coupling was addressed with an experimental flow cytometry approach. oCaPs were surface-stained with a panel of monoclonal Env apex antibodies specific for the pre-fusion conformation (PG9, PGT145). Additional stainings were done with a CD4bs-directed antibody (b12) as well as with a SARS-CoV-2-specific anti-S antibody (TRES567hu [239]) as isotype control. The stained nanoparticles were further incubated with AlexaFluor®-647-coupled secondary anti-human IgG antibody and analyzed by flow cytometry (Fig. 19). In contrast to the isotype control, PG9 and PGT145 as well as b12 recognized and bound to the oCaPs (CaP-lnkr-(Env-Ald_6/FGE)). Interestingly, the median fluorescence intensity (MFI) of the b12 staining was thrice as high as the MFIs of the trimer-specific antibody stainings

(3922 vs. 1310 and 1303), which perfectly resembles the ratio of CD4bs and apex antibody binding sites on one trimer (3:1 vs. 1:1). As a consequence, this experimental FACS approach gave strong evidence that the conformation of the Env trimers was preserved on the surface of oCaPs.

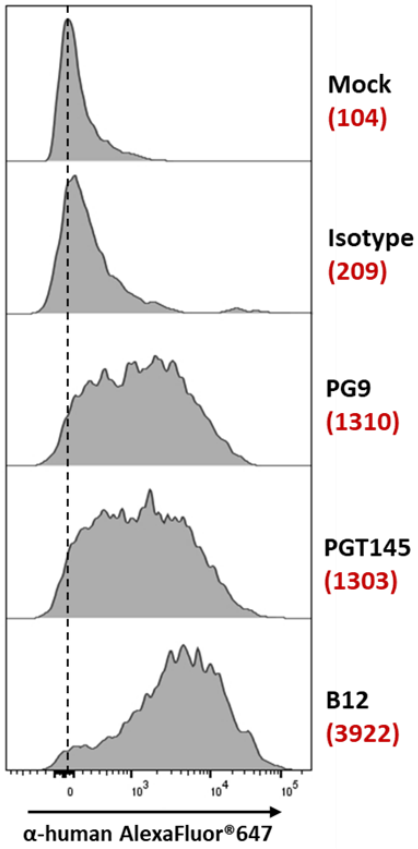

Figure 19) Biological characterization of oCaPs

Surface FACS analysis of CaP-lnkr-(Env-Ald$_6$/FGE). The oCaPs were stained with trimer-specific apex antibodies PG9 and PGT145 as well as CD4bs antibody b12. The isotype control staining was done with a human monoclonal SARS-CoV-2 S-antigen antibody (TRES567hu). Secondary antibody staining was performed with AlexaFluor®-647-conjugated anti-human IgG. The mock group was incubated in buffer only. Numbers (red) indicate the median fluorescence intensities. Modified from Damm *et al.*, (2022).

A crucial requirement for ISH is the recognition and uptake of nanoparticles functionalized with the antigen of interest by antigen-specific naïve B cells in a B cell receptor-dependent manner [220]. As shown above, rCaPs induced activation of Env-specific PGT121 B cells in a comparable range than lentiviral VLPs (Fig. 8). Since the CaP design has now been optimized by orthogonal Env conjugation, this *in vitro* activation assay was repeated comparing PGT121 B cell activation in the

presence of dilution series of rCaPs and oCaPs normalized to the bulk Env concentration (200 – 0.3 ng/mL) (Fig. 20 A). While the amount of activated, viable CD19+ B cells was comparable at the highest and lowest Env concentration between both types of nanoparticles (73 % vs. 74 %; 7 % vs. 7 %), oCaPs induced a 1.3 – 2-fold higher activation of PGT121 B cells at the bulk Env concentrations inbetween saturation and background (40, 8 and 1.6 ng/mL).

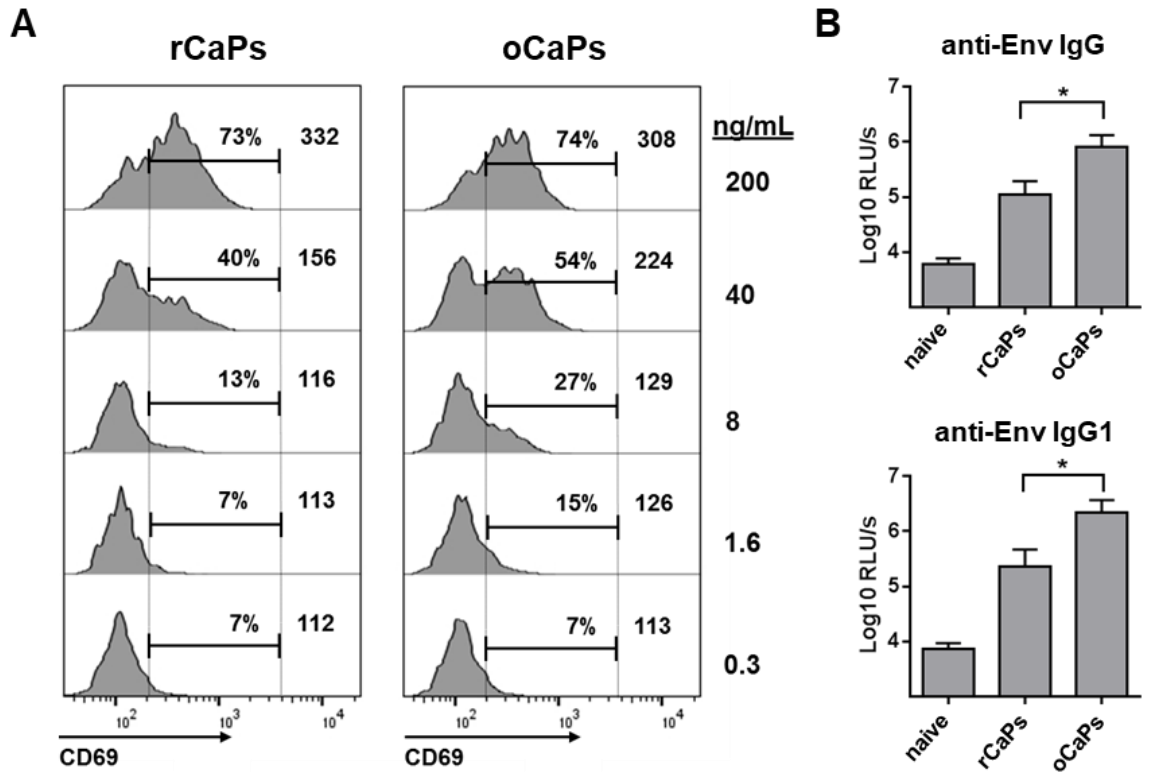

Figure 20) Functional and immunological comparison of rCaPs and oCaPs

(A) *In vitro* B cell activation assay. Naïve Env-specific B cells isolated from PGT121 B cell receptor-transgenic mice were stimulated for 18 h with different dilutions of rCaPs and oCaPs normalized to the bulk concentration of Env (0.3 – 200 ng/mL). Afterwards, the B cells were stained with fluorescent anti-CD19 and anti-CD69 as well as with a viability dye and analyzed by flow cytometry. The histograms represent the expression of early activation marker CD69 on the surface of viable CD19+ cells. Additionally, the percentages of CD69+ cells (in %) and the MFI values are given in numbers. One representative experiment out of three independent trials with similar results is shown. **(B)** Serum ELISA. Env-specific total IgG (top) and IgG1 (bottom) humoral immune responses (in Log10 RLU/s) in mice three weeks after intramuscular immunization with rCaPs or oCaPs. The columns represent the means of six animals per group ± SEM. * $p < 0.05$; one-way ANOVA with Tukey's multiple comparison post-hoc test. Modified from Damm *et al.*, (2022).

Finally, the influence of orthogonal coupling on the induction of Env-specific humoral immune responses has been evaluated. To this end, wildtype C57bl/6NRj mice were immunized with CpG-adjuvanted rCaPs and oCaPs intramuscularly. Blood was taken after three weeks and serum ELISAs were performed to analyze the antibody response (Fig. 20 B). Interestingly, total anti-Env IgG antibody responses were improved in mice that received oCaPs. Subtype ELISA analysis revealed that this effect was predominantly due to an increased magnitude of Env-specific IgG1 responses in oCaP mice compared to rCaP mice. IgG2c levels have not been affected by the type of nanoparticle (data not shown).

These results clearly indicated functional and immunological advantages of BCR binding by oCaPs over rCaPs (see discussion and Fig. 21).

In total, the design of T helper rCaPs shown to induce ISH in mice has been optimized with a two-step orthogonal, site-specific coupling mechanism. oCaPs were functionalized with a high density of conformationally preserved Env trimers and demonstrated an improved induction of both Env-specific B cell activation and increased magnitudes of humoral immune responses in functional *in vitro* and *in vivo* assays. Thus, oCaPs are a reliable platform for future preclinical and clinical vaccine trials against various pathogens.

3. Discussion

The two major achievements of this study were i) the indication that T helper CaPs can be used as a replacement for T helper VLPs in the induction of ISH effects, which comes along with additional advantages such as the dispensability of adjuvants and the avoidance of HIV-specific CD4+ T cell induction, and ii) that the nanoparticle design was optimized by an aldehyde-tag-based, orthogonal coupling mechanism, which preserves the conformation of the Env trimers on the CaP surface and leads to better BCR crosslinking.

CaPs encapsulating TLR ligands or peptides have been used for preclinical, immunomodulatory studies before [104, 240] and are physiologically well tolerated, since the main chemical reagents, calcium phosphate and silicon dioxide, are part of human bone [121] and are used in the food industry [241], respectively. The biological safety of polyethylenimine is yet controversial [242]. This cationic polymer, however, may be easily replaced by another chemically inert one for the stabilization of the nanoparticle matrix, before moving on in clinical trials and applications. The zetapotential of functionalized rCaPs and oCaPs was between +20 mV and +27 mV and the orthogonally coupled nanoparticles had hydrodynamic sizes between 104 nm and 120 nm in diameter. These properties render the particles likely to enter the lymphatic system and to be taken up by cells [131, 100]. Interestingly, the hydrodynamic diameters of rCaPs were about thrice as big as those of oCaPs (Table 1, Table 2). The principle of random coupling of Env trimers to the surface of CaPs was based on the targeting of primary amines on the antigen by sulfo-SMCC crosslinker-mediated NHS esters [101]. In one gp140 Env molecule, 33 lysine residues were expected to have a solvent-exposed side chain and, thus, could be harnessed for random coupling [243,244].

After synthesis, the capability of rCaPs to induce activation of Env-specific B cells *in vitro* was evaluated in advance to *in vivo* experiments. B cell receptor-transgenic PGT121 mice were used as B cell donors, since approximately 70 % of their naïve B cell repertoire bear the broadly-neutralizing Env-antibody PGT121 as IgM (BCR) on the surface [232]. One Env trimer exposes three identical epitopes for PGT121 and binding of this antibody is not restricted to a specific antigen conformation [28]. Importantly, rCaPs induced a comparable magnitude of PGT121

B cell activation than lentiviral VLPs, which served as a positive control for BCR-dependent B cell activation [245]. On the contrary, both kinds of nanoparticles were not able to induce activation of *wt* B cells, as expected. In order to control the inducibility of these B cells, LPS-treated controls were performed to demonstrate the total polyclonal capability of B cell activation [246]. On the other hand, since *wt* B cells did not show any activation in the presence of rCaPs or lentiviral VLPs, this means that all nanoparticle preparations were free of polyclonal activators such as endotoxin. The PGT121 B cell activation by soluble Env-His_8 was significantly reduced in comparison to rCaPs, which is in line with other studies demonstrating that liposomes conjugated with Env are superior over soluble Env trimers in Env-specific B cell activation [112,113].

To induce *in vivo* ISH effects, mice were initially immunized with a licensed Tetanus Toxoid-based vaccine (Tetanol®pur) and boosted with rCaPs intramuscularly. This type of application was previously shown to be the most appropriate delivery route for B and T cell antigens via CaPs into draining lymphoid organs [104]. rCaP-mediated ISH strongly increased the magnitude of Env-specific IgG1 levels in contrast to mock-prime or nanoparticle control groups. Despite a dose of 10 µg Env on nanoparticles per mouse, mock-primed mice demonstrated poor Env-specific humoral immune responses. In previous studies, immunizations with HEL-functionalized nanoparticles (CaPs or VLPs) alone were sufficient to induce strong immune responses in highly sensitive C3H mice [104,247]. Despite the capability of rCaPs to directly activate Env-specific B cells *in vitro*, CD4+ T cell help is additionally necessary to induce primary *in vivo* antibody responses [248]. As a consequence, the poor humoral immune responses induced by rCaPs alone might be the result of i) a generally weak MHC-II-restricted CD4+ T cell help towards Env trimers in *wt* mice [249,250] or ii) a suboptimal immunogenicity of non-adjuvanted CaPs. The first hypothesis is supported by the fact that the encapsulation of Tetanus Toxoid p30 peptide, which is a universal T helper epitope [249], into rCaPs (rCaP-p30) was enough to significantly increase the magnitude of the Env-specific humoral immune response in mock-primed mice. A similar observation was already made in a previous study, where the encapsulation of p30 into CaPs functionalized with HEL has overcome the lack of HEL-derived CD4+ T cell epitopes in C57bl/6 mice that are genetically predisposed not to provide anti-HEL CD4+ T cell help [104]. Nevertheless, the Env-specific antibody response in ISH mice (Tetanol®pur +

rCaP-p30) was about 10-fold higher than the “rCaP-p30 / mock-prime” group and more than 100-fold higher than the “rCaP only” group. Induction of Tetanus-mediated ISH effects was previously shown in mice immunized with p30-incorporating lentviral VLPs after a prime administration of Tetanol®pur [224]. This experimental setup was reproduced in the current study as a positive control group with lentiviral VLPs that incorporated p30 and displayed membrane-anchored BG505 Env trimers on the surface (Env-VLP-p30) to obtain a direct comparison of VLP- and CaP-mediated ISH effects. The dosage of Env-VLP-p30 normalized to the bulk amount of Env per mouse was adapted from previous studies and was about 33-fold lower than the CaP dosage (0.3 µg vs. 10 µg) [211,224]. Most importantly, the strength and phenotype of the ISH between rCaP-p30- and Env-VLP-p30-immunized mice was comparable, indicating that T helper VLPs can be replaced by synthetic T helper CaPs in future preclinical and clinical vaccine applications. The phenotype of ISH was consistent with the results of the cytokine profiling of p30-specific CD4+ T cells. ISH mice showed significantly elevated levels of IL-5-secreting, p30-specific T helper cells. ISH for Env-specific B cells given by these CD4+ T cells may be responsible for the dominant anti-Env IgG1 response, while elevated levels of cells secreting Th1 cytokines IFN-γ and TNF-α were sufficient to additionally increase the magnitude of Env-specific IgG2c responses in a significant manner in the same mice [180,251].

In the past, as an alternative for the recruitment of heterologous, non-Env T cell help, TLR ligands were encapsulated into CaPs for immunomodulatory vaccine trials. Here, incorporation of TLR9 ligand CpG resulted in the highest increase of IgG antibody responses against a model antigen beside a number of other advantages [104]. Furthermore, CpG 1018 is approved as an adjuvant for clinical applications [234]. In this study, the hypothesis that ISH can compete with the modulatory effects of adjuvants was tested by direct comparison of animal groups that have received either rCaP-p30 in an ISH setup or rCaP-CpG. In fact, both groups demonstrated a comparable magnitude of Env-specific total IgG responses. Nevertheless, while Tetanus-mediated ISH induced an anti-Env IgG1-dominated response, CpG adjuvantation resulted in predominant IgG2c levels. These findings, however, were in line with immune response phenotypes in previous studies [104,224]. Moreover, it is possible to alter the ISH-mediated immune response phenotype by using different heterologous T helper epitopes [225,227].

The success of a vaccine is not only dependent on the elicitation of protective humoral immune responses, but also on avoiding the vaccine-mediated induction of immune mechanisms that may increase the susceptibility for infection [252]. Multiple studies have demonstrated that vaccine-induced HIV-specific CD4+ T cells may act as a target for HIV and promote the infection after inoculum-mediated activation and expansion [213,214]. To evaluate, whether the recruitment of non-HIV-specific CD4+ T cells via ISH can bypass the induction of HIV-specific T cell help, the ISH and CpG-adjuvanted CaP mice were analyzed for the presence of Env-specific CD4+ T cell responses. To this end, splenocytes of completely immunized mice (w18) were co-cultured with Env-specific B cells previously incubated with lentiviral VLPs for the restimulation of CD4+ T cells, since no universal Env peptide is described in the literature. This co-culture assay as a prerequisite for intracellular cytokine staining of Env-specific T cells has been established in this study. Indeed, while both groups (ISH vs. CpG) showed similar levels of anti-Env total IgG, Env-specific CD4+ T cells that secrete pro-inflammatory cytokines IL-2, TNF-α and IFN-γ [253] were only detected in the rCaP-CpG group, but not in the ISH group. The pronounced Env-specific CD4+ T cell responses in rCaP-CpG mice might be a result of TLR9 ligation in DCs [126,254]. IFN-γ-secreting CD4+ T cells were particularly in focus in this experiment, since non-human primate SIV infection models have shown that vaccinated macaques with a high number of vaccine-induced IFN-γ-secreting T cells were more likely to be infected with challenge virus than animals with a low SIV-specific CD4+ T cell number [213]. Thus, the current study indicates that CpG-incorporation into CaPs, but not ISH, may result in immune responses that potentially enhance the susceptibility for HIV acquisition.

To summarize the immunological findings, the encapsulation of non-HIV peptides as heterologous T helper epitopes into rCaPs induced ISH effects that modified the phenotype and magnitude of the Env-specific antibody response in a comparable range than a commercial adjuvant, but without the additional induction of HIV-specific CD4+ T cells that are suspected to increase the susceptibility for HIV infection. Thus, these findings provide multiple reasons to further push the concept of ISH in the context of HIV-1 vaccination into clinical studies.

In fact, nanoparticle delivery platforms for clinical applications in HIV-1 vaccine research have been tremendously put into spotlight during the last decade

[255]. The targeting of cells and tissues as well as the immune response induction requires a surface functionalization with either antigens, antibodies or small molecules such as peptides [256]. The HIV-1 surface glycoprotein Env is the only target for the humoral immune system on native virions. Therefore, in the context of an HIV-1 vaccine candidate, the surface functionalization of nanoparticles with Env is required to improve B cell targeting and the immunogenicity towards the antigen. A multitude of studies describe various mechanisms for the generation of nanoparticles conjugated with Env trimers [257]. In this study, T helper CaPs were functionalized with Env trimers in a randomly oriented manner via sulfo-SMCC crosslinkers. However, state-of-the-art coupling mechanisms manage to surface-functionalize nanoparticles in a way that preserves the pre-fusion conformation of stabilized Env trimers which contains epitopes for broadly-neutralizing antibodies [110,113]. Furthermore, site-specific Env immobilization may contribute to make the trimer bases, which contains immunodominant epitopes that lead to non-neutralizing antibody responses, inaccessible for B cell receptors (BCRs) [258]. In order to improve the design of T helper CaPs, a two-step coupling mechanism for orthogonal Env functionalization of CaPs was planned, established and evaluated in the course of this study. This mechanism is based on two highly selective and well-characterized bioconjugation reactions – oxime ligation (Step-one) and copper-catalyzed azide-alkyne cycloaddition (Click reaction; Step-two) [130,259]. BG505 Env trimers based on the subtype A transmitted/founder virus BG505.B1 were used as the antigen of choice for orthogonal coupling, since they are broadly applied as vaccine candidates and allow a direct comparison to rCaPs [56,260]. Moreover, native-like soluble BG505 NFL trimers were reported to be predominantly in a non-dissociated, trimeric state after affinity chromatography alone, without the need for further size-exclusion purification [76]. A genetically encoded aldehyde-tag was introduced at the C-terminus of Env as prerequisite for the coupling mechanism.

Initially, it was planned to directly conjugate aminooxy-functionalized nanoparticles with aldehyde-tagged Env trimers. However, since the oxime ligation requires a low acidic environment and the calcium phosphate matrix is not stable under these conditions, this problem was bypassed via an additional crosslinker and second bioconjugation step at neutral pH. In theory, pH-insensitive nanoparticles such as liposomes can be coupled in a single step via the aldehyde-

tag mechanism. However, since missing flexibility in the proximity of conjugation reactions is reported to impede the coupling efficiency, the two-step mechanism may even be beneficial in this regard [109]. Oxime ligations form covalent bonds between the reaction partners and, thus, have advantages in comparison to coupling strategies based on affinity interactions or random antigen immobilization via targeting of primary amines with a low conjugation efficiency [113,261]. The site-specific bioconjugation can compete well with already published mechanisms harnessing recombinant cysteines and maleimide head groups or orthogonal immobilization on biocompatible silica nanoparticles [109,137].

The Fgly conversion rate and both bioconjugation steps were analyzed independently in terms of efficiency and specificity in order to assess the total performance of the two-step coupling mechanism. In a prokaryotic expression system, 85 % of the C-terminal aldehyde-tags in the maltose binding protein (MBP) demonstrated converted Fgly residues upon co-expression of FGE from M. tuberculosis [167]. Another study reported that Fgly conversion in 6-mer aldehyde-tags introduced downstream of Fc domains was done at a rate of 28 ± 1 % (endogenous FGE only) and 45 ± 1 % (FGE overexpression) during protein expression in eukaryotic CHO cells [166]. In this study, the Fgly conversion rate was addressed by mass spectrometry (MS) analysis and gel shift assays. In general, Env expression takes place in the secretory pathway. Due to extensive co-translational modifications such as glycosylation, Env may be exposed to FGE activity a proportional amount of time [19]. Since three heterodimers with individual aldehyde-tags form one Env trimer, the Fgly conversion in one gp120-gp41 subunit would be sufficient for theoretical trimer coupling. MS analysis has proven that Fgly conversion was detectable in both the endogenous (Env-Ald_6) and the overexpression setting (Env-Ald_6/FGE). Nevertheless, the calculated conversion rate based on the MS data was much lower in Env-Ald_6 (7 % vs. 42 %). Surprisingly, despite this low endogenous conversion rate, the gel shift assay demonstrated efficient oxime ligations of both Env-Ald_6 and Env-Ald_6/FGE with a 40 kDa aminooxy-$PEG_{[n]}$ linker (71.8 % vs. 92.2 %). Assuming a statistically necessary conversion rate of 33.3 % to introduce one reactive aldehyde group per trimer, the gel shift assay suggested minimum conversion rates of 23.9 % (endogenous setting; 0.718 x 33.3) and 30.7 % (overexpression setting; 0.922 x 33.3), respectively. Despite the divergence of the calculated conversion rates from both

assays, the data clearly draw the conclusion that transient FGE overexpression is strongly recommended for future production of aldehyde-tagged Env.

The oxime ligation (Step-one) was first evaluated in terms of specificity by reactions of aldehyde- and His-tagged Env proteins with a fluorescent aminooxy-dye. Aminooxy groups react most preferentially with aldehyde groups, but in declining affinity also with ketones, amides and carboxylic acids. Native Env does not contain any naturally occurring aldehyde or ketone groups. Nevertheless, major unspecific targeting of other Env domains except the recombinantly introduced aldehyde-tag by aminooxy groups had to be excluded. Especially the glycan shield was a matter of concern, since various publications describe the immobilization of monosaccharides or more complex glycans on gold nanoparticles via aminooxy-terminated linker molecules [262–264]. However, this immobilization was done by targeting free C1 atoms on the ring structures and the reactions were catalyzed via aniline. The Env glycan shield is comprised of N-linked complex or high-mannose glycans, where free C1 atoms do not occur, since they are always conjugated by 1,4- or 1,6-glycosidic bonds and, thus, inaccessible [265–267]. However, GlcNAc and Neu5Ac residues located at the stem and caps of oligosaccharides, respectively, contain amide moieties, which are potential but hardly reactive targets of aminooxy groups [268,269]. These moieties might be responsible for the weak signals in the oxime reporter gel assay with Env-His_8, but this amount of unspecific binding is neglectable, especially because only 0.5 % of Env-His_8 was bound in the gel shift assay. Studies indicating the presence of O-glycosylation in Env are rare [270]. The amino acids asparagine and glutamine contain additional amide groups. Moreover, both Neu5Ac as well as aspartic and glutamic acid bear free carboxylic acid groups. Yet, in the absence of a catalytic reagent, it is unlikely that the propargyl-PEG_3-aminooxy linker would react with above mentioned moieties. In summary, the genetically encoded aldehyde-tags at the C-termini of Env were the specific and preferential targets for oxime ligations.

The conformational stability of BG505 Env trimers at low acidic environment (pH 4.5) required for an optimal oxime ligation efficiency was a major concern in the course of this study. Thus, the conformational integrity of Env was evaluated by ELISA using trimer-specific antibodies (PG9, PG16, PGT145) after antigen treatment at neutral, low acidic or highly acidic environment (pH 7.0, pH 4.5 and pH

3.0, respectively). These antibodies are commonly applied to confirm the closed conformation of native-like trimers [61,139]. Additional detection was done with glycan-binding, trimer-unspecific antibody 2G12 to control an equal amount of coated Env molecules. As a result, low acidic environment had no influence of the structural integrity of the trimers, whereas pH 3.0 as a positive control induced dramatic loss of conformation. This is consistent with other studies that observed a declining stability of BG505 Env trimers at pH values below 3.6 [271,272]. The preservation of the pre-fusion conformation after the complete two-step coupling mechanism was confirmed again later by surface staining of oCaPs with a panel of monoclonal Env antibodies and flow cytometry analysis. Here, the MFI values of the different antibodies were in the same ratio (3 : 1) as their potential binding sites on the Env trimers [55]. This strongly indicates that the aldehyde-tag-mediated coupling mechanism resulted in a dense array of conformationally preserved Env spikes on the surface of oCaPs. On a side note, since the oxime ligation reporter assay with AlexaFluor®-647-aminooxy ran highly specific and efficient and the preservation of the trimeric conformation was proven after the reaction, this setup can be used in the future for conformation-sensitive labeling of Env trimers as a requirement for multiple applications such as antigen-staining of memory B and plasma cells for FACS as well as localization and tracking of conformational trimers in living cells and lymphoid organs of vaccinated animals [273–275]. The conformational labeling via oxime ligation is, thus, an advantage to unspecific labeling via targeting of primary amines, which easily leads to dissociation of the pre-fusion conformation, and an alternative to a parallel approach that introduces GFP at a specific site within the Env ORF which did not lead to loss of conformation after protein expression [238].

The advantages of nanoparticle-immobilized antigens in comparison to soluble forms in terms of immunogenicity and immunomodulation have been demonstrated in numerous studies before [85,137,140,222]. Functional *in vitro* assays, i.e. the activation of antigen-specific B cells, can act as surrogate markers to predict the outcomes of subsequent *in vivo* trials [106,113]. In this study, the superior *in vitro* activation of Env-specific, naïve B cells by rCaPs compared to soluble Env trimers was a reproduction of these studies' findings with the CaP system. However, since an orthogonal coupling mechanism was additionally established in this study, a functional comparison between rCaPs and oCaPs was reasonable to evaluate the advantages of orthogonal antigen immobilization. In fact, the *in vitro* B cell activation

assay with rCaPs and oCaPs demonstrated that oCaPs induced an improved activation of PGT121 B cells in several nanoparticle dilution steps than rCaPs. B cell activation in general is triggered by BCR crosslinking. Recently, it was shown that BCRs are not equally distributed on the B cell surface. They are rather clustered in multiple protein islands within the plasma membrane that consist of approximately 30 BCRs each. The diameters of these islands have an average size of 150 nm [276]. The hydrodynamic diameter of oCaPs indicates that one nanoparticle may cover a BCR island completely. Due to orthogonal coupling, oCaPs display a dense array of repetitive, identical epitopes. Thus, they display an increased valence of accessible epitopes to the BCRs compared to rCaPs (Fig. 21). This situation may favor the inter-BCR Env binding (BCR crosslinking) [277] and would be a possible explanation for the better activation of PGT121 B cells by oCaPs with bulk Env concentration between saturation and background.

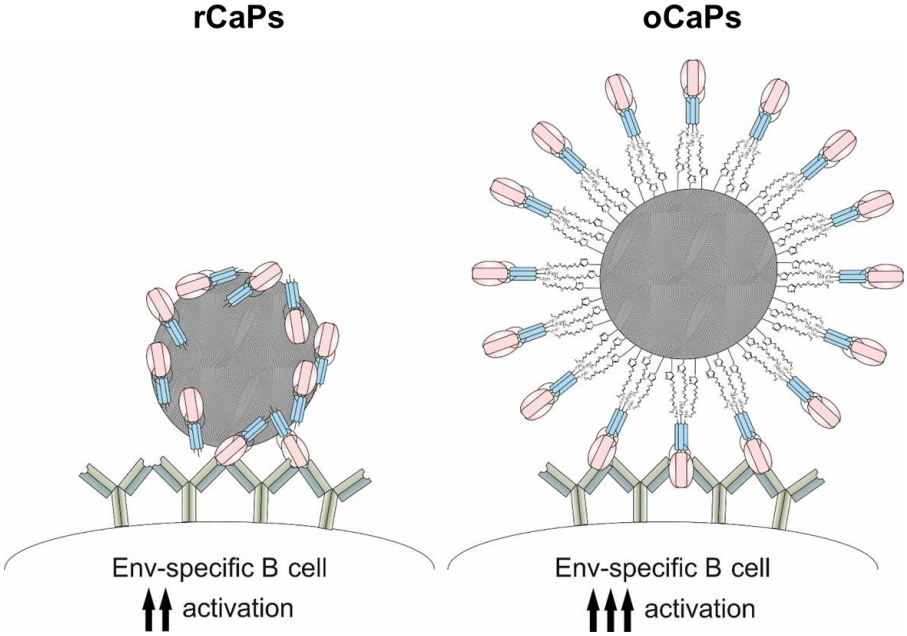

Figure 21) Improvement of BCR crosslinking by oCaPs

oCaPs display a high number of well-accessible, identical Env epitopes on the surface in comparison to rCaPs. This feature may facilitate an improved BCR recognition and crosslinking. (Adapted from Damm *et al.*, 2022).

Native HIV-1 virions display approximately 14 Env trimers on the surface [20]. The trimers are comprised of non-covalently linked subunits and, thus, they may dissociate or dynamically shift between different conformational states [278]. These escape mechanisms (among others) retard the generation of broadly-neutralizing

antibodies. The quantitative, orthogonal immobilization of conformationally stabilized Env trimers on the surface of nanoparticles for vaccination may overcome this bias [279]. The calculated amount of Env trimers on the surface of oCaPs is comparable to the dense array of well-ordered spikes described for synthetic liposomes [109]. On another note, antigen spacing may also play a role in B cell activation [280]. This concern can be addressed in future experiments that include alterations of the crosslinker length and variations of reactive groups on the nanoparticle surface.

Finally, the advantage of oCaPs over rCaPs was demonstrated *in vivo* by intramuscular immunization of *wt* mice with CpG-adjuvanted oCaPs and rCaPs. Here, oCaP-immunized mice showed significantly higher anti-Env total IgG and IgG1 levels than rCaP mice after one dose of nanoparticles. This is in line with the B cell activation results. Beside Tetanus-mediated ISH, a Th2 bias in mice after Env immunization is typical [169,222]. However, the mice sera were unsuitable for neutralization assays, since murine CDRH3 domains of IgG heavy chains in *wt* mice are too small to potentially neutralize tier-2 HIV strains [258,281]. Future immunization experiments in transgenic mice either with humanized VDJ segments or recombinant knock-ins of germline precursor sequences of bnAbs may give more insights in the potential of oCaPs to elicit neutralizing immune responses [239,282].

Taken together, this study provides a proof-of-principle that orthogonal immobilization of Env trimers on the surface of nanoparticles via aldehyde-tag-mediated oxime ligation under low acidic environment and medium temperature is feasible and highly efficient without the loss of antigen conformation. This feature is highly relevant for the rational design of nanoparticle-based HIV-1 vaccine platforms for clinical applications. The current study additionally shows that orthogonal coupling has many functional advantages over random coupling. Furthermore, this approach can be easily applied with antigens from different pathogens such as the spike proteins of coronaviruses, surface glycoproteins of Ebola and Marburg filoviruses as well as E-antigen dimers of Zika and Dengue flaviviruses [283–285]. Together with the possibility to induce ISH-mediated immunomodulation, these nanoparticles might be powerful tools for future diagnostic applications and vaccine development.

4. Material and Methods

4.1. Material

If not specified otherwise, the supplier or manufacturer was located in Germany.

Table 3) Disposables

Name of Material	Manufacturer
6-Well cell culture plate	Greiner Bio-One, Frickenhausen
24-Well cell culture plate	Greiner Bio-One, Frickenhausen
48-Well cell culture plate	Greiner Bio-One, Frickenhausen
96-Well cell culture plate (U bottom)	Greiner Bio-One, Frickenhausen
96-Well cell culture plate (V bottom)	A. Hartenstein GmbH, Würzburg
96-Well microtest plate (flat bottom)	Sarstedt, Nümbrecht
Alcohol swabs	Vivomed GmbH, Geislingen
Amicon Ultra-4 centrifugal filters (10 kDa)	Merck, Darmstadt
Beaker	Duran Schott, Wertheim/Main
Blotting filters / Whatman paper	BIO-RAD, München
Bolt™ empty cassettes (1.0 mm)	Thermo Fisher, Waltham, USA
Bolt™ 4-16 % Bis-Tris gels (1.0 mm)	Thermo Fisher, Waltham, USA
CA Membrane Filter (0.2 µm)	Membrane Solutions, Kent, USA
CA Membrane Filter (0.45 µm)	Membrane Solutions, Kent, USA
Cell culture flask (25 cm²)	Greiner Bio-One, Frickenhausen
Cell culture flask (75 cm²)	Greiner Bio-One, Frickenhausen
Cell culture flask (175 cm²)	Greiner Bio-One, Frickenhausen
Countess™ Cell Counting Chamber Slides	Thermo Fisher, Waltham, USA
Counting chamber, CE-certified	Hartenstein, Würzburg
Econo-Pac® Chromatography Columns	BIO-RAD, München
ELISA plates, 96 Well, high binding, white	gbo, Rimbach
Erlenmeyer flask (500 mL)	Duran Schott, Wertheim
Erlenmeyer flask (1000 mL)	Duran Schott, Wertheim
FACS tubes, mini	Axygen, Union City, UK
Falcon reaction tube (15 mL)	Sarstedt, Nümbrecht
Falcon reaction tube (50 mL)	Sarstedt, Nümbrecht
gentleMACS C tubes	Miltenyi Biotec, Bergisch Gladbach
LS Columns	Miltenyi Biotec, Bergisch Gladbach
Micro-Fine™ Insulin syringes (0.3 mL; 0.3 mm x 8 mm)	Becton Dickinson, Franklin Lakes, USA
Micro-Fine™ Insulin syringes (0.5 mL; 0.33 mm x 12.7 mm)	Becton Dickinson, Franklin Lakes, USA
Microtainer® SST Tubes	Becton Dickinson, Franklin Lakes, USA
Minicap capillaries	Hirschmann Laborgeräte GmbH, Eberstadt
Minisart® syringe filters (0.22 µm)	Sartorius, Göttingen
Minisart® syringe filters (0.45 µm)	Sartorius, Göttingen
Mr. Frosty	Nalgene, Rochester, NY, USA
Ni-NTA HisSorb™ plates	QIAGEN GmbH, Hilden

Nitrocellulose membrane (0.45 µm)	GE Healthcare, Chalfont St Giles, UK
Nunc MaxiSorp ELISA plates	Thermo Fisher Scientific, Schwerte
PETG Erlenmeyer flask (125 mL)	Thermo Fisher Scientific, Schwerte
PETG Erlenmeyer flask (250 mL)	Thermo Fisher Scientific, Schwerte
PETG Erlenmeyer flask (500 mL)	Thermo Fisher Scientific, Schwerte
Pipet tip (0.1 - 10 µL)	Ratiolab, Dreieich
Pipet tip (1 - 20 µL)	Ratiolab, Dreieich
Pipet tip (100 - 1000 µL)	Ratiolab, Dreieich
Pipet tip (20 - 200 µL)	Sarstedt, Nümbrecht
Polypropylene centrifuge tubes	Beckman Coulter, Brea, USA
Polystyrene cuvettes	Sarstedt, Nümbrecht
Pre-Separation Filters (30 µm)	Miltenyi Biotec, Bergisch Gladbach
Reaction tube (1.5 mL)	Brand, Wertheim
Reaction tube (2.0 mL)	Sarstedt, Nümbrecht
SDS-PAGE gel running chamber	Thermo Fisher Scientific, Schwerte
SealPlate®	EXCEL Scientific, Victorville, USA
Stericup 0.22 µm	Merck, Darmstadt
Stericup 0.45 µm	Merck, Darmstadt
Sterile plastic pipets (5 mL)	Corning Inc., Corning, USA
Sterile plastic pipets (10 mL)	Corning Inc., Corning, USA
Sterile plastic pipets (25 mL)	Corning Inc., Corning, USA
Sterling nitrile gloves	O&M Halyard, Mechanicsville, USA
Suprasil® quartz cuvette	PerkinElmer, Waltham, MA, USA
Syringe Luer-Lok™ 50 mL	Becton Dickinson, Franklin Lakes, USA
YMC Triart C18 column	YMC Europe GmbH, Dinslaken
Volumetric cylinder	Duran Schott, Wertheim/Main
Volumetric flask	Duran Schott, Wertheim/Main

Table 4) Devices

Device	**Manufacturer**
5430/5430 R Centrifuge	Eppendorf AG, Hamburg
Agarose gel chamber	Institute for Virology, Erlangen
Apreo S LoVac microscope	ThermoFisher Scientific, Waltham, MA, USA
BDK Laminar Flow System	Weiss Umwelttechnik, Reiskirchen
Blotting device TE77XP	Hoefer, Holliston, USA
Centrifuge, 48 R	Hettich GmbH & Co. KG, Tuttlingen
Centrifuge Mikro 200R	Hettich GmbH & Co. KG, Tuttlingen
Centrifuge, Mikro 24-48	Hettich GmbH & Co. KG, Tuttlingen
Centrifuge Rotina 420 R	Hettich GmbH & Co. KG, Tuttlingen
Christ Alpha 2-4 LSC instrument	Martin Christ GmbH, Osterode am Harz
Countess™ Automated cell counter	Thermo Fisher Scientific, Schwerte
DS-11 FX+ spectrophotometer “Nanodrop”	DeNovix, Wilmington, USA
Electroporator TriGrid™ Delivery System	Ichor Medical Systems, San Diego, CA, USA
Endosafe Nexgen-PTS handheld spectrophotometer	Charles River, Boston, USA
ESEM Quanta 400 instrument	FEI Co., Hillsboro, USA
Freezer -20°C	Bosch, Gerlingen-Schillerhöhe

Freezer -80°C	Thermo Fisher Scientific, Schwerte
Gel camera E.A.S.Y® doc plus	Herolab GmbH, Wiesloch
Gel station	PEQLAB, Erlangen
gentleMACS™ dissociator	Miltenyi Biotec, Bergisch Gladbach
HT-minitron (shaking incubator for cells)	Infors, Bottmingen
Ice machine	ZIEGRA Eismaschinen GmbH, Isernhagen
Incubator, CB 220	Binder, Schwerte
Incubator (for bacteria)	Heraeus, Hanau
Incubator (for cells)	Sanyo, Osaka, Japan
INTAS advanced fluorescence imager	Intas Science Imaging Instruments GmbH, Ahmedabad, India
Keyence Biorevo BZ-9000	Keyence, Neu-Isenburg
Leica TCS SP8X FALCON	Leica, Wetzlar
LSR-II	Becton Dickinson, Franklin Lakes, USA
Magnetic stirrer MR 3001	Heidolph Instruments, Schwabach
Microplate washer, Asys Atlantis	Biochrom, Berlin
Microscope, AE 2000	MoticEurope, S.L.U., Barcelona, Spain
Microscope Axiovert 25	Carl Zeiss AG, Oberkochen
Microscope, Telaval 31	ZEISS Oberkochen
Mini Gel Tank and Blot Module Set	Thermo Fisher Scientific, Schwerte
MS2 Minishaker	IKA, Staufen
M-Series AA spectrometer	Thermo Electron Corporation, Schwerte
Multichannel, Transferpette® p5-50	Brand, Grossostheim
Mutlichannel, Transferpette® p30-300	Brand, Grossostheim
Multilabel plate reader, Victor X4	Perkin Elmer, Hamburg
ND-1000 NanoDrop®	PEQLAB, Erlangen
Neubauer counting chamber	A. Hartenstein GmbH, Würzburg
Orion Microplate Luminometer	Berthold Detection Systems, Pforzheim
pH-Meter	Mettler Toledo, Wien, Austria
Pipettes	Gilson, Middleton, WI, USA
Pipetus	Hirschmann Laborgeräte, Eberstadt
Power Pac 300	BIO-RAD, München
Power supply, EPS 301	Pharmacia, Lissabon, Portugal
QuadroMACS™ Separator	Miltenyi Biotec, Bergisch Gladbach
Refrigerator 4°C	Liebherr, Biberach an der Riß
Rolling incubator, REAX 2	Heidolph, Schwabach
Scale	Kern, Balingen
Scale	Sartorius AG, Göttingen
SDS gel running chamber	Thermo Fisher Scientific, Schwerte
Shaking incubator for bacterial culture	Infors, Bottmingen
Sonotrode (UP50H, Sonotrode N7, amplitude 70%, pulse duration 0.8 s	Hielscher Ultrasonics GmbH, Teltow
Sorvall RC-5B Refrigerated Superspeed Centrifuge	DuPont Instruments, Wilmington, DE, USA
Sorvall RC5B Plus	DuPont Instruments, Wilmington, DE, USA
Sorvall WX Ultra Series centrifuge	Thermo Electron Corporation, Schwerte
Sprout Minicentrifuge	Biozym, Hessisch Oldendorf
Thermal cycler MJ Mini	BIO-RAD, München

Thermomixer compact	Eppendorf AG, Hamburg
timsTOF Pro mass spectrometer	Bruker Daltonik GmbH, Bremen
Ultimate 3000 RS system	Bruker Daltonik GmbH, Bremen
Ultracentrifuge L7-55	Beckman Coulter, Brea, USA
Ultracentrifuge Optima XPN-80	Beckman Coulter, Brea, USA
UV-transilluminator	Clare Chemical Research, Denver, USA
Varian Cary 300 Bio spectrophotometer	Agilent Technologies, Santa Clara, USA
Vortex mixer	Phoenix Instrument GmbH, Garbsen
Water bath	Mason technology, Dublin, Ireland
ZetaSizer Nano S90	Malvern Pananalytical, Kassel
Zetasizer Nano ZS (λ = 633 nm)	Malvern Instruments, Malvern, UK

Table 5) Chemicals

Chemical / Solution	**Manufacturer**
0.1 M DTT	Thermo Fisher Scientific, Waltham, MA, USA
2-Mercaptoethanol, 50 mM in PBS, sterile	PAN-Biotech, Aidenbach
(3-azidopropyl)triethoxysilane	Select Lab, Münster
(3- mercaptopropyl)trimethoxysilane (MPS)	Sigma-Aldrich, Taufkirchen
3-(N-morpholino)propanesulfonic acid	Carl Roth, Karlsruhe
3.1 Buffer (NEB Buffer r3.1)	New England Biolabs, Ipswich, MA, USA
3,3',5,5'-Tetramethylbenzidine (TMB)	KPL, Gaithersburg, USA
4-(2-hydroxyethyl)-1-piperazineethanesulfonic acid (HEPES)	Thermo Fisher Scientific, Waltham, MA, USA
6x Purple DNA Loading Dye	New England Biolabs, Frankfurt am Main
Acetic acid	Sigma-Aldrich, Taufkirchen
Agarose	SERVA GmbH, Heidelberg
Agarose bound Galanthus Nivalis lectin	Vector laboratories inc., Burlingame
AlexaFluor®-647-hydroxylamine	Thermo Fisher Scientific, Schwerte
AlexaFluor®-488-azide	Thermo Fisher Scientific, Schwerte
AlexaFluor®-488 phalloidin	Thermo Fisher Scientific, Schwerte
Aminoguanidine hydrochloride (AGHC)	Sigma-Aldrich, Taufkirchen
Ammonium persulfate (APS)	Merck, Darmstadt
Ampicillin	Sigma-Aldrich, Taufkirchen
Aqua ad iniectabilia	B. Braun Melsungen AG, Melsungen
Aqueous ammonia solution (7.8 wt%)	Carl Roth, Karlsruhe
Bacto-agar	Becton Dickinson, Heidelberg
Boric Acid	Carl Roth, Karlsruhe
Bovine serum albumin (BSA)	Carl Roth, Karlsruhe
Brefeldin A (1000x)	eBioscience, Frankfurt am Main
Bromophenol blue	Sigma-Aldrich, Taufkirchen
Calcium Lactate	Sigma-Aldrich, Taufkirchen
Cell Trace™ CFSE	Thermo Fisher Scientific, Schwerte
Copper(I) sulfate ($CuSO_4$)	Jena Bioscience, Jena
CutSmart Buffer	New England Biolabs, Frankfurt am Main

D-(+)-trehalose solution	Sigma-Aldrich, Taufkirchen
Diammonium hydrogen phosphate	VWR, Radnor, PA, USA
Dimethyl sulfoxide (DMSO)	VWR, Radnor, PA, USA
Disodium phosphate (Na_2HPO_4 x 2(H_2O))	Sigma-Aldrich, Taufkirchen
dNTPs	GE Healthcare, Freiburg
Dulbecco's Modified Eagle Medium (DMEM)	Gibco, Waltham, MA, USA
Dulbecco's Phosphate Buffered Saline (DPBS)	Gibco, Waltham, MA, USA
Ethanol (EtOH)	Merck, Darmstadt
Ethidiumbromide	SERVA, Heidelberg
Ethylene glycol-bis(β-aminoethyl ether)-N,N,N′,N′-tetraacetic acid (EGTA)	Sigma-Aldrich, Taufkirchen
Ethylenediaminetetraacetic acid (EDTA)	VWR, Radnor, PA, USA
Fetal calf serum (FCS)	Capricorn Scientific GmbH, Ebsdorfergrund
Fetal calf serum (FCS)	Sigma-Aldrich, Taufkirchen
Fixable Viability Dye eFluor™ 450	eBioscience, Frankfurt am Main
FreeStyle™ 293 Expression Medium	Thermo Fisher Scientific, Waltham, MA, USA
Gel Loading Dye, Purple (6X)	New England Biolabs, Ipswich, MA, USA
GeneRuler™ DNA Ladder Mix	Thermo Fisher Scientific, Waltham, MA, USA
GlutaMax™ (100x)	Thermo Fisher Scientific, Waltham, MA, USA
Glycerol	Merck, Darmstadt
Glycine	SERVA, Heidelberg
Hydrogen peroxide	Merck, Darmstadt
Iodoacetamide	Merck, Darmstadt
Isofluran	CP Pharma, Burgdorf
Isopropanol	Merck, Darmstadt
Liberase™	Sigma-Aldrich, Taufkirchen
Lipopolysaccharide (LPS)	Sigma-Aldrich, Taufkirchen
Luminol sodium salt	VWR, Radnor, PA, USA
Lysogeny broth with agar (LB-broth)	SERVA GmbH, Heidelberg
Methanol	Merck, Darmstadt
Methyl-α-D-mannopyranosid	Sigma-Aldrich, Taufkirchen
Monopotassium phosphate ($KH(PO_4)_2$)	Sigma-Aldrich, Taufkirchen
MOPS	Sigma-Aldrich, Taufkirchen
NativeMark™ Unstained Protein Standard	Life Technologies, Carlsbad, USA
N,N,N´,N´-Tetraacetylethylenediamine (TEMED)	AppliChem GmbH, Darmstadt
Opti-MEM reduced serum medium	Thermo Fisher Scientific, Schwerte
Opti-PRO™ SFM serum-free	Thermo Fisher Scientific, Schwerte
PageRuler™ Prestained Protein ladder	Thermo Fisher Scientific, Waltham, MA, USA
Paraformaldehyde solution (PFA)	Morphisto, Frankfurt am Main
Penicillin	Sigma-Aldrich, Taufkirchen
Phenol red	Merck, Darmstadt
Phosphoric Acid	Carl Roth, Karlsruhe
Polyethyleneimin, Branched, (PEI 25K™)	Sigma-Aldrich, Taufkirchen
Polyethyleneimin, Linear, (PEI 25K™)	Polysciences, Warrington, PA, USA

Potassium Phosphate, dibasic (K_2HPO_4)	Sigma-Aldrich, Taufkirchen
Potassium Phosphate, monobasic (KH_2PO_4)	Sigma-Aldrich, Taufkirchen
Propargyl-PEG3-aminooxy	BroadPharm, San Diego, CA, USA
RPMI 1640	Thermo Fisher Scientific, Waltham, MA, USA
Saponin	Sigma-Aldrich, Taufkirchen
Skimmed milk powder	Heirler-Cenovis GmbH, Radolfzell
Sodium ascorbate (SAsc)	Sigma-Aldrich, Taufkirchen
Sodium chloride (NaCl)	Sigma-Aldrich, Taufkirchen
Sodium dodecyl sulfate (SDS)	SERVA GmbH, Heidelberg
Sodium hydroxide (NaOH)	Sigma-Aldrich, Taufkirchen
Sodium thiocyanate	Sigma-Aldrich, Taufkirchen
Streptomycin (Strep)	Sigma-Aldrich, Taufkirchen
Sucrose	PanReac AppliChem, Darmstadt
Sulfosuccinimidyl-trans-4-(N-maleimidomethyl)cyclohexane-1-carboxylate (sulfo-SMCC)	Merck, Darmstadt
SUNBRIGHT® ME-400CA (GSL)	NOF Corporation, Tokyo, Japan
Super optimal broth with glucose (SOC)	Thermo Fischer Scientific, Schwerte
Tetraethylorthosilicate (TEOS)	Sigma-Aldrich, Taufkirchen
Tris(hydroxymethyl)aminomethane (TRIS)	Carl Roth, Karlsruhe
TRIS-HCl	Merck, Darmstadt
Tris(3-hydroxypropyltriazolylmethyl)amine	Sigma-Aldrich, Taufkirchen
Trypanblue	Thermo Fisher Scientific, Schwerte
Trypsin	Gerbu, Heidelberg
Tween-20	AppliChem GmbH, Darmstadt
Ultra Pure™ Agarose	Invitrogen, Carlsbad, USA
Ultrapure ELGA LabWater	Purelab, Celle

Table 6) Buffers

Buffer / Solution	**Composition**
0.1 % Saponin in PBS (Permeabilization Buffer)	100 mL DPBS 100 µL Saponin
10x Transfer buffer	30.3 g Tris 144.2 g glycine ad 1 L H_2O
2 % skimmed milk solution	20 g/L skimmed milk powder in PBS/T
2x oxime labeling buffer	500 mM NaOAc in H_2O (ad pH 4.5)
35 % Sucrose solution	17.5 g sucrose ad 50 mL DPBS
5 % skimmed milk solution	50 g/L skimmed milk powder in PBS/T

6x SDS sample buffer	10 mL 1.5 M Tris-HCL pH 6.8 3.78 g glycerol 1.9 g SDS 0.93 g DTT 600 µL 0.2 % bromphenol blue in 50 mM EDTA
70 % Ethanol	70 mL Ethanol 30 mL H_2O
ACK Buffer	100 nM NH_4Cl 1 mM $KHCO_3$ 1 mM EDTA in H_2O
Bacteria Lysis Buffer	10 mL 10 % SDS 10 mL 2 M NaOH
Bacteria Neutralization Buffer	1.32 M Potassium acetate ad 500 mL H_2O (adjusted with acetic acid to pH 4.8 - 6.0)
Bacteria Resuspension Buffer	5 mL 1 M Tris pH 7.5 2 mL 0.5 M EDTA 10 mg RNAse A 93 mL H_2O
Click reaction MasterMix	60 µL 20 mM $CuSO_4$ 120 µL 50 mM THPTA
Click reaction (nanoparticles)	50 µL oxime ligation mix 7.5 µL Click reaction MasterMix 25 µL 11 g/L AGHC 25 µL 20 g/L SAsc 25 µL nanoparticle suspension 367 µL 0.1 M K_2PO_4 (pH 7.0)
Click reaction (nanoparticles)	50 µL oxime ligation mix 7.5 µL Click reaction MasterMix 25 µL 11 g/L AGHC 25 µL 20 g/L SAsc 2.5 µL 10 mM AlexaFluor®-488-azide 390 µL 0.1 M K_2PO_4 (pH 7.0)
ELISA coating buffer	15 mM Na_2CO_3 35 mM $NaHCO_3$ in H_2O (pH 9.6)
Endotoxin removal buffer A	12.5 mL 1 M MOPS (pH 7.0) 37.5 mL 5 M NaCl 25 mL Triton-X 100 50 mL isopropanol ad 250 mL H_2O
Endotoxin removal buffer B	100 mL 1 M NaAc (pH 5.0) 150 mL 5 M NaCl 10 mL Triton-X 100 ad 1 L H_2O
Enhanced chemiluminescence solution (ECL solution)	10 mL Solution A 100 µL Solution B 3.4 µL Hydrogen peroxide (30 %)
FACS Buffer	1 % BSA 1 mM EDTA in DPBS
Fixation buffer	50 mL 4 % PFA 50 mL DPBS

Gel Fixation buffer	600 mL H_2O 300 mL 98 % ethanol 100 mL acetic acid
K_2PO_4 buffer (0.1 M; pH 7.0)	61.5 mL 1 M K_2HPO_4 38.5 mL 1 M KH_2PO_4 900 mL H_2O
Lectin elution buffer	19.5 g Methyl-α-mannopyranosid 100 mL Lectin washing buffer
Lectin washing buffer	500 mL DPBS 1 mM EDTA and 1 mM EGTA
MACS Buffer	1 % BSA 1 mM EDTA in DPBS
MACS Dissociator Buffer	0.5 % BSA 2 mM EDTA in DPBS
Oxime ligation (gel shift)	2x oxime ligation buffer 6 µg Env 500 µM gel shift linker ad 50 µL H_2O
Oxime ligation (propargyl-PEG_3-aminooxy)	2x oxime ligation buffer 6 µg Env 125 µM / 250 µM / 500 µM linker ad 50 µL H_2O
Oxime ligation (reporter assay)	2x oxime ligation buffer 6 µg Env 500 µM AlexaFluor®-488-hydroxylamine ad 50 µL H_2O
PBS/T	0.1 % Tween-20 in DPBS without bivalent cations
PEI stock	10 mg/mL in H_2O for transfection 1:10 diluted in H2O
Phosphate buffered saline (PBS/O)	8 g NaCl 1.15 g Na_2HPO_4 x $2H_2O$ 0.2 g KH_2PO_4 0.2 g KCl in 1 L H_2O, pH 7.3
SDS running buffer	25 mM Tris 192 mM glycine 0.1 % SDS in H2O
SDS Separating gel 8 %	4.7 mL H_2O 2.6 mL 30 % acrylamide/bis solution 2.5 mL 1.5 M Tris (pH 8.8) 0.1 mL 10 % SDS 0.1 mL APS 0.004 mL TEMED
SDS Separating gel 10 %	4.0 mL H_2O 3.3 mL 30 % acrylamide/bis solution 2.5 mL 1.5 M Tris (pH 8.8) 0.1 mL 10 % SDS 0.1 mL APS 0.004 mL TEMED

SDS Separating gel 12 %	3.3 mL H_2O 4.0 mL 30 % acrylamide/bis solution 2.5 mL 1.5 M Tris (pH 8.8) 0.1 mL 10 % SDS 0.1 mL APS 0.004 mL TEMED
Solution A for ECL	0.1 M Tris-HCl (pH 8.6) 250 mg/L luminol sodium salt in 100 mL H_2O
Solution B for ECL	110 mg p-coumaric acid 50 mL DMSO
Stacking gel	1.4 mL H_2O 0.33 mL 30 % acrylamide/bis solution 0.25 mL 1.5 M Tris (adjust to pH 6.8) 20 µL SDS 10 % 20 µL APS 2 µL TEMED
TBE Buffer	10.8 g/L Tris 5.5 g/L H_3BO_4 2 mM EDTA in H_2O
Transfer buffer with methanol	100 mL methanol 100 mL 10x Transfer buffer 800 mL H20
Trypsin-EDTA	0.12 % Trypsin 0.5 mM EDTA 0.0005 % Phenol red in PBS

Table 7) Media

Medium	**Composition**
D0 (Serum-free)	500 mL DMEM 5.5 mL GlutaMax
D1.5 (1.5 % FCS)	500 mL DMEM 7.5 mL FCS 1 mL Pen/Strep 5.5 mL GlutaMax
D10 (10 % FCS)	500 mL DMEM 50 mL FCS 1 mL Pen/Strep 5.5 mL GlutaMax
Fluoromount-G™ Mounting Medium	Thermo Scientific, Schwerte
FreeStyle™ 293 Expression Medium	Thermo Scientific, Schwerte
Freezing medium	10 % DMSO in FCS
LB medium	10 g/L Pepton from Casein 5 g/L Yeast-Extract 5 g/L NaCl in H_2O, pH 7.2
R0	500 mL RPMI 1640 5.5 mL GlutaMax

R10	500 mL RPMI 1640 50 mL FCS 5.5 mL GlutaMax 5.5 mL HEPES 1 % Pen/Strep 500 µL 2-Mercaptoethanol
SOC Medium	20 g/L Bacto Trypton 5 g/L Bacto Yeast Extrakt 500 mg/L NaCl 186 mg/L KCl (from 100x solution) in H_2O, pH 7; autoclave When cooled down, add: 200 mg/L $MgCl_2$ $6H_2O$ (from 200x solution) 3.6 g/L D(+) Glucose (from sterile 50x solution)
Solid Agar	36 g Bacto-agar in 1 L LB medium (prior to autoclaving) autoclaving 20 min (121°C) after cooling down to 50°C, add antibiotic

Table 8) Antibodies

Name	Clone	Host, isotype	Manufacturer
17b		Human	NIH, Bethesda, MD, USA
2G12		Human	Polymun Scientific, Klosterneuburg, Austria
anti-goat/sheep IgG (HRP)	polyclonal	Rabbit	Dianova, Hamburg
anti-gp120		Goat	Acris Antibodies GmbH, Herford
anti-His		Mouse	Dianova, Hamburg
anti-human IgG (AlexaFluor®-488)	polyclonal	Goat	Jackson Immuno Research, West Grove, PA, USA
anti-human IgG (AlexaFluor®-647)	M1310G05	Rat, IgG2a	Biolegend, San Diego, CA, USA
anti-human IgG (HRP)	polyclonal	Goat	Dianova, Hamburg
anti-human/mouse CD44 (FITC)	IM7	Rat, IgG2b	eBioscience, Waltham, MA, USA
anti-mouse IgG (HRP)	polyclonal	Goat	Dianova, Hamburg
anti-mouse IgG1 (HRP)		Goat	Southern Biotech, Birmingham, AL, USA
anti-mouse IgG2c (HRP)		Goat	Southern Biotech, Birmingham, AL, USA
anti-mouse CD4 (BV 650)	RM4-5	Rat, IgG2a	Biolegend, San Diego, CA, USA
anti-mouse CD11c (PerCP)	N418		Biolegend, San Diego, CA, USA
anti-mouse CD16/CD32	93	Rat IgG2a	eBioscience, Waltham, MA, USA
anti-mouse CD19 (PE-Cy7)	1D3	Rat, IgG2a	BD Pharmingen, Franklin Lakes, NJ, USA
anti-mouse CD19 (PerCP)	6D5		Biolegend, San Diego, CA, USA
anti-mouse CD19 (Qdot 655)	6D5		Molecular Probes, Eugene, OR, USA
anti-mouse CD25 (APC)	PC61	Rat, IgG1	BD Pharmingen, Franklin Lakes, NJ, USA

anti-mouse CD28	37.51	Golden Syrian Hamster IgG	eBioscience, Waltham, MA, USA
ati-mouse CD40 (PE)		Rat	eBioscience, Waltham, MA, USA
anti-mouse CD4 (FITC)	GK1.5	Rat IgG2b	BD Pharmingen, Franklin Lakes, NJ, USA
anti-mouse CD44 (APC)	IM7	Rat IgG2b	BD Pharmingen, Franklin Lakes, NJ, USA
anti-mouse CD45R/B220 (APC)		Rat	BD Pharmingen, Franklin Lakes, NJ, USA
anti-mouse CD45R/B220 (PE-Cy7)	RA3-6B2	Rat IgG2a	BD Pharmingen, Franklin Lakes, NJ, USA
anti-mouse CD62L (APC)		Rat	eBioscience, Waltham, MA, USA
anti-mouse CD62L (PE)	MEL-14	Rat, IgG2a	BD Pharmingen, Franklin Lakes, NJ, USA
anti-mouse CD69 (PE-Cy7)	H1.2F3	Armenian Hamster, IgG	eBioscience, Waltham, MA, USA
anti-mouse CD80 (APC)	16-10A1	Armenian Hamster, IgG2	BD Biosciences, Franklin Lakes, NJ, USA
anti-mouse CD80 (FITC)		Armenian Hamster, IgG	eBioscience, Waltham, MA, USA
anti-mouse CD86 (FITC)	GL-1		Biolegend, San Diego, CA, USA
anti-mouse IFN-γ (PE)	XMG1.2	Rat IgG1	eBioscience, Waltham, MA, USA
anti-mouse IL-2 (APC)	JES6-5H4		eBioscience, Waltham, MA, USA
anti-mouse IL-4 (AlexaFluor®-488)	11B11	Rat IgG1	eBioscience, Waltham, MA, USA
anti-mouse MHC-II (APC eFluor 780)		Rat	eBioscience, Waltham, MA, USA
anti-mouse TNF-α (PE-Cy7)	MP6-XT22	Rat IgG1	eBioscience, Waltham, MA, USA
anti-p24		Mouse	Überla lab
b12		Human	NIH, Bethesda, MD, USA
PG16		Human	NIH, Bethesda, MD, USA
PG9		Human	NIH, Bethesda, MD, USA
PGT145		Human	NIH, Bethesda, MD, USA
TRES567hu		Humanized	Antonia Sophia Peter

Table 9) Proteins

Name	**Application**	**Provider**
conS.gp140.CFI.avi	ELISA standard	Dr. Jamie Peacock, Duke University, Durham, NC, USA
p24	ELISA standard	Aalto Bio Reagents, Dublin, Ireland
BG505 NFL gp140-His (Env-His_8)	Nanoparticle functionalization	self-made
BG505 NFL gp140-LCTPSR (Env-Ald_6)	Nanoparticle functionalization	self-made

Table 10) Enzymes

Name	Buffer	Manufacturer
AgeI-HF	NEBuffer rCutSmart	New England BioLab Inc., Ipswich, USA
BamHI-HF	NEBuffer rCutSmart	New England BioLab Inc., Ipswich, USA
DpnI	NEBuffer rCutSmart	New England BioLab Inc., Ipswich, USA
EcoRI	NEBuffer rCutSmart	New England BioLab Inc., Ipswich, USA
Glu-C	Glu-C buffer	New England BioLab Inc., Ipswich, USA
HindIII-HF	NEBuffer rCutSmart	New England BioLab Inc., Ipswich, USA
Ligase	T4 DNA Ligase Buffer	New England Biolabs, Frankfurt am Main
NcoI	NEBuffer rCutSmart	New England BioLab Inc., Ipswich, USA
NheI-HF	NEBuffer rCutSmart	New England BioLab Inc., Ipswich, USA
Phusion High-Fidelity DNA-Polymerase	Phusion HF Buffer	Thermo Fisher Scientific, Schwerte
SmaI	NEBuffer rCutSmart	New England BioLab Inc., Ipswich, USA
Sph-I	NEBuffer rCutSmart	New England BioLab Inc., Ipswich, USA
Taq DNA-Polymerase	Taq Buffer	Genaxxon Bioscience, Ulm
XbaI-HF	NEBuffer rCutSmart	New England BioLab Inc., Ipswich, USA

Table 11) Peptides

Name	Sequence	Application
p30	FNNFTVSFWLRVPKVSASHLE	Nanoparticle encapsulation

Table 12) Vaccines and Adjuvants

Name	Manufacturer
CpG	Eurofins MWG Operon, Ebersberg
Tetanol®pur	Novartis Vaccines and Diagnostics, Marburg

Table 13) Cells and Bacteria

Strain	Genotype	Source
DH10B E. coli	Δ(ara-leu) 7697 araD139 fhu ΔlacX74 galK16 galE15 e14- φ80dlacZΔM15 recA1 relA1 endA1 nupG rpsl (StrR) rph spoT1 Δ(mrr-hsdRMS-mcrBC)	New England BioLab Inc., Ipswich, USA
HEK293T	human Ad5/SV40 (T)-transformed kidney epithelial cells	DSMZ, Leibniz Institut, Braunschweig
HEK293F	human Ad5/SV40 293 F-transformed kidney epithelial cells	Thermo Fisher Scientific, Waltham, MA, USA
HeLa		CLS Cell Lines Service GmbH, Eppelheim
STBL2 E. coli	F-mcrA Δ(mcrBC-hsdRMS-mrr) recA1 endA1longyrA96 thisupE44 relA1 λ- Δ(lac-proAB)	Invitrogen, Waltham, MA, USA
XL10-Gold E. coli	TetrD(mcrA)183 D(mcrCB-hsdSMR-mrr)173 endA1 supE44 thi-1 recA1 gyrA96 relA1 lac Hte [F´ proAB lacIqZDM15 Tn10 (Tetr) Amy Camr]	Stratagene, San Diego, CA, USA

Table 14) Primers

Name	Sequence	Application
CMV_fwd	5'-CGCAAATGGGCGGTAGGCGTG-3'	Sequencing
BG505_seq_1	5'-CGAGCTGCGAGACAAGAAAC-3'	Sequencing
BG505_seq_2	5'-ACCTGGAAGTGACAACTCAC-3'	Sequencing
BG505_seq_3	5'-GTTTCTGGGAGCCGCTGG-3'	Sequencing
conB_seq_1	5'-CCTGCTGAACACCAACTC-3'	Sequencing
conB_seq_2	5'-GATCGTGAAGAAGCTGCGC-3'	Sequencing
BGH_rev	5'-TAGAAGGCACAGTCGAGG-3'	Sequencing
BG505_seq_as1	5'-CACTCTTCGTTTAGCGCGGG-3'	Sequencing
BG505_seq_as2	5'-CTGAAGGGCAGGGTCCTG-3'	Sequencing
BG505_seq_as3	5'-GCTCCACCATATTGTTCTTCC-3'	Sequencing
BG505_gp41del_fwd	GGGAGCGGAGGAGGAGGCAGCCACCATCAT CACCACCATCACCATTGA	Removal of gp41 ectodomain
BG505_gp41del_rev	GTGGTGATGATGGTGGCTGCCTCCTCCTCCG CTCCC	Removal of gp41 ectodomain
LCTPSR_fwd	CTCCCTGTGCACCCCCTCCCGGTGATAAGCT TAAGTTTAAACCGCTGATCAGC	Replacment of His_8 with Ald_6
LCTPSR_rev	AGCTTATCACCGGGAGGGGGTGCACAGGGA GCCTCCTCCGCCATC	Replacment of His_8 with Ald_6

Table 15) Plasmids

Plasmid	Application	Supplier
pBG505-NFL-gp120-His	Purification control	self-made
pBG505-NFL-gp140-His	Env-His_8 production	Prof. Dr. Rich Wyatt
pBG505-NFL-gp140-Ald_6	Env-Ald_6 production	self-made
pBG505-NFL-gp140-G/TMCD	VLP Production	self-made
pcDNA3.1-hSUMF1	FGE overexpression	AddGene
pConB-gp140opt-GCD	Template for cloning	Dr. Ghulam Nabi
pHgpsyn	VLP production	Prof. Dr. Klaus Überla
pHgpsyn-TTp30	VLP production	Dr. Vladimir Temchura

Table 16) Kits

Name	Manufacturer
AlexaFluor™ 647 Protein Labeling Kit	Thermo Fisher Scientifc, Schwerte
B cell Isolation Kit, mouse	Miltenyi Biotec, Bergisch Gladbach
CD11c MicroBeads, mouse	Miltenyi Biotec, Bergisch Gladbach
CD4+ T cell Isolation Kit, mouse	Miltenyi Biotec, Bergisch Gladbach
Mouse IL-4 Ready-Set-Go!™ Kit	Thermo Fisher Scientific, Schwerte
Mouse IL-5 Ready-Set-Go!™ Kit	Thermo Fisher Scientific, Schwerte
NativePAGE™ Novex Bis-Tris Gel System	Life Technologies, Carlsbad, USA
Pierce™ BCA Protein Assay Kit	Thermo Fisher Scientific, Waltham, MA, USA
Pierce™ Silver Stain Kit	Thermo Fisher Scientific, Waltham, MA, USA
PureLink™ HiPure Plasmid Maxiprep Kit	Thermo Fisher Scientific, Waltham, MA, USA
QuikChange II Site-directed Mutagenesis Kit	Agilent Technologies, Santa Clara, CA, USA

Table 17) Mice

Animal	Genotype	Supplier
BCR-transgenic PGT121 mice	B6(Cg)-Tyrc-2J/JMutH121	Prof. Dr. Michel Nussenzweig
C57bl/6NRj mice	*a (a/a)* non agouti	Janvier, Le Genest-Saint-Isle, France

4.2. Methods

4.2.1. Molecular biology

4.2.1.1. Transformation of competent bacteria

A mixture of 10 µL XL10-Gold ultracompetent bacteria and 500 ng DNA was incubated on ice for 10 min. Uptake of DNA was initiated by a 35 s heat shock in a 42°C water bath followed by a 1 min return on ice. 300 µL SOC medium were then added and the transformed cells were incubated for 1 h at 37°C and 330 rpm. Small volumes of the bacterial suspension were plated on agar dishes supplemented with an antibiotic that matches the resistance encoded by the transformed plasmid DNA. After overnight incubation at 37°C, bacterial colonies were picked and transferred to 5 mL aliquots of LB medium with matching antibiotic resistance. The suspensions were further incubated at 37°C and 330 rpm for subsequent small-scale DNA isolation (4.2.1.2), sequencing and glycerol stocking (4.2.1.3).

4.2.1.2. Plasmid DNA isolation

Small-scale DNA mini-preparation

1.5 mL of grown bacterial suspension were transferred into 1.5 mL reaction tubes and centrifuged for 3 min at 8000 rpm. After resuspension of the cell pellets in 100 µL Bacteria Resuspension Buffer, 100 µL of Bacteria Lysis Buffer were added and the mixtures were carefully inverted 5 – 10 times. 5 min later, another 100 µL of Bacteria Neutralization Buffer were added and the tubes were again mixed by inversion and incubated for 10 min on ice. Cell debris was pelleted by centrifugation for 15 min at 15000 rpm. The supernatants were transferred into fresh reaction tubes. 300 µL isopropanol were added respectively. The mixtures were thoroughly vortexed and centrifuged again under the same conditions. The pellets were washed with 300 µL ethanol (70 %) and centrifuged a third time. The

supernatants were then discarded and the pellets were dried for 10 min, before being resuspended in 50 µL TE buffer.

Large-scale DNA maxi-preparation

Plasmid DNA from 250 mL grown bacterial culture was isolated using the PureLink™ HiPure Plasmid Maxiprep Kit following manufacturer's guidelines. DNA concentration was defined by NanoDrop measurement at 260 nm absorption.

4.2.1.3. DNA quality control

Digestion and agarose gel electrophoresis

Isolated plasmid DNA was digested with various restriction enzymes and separated on agarose gels to check for proper plasmid content and PCR products. All enzymes were used in excess compared to the amount of DNA and had optimal performance at 37°C in the presence of CutSmart buffer. Digestion reactions at final volumes of 20 µL consisting of 1 µg DNA, 2 µL 10x CutSmart buffer, 1 µL of each enzyme and water were incubated for 2 h at 37°C. The reactions were then supplemented with 4 µL of 6x Purple Loading Dye and separated via agarose gel electrophoresis. Agarose gels were prepared by boiling a suspension of 1 % (w/v) UltraPure™ Agarose in 100 mL TBE buffer. The liquid gel was cooled down to room temperature and 10 mg/mL ethidium bromide were added. The gel was poured into an electrophoresis chamber with a matching comb. After polymerization, the gel was covered in TBE buffer, 12 µL Loading Dye-supplemented DNA were loaded into each pocket and a voltage of 130 V was applied. DNA fragments were finally detected with a Quantum ST5 Imaging System. The fragment size was evaluated by comparison with a DNA standard ladder (GeneRuler 1 kb).

Sequencing

Env open-reading frames of recombinant plasmids were further quality-checked by sequencing. Four forward primers (CMV_fwd, BG505_seq_1, BG505_seq_2, BG505_seq_3) as well as four reverse primers (BGH_rev, BG505_seq_as1, BG505_seq_as2, BG505_seq_as3) were used to obtain two antiparallel, full-length sequences of the Env-encoding region. Sequencing reactions consisting of 500 ng DNA and 0.5 pmol/µL sequencing primer (Table 14) in a total volume of 8 µL H_2O were sent to Macrogen Europe (Amsterdam, Netherlands). Sequences were analyzed with SnapGene software.

Bacterial glycerol stocks

Glycerol stocks of plasmid DNA-containing, bacterial cultures, that were quality-controlled as described above, were produced by mixing the bacterial suspension 1:1 (v/v) with previously autoclaved glycerol. The glycerol stocks were then stored at -80°C and further used for inoculation of LB medium for DNA preparation.

4.2.1.4. Cloning of recombinant Env constructs

Plasmid information and cloning strategies

All recombinant constructs encoding soluble forms of Env were produced by mutagenesis PCR. The vector pBG505-NFL-gp140-His [76] was used as the basis for two recombinant variants used in this study, i) pBG505-NFL-gp120-His and ii) pBG505-NFL-gp140-Ald$_6$. i) A mutagenesis PCR with the primer pair BG505_gp41del_fwd and BG505_gp41del_rev was performed to remove the nucleotides coding for the gp41 ectodomain. The primers are designed to connect the nucleotides encoding the central 2x G$_4$S flexible linker with the C-terminal His-tag in order to pass over the gp41 region during DNA amplification, resulting in a construct coding for a monomeric gp120 with a C-terminal flexible linker and His-tag (pBG505-NFL-gp120-His). ii) The nucleotide sequence coding for the aldehyde tag (Ald$_6$; LCTPSR) was optimized to human codon usage according to the GenScript Codon Usage Frequency Chart (www.genscript.com). The primer pairs LCTPSR_fwd and LCTPSR_rev contain the optimized sequence (ctgtgcacccctcccgg) between the nucleotides for the C-terminal G$_4$S linker and the stop codon. Amplification of pBG505-NFL-gp140-His with these primers results in a PCR product in which the 8x His-tag nucleotides are replaced by the aldehyde-tag sequence (pBG505-NFL-gp140-Ald$_6$).

Additionally, a plasmid coding for a membrane-embedded BG505 Env trimer (pBG505-NFL-gp140-G/TMCD) was provided by Dr. Ghulam Nabi. Here, the Env-encoding sequence of pBG505-NFL-gp140-His was fused to a nucleotide sequence coding for the transmembrane and cytoplasmic domains of VSV-G (aa 52 – 122 from Genbank entry CAA24524.1). The basis of this construct was the previously published vector pHEL-GCD [221]. The plasmid pHgpsyn-TTp30 was kindly provided by Dr. Hassan Elsayed and Dr. Vladimir Temchura [224]. This construct codes for codon-optimized HIV-1 GagPol. The nucleotides encoding the

Tetanus Toxoid-derived peptide p30 (FNNFTVSFWLRVPKVSASHLE) were recombinantly introduced into the Gag ORF inbetween the sequences for p17 (matrix protein) and p24 (capsid protein). The backbone of all used plasmids is pcDNA3.1.

Mutagenesis PCR

The QuikChange II Site-directed Mutagenesis Kit was used to generate pBG505-NFL-gp120-His, while the C-terminal aldehyde-tag was introduced utilizing the Phusion High-Fidelity PCR Kit. pBG505-NFL-gp140-His served as template DNA for both PCR reactions (Table 18). After amplification, 2 µL DpnI was added to each reaction. The samples were incubated for 5 min at 37°C to digest the parental, non-mutated supercoiled DNA. 5 µL of the mixtures were analyzed by agarose gel electrophoresis (4.2.1.3). XL10-Gold ultracompetent bacteria were transformed with 20 µL, 10 µL and 5 µL of the reaction mixtures for DNA preparation (4.2.1.2), glycerol stocking and quality sequencing (4.2.1.3).

Table 18) Mutagenesis PCR

PCR Kit	PCR reaction	Thermocycler protocol	
QuikChange	37.5 µL H_2O 5 µL 10x QuikChange reaction buffer 1 µL DNA (~ 500 ng) 1.5 µL BG505_gp41del_fwd (~ 150 ng) 1.5 µL BG505_gp41del_rev (~ 150 ng) 1 µL dNTP mix (10 mM) 1.5 µL QuikSolution reagent 1 µL QuikChange Lightning polymerase	1. 95°C 2. 95°C 3. 60°C 4. 68°C 5. GoTo 2 (17x) 6. 68°C 7. 4°C	120 s 20 s 10 s 30 s / kb 300 s hold
Phusion	23 µL H_2O 10 µL 5x Phusion GC buffer 2 µL DNA (~ 1 µg) 2 µL LCTPSR_fwd (~ 200 ng) 2 µL LCTPSR_rev (~ 200 ng) 8 µL dNTP mix (2.5 mM) 2.5 µL DMSO 0.5 µL Phusion™ polymerase	1. 98°C 2. 98°C 3. 45 - 61°C 4. 72°C 5. GoTo 2 (34x) 6. 72°C 7. 12°C	60 s 30 s 30 s 240 s 600 s hold

4.2.2. Cytology

4.2.2.1. Cell culture and transfection

Adherent HEK293T cells

HEK293T cells were cultured as monolayers in cell culture flasks at 37°C in incubators adjusted to 65 % humidity and 5% CO_2 in D10 medium. Upon reaching 80 – 95 % confluency, the medium was discarded and the cells were manually washed off with fresh D10 and split into fresh cell culture flasks. For transfection of HEK293T cells, a confluency of 70 – 90 % was required and the medium was exchanged with D0 medium. 10 µg DNA / 25 cm^2 cells were diluted in D0 medium (1.5 mL D0 per 175 cm^2 flask) and a threefold excess of linear PEI was added. After thorough mixing, the solutions were incubated for 15 min at RT for formation of PEI:DNA complexes and were finally dripped equally onto the cell monolayer. 6 h later, the supernatant was replaced with D1.5 medium to remove PEI. Supernatant of transfected cells was harvested 48 – 72 h after transfection.

HEK293F suspension cells

Suspension-adapted HEK293F cells are widely used for the expression of large amounts of soluble Env trimers [55,59,61]. The cells were cultivated with Freestyle™ 293 expression medium (FMe) in disposable PETG Erlenmeyer flasks in a shaking incubator at 150 rpm, 37°C and 65 % humidified air supplemented with 8 % CO_2. Thrice a week, the culture was controlled for bacterial contamination by inoculation of 4 mL LB medium or FCS with 200 µL HEK293F supernatant. The cell density was monitored using a Neubauer cell counting chamber and was constantly kept between 0.3 – 3 x 10^6 cells/mL. Reduction of cell density was done by discarding a fraction of cell suspension and replacing the missing volume with fresh medium. HEK293F cells were transfected at an optimal density of 1 x 10^6 cells/mL. 1 µg DNA per mL cell culture was diluted together with a threefold excess of linear PEI in OptiPro-SFM, mixed, incubated for 15 min at RT and finally added to the cell suspension. After 6 h incubation in the shaking incubator, the cells were centrifuged at 300 g and modest temperature. The PEI-containing supernatant was discarded and the cells were resuspended in the same volume of fresh FMe. The supernatant of transfected cells was harvested after 72 h for further Env purification.

HeLa cell culture

HeLa cells were cultivated by Kathrin Kostka in D10 medium at 37°C in 5 % CO_2 atmosphere.

4.2.2.2. Isolation of primary immune cells from mice

Preparation of splenocytes

All steps except erythrocyte lysis (RT) and collagenase treatment (37°C) were performed with ice-cold buffers. Centrifugation of primary cells was done for 3 min at 12°C and 300 g. Animals were sacrificed by cervical dislocation, before the spleens and/or lymph nodes were removed. The spleens were generally homogenized in ice-cold MACS Dissociator Buffer (1 – 3 organs in 3 mL) by mixing with a gentleMACS™ Dissociator. The splenocytes were then filtered through a 70 µm strainer, centrifuged and washed with R10 medium. The cells were warmed to RT, centrifuged again and resuspended in 1 mL ACK buffer per spleen for erythrocyte lysis. After 8 min incubation at RT, the lysis suspension was filled up to 30 mL with R10 to stop the reaction. The cells were washed once with R10 and were finally resuspended in 1 mL medium per spleen. An aliquot of splenocytes was diluted 1:100 in R10 and the cell density was analyzed using the Countess™ Automated cell counter. The isolated splenocytes were filled up to 15 mL with MACS buffer, centrifuged and resuspended in a volume of MACS buffer dependent on the total cell count and the magnetic cell separation kit.

B cells

B cells from splenocytes of both *wt* C57bl/6NRj and PGT121 B cell receptor-transgenic mice were purified using the murine B cell isolation kit (Miltenyi Biotec) according to the manufacturer's protocol. The kit's antibody beads bind and immobilize all splenocyte-derived immune cells except B cells (negative selection). Thus, the B cell fraction ran through the MACS column after loading, was collected, centrifuged and resuspended in R10 on ice. The cell concentration was determined as described above.

T helper cells

CD4+ T cells were purified as described for B cells by negative selection from splenocytes using the murine CD4+ T cell isolation kit (Miltenyi Biotec) following manufacturer's instructions.

Dendritic cells

For DC isolation, the spleens were pre-treated with Liberase™ to dissolve the cell tissue. To this end, the spleens were placed in 12-well plates filled with Liberase™. Liberase™ was additionally injected into the spleens with syringes. The spleens were then cut into pieces and incubated for 45 min at 37°C. The remaining tissue as well as the cell suspension was then manually filtered through 70 µm strainers followed by splenocyte preparation as described above. DCs were finally purified using the murine CD11c MicroBeads (Miltenyi Biotec) following the manufacturer's protocol. Here, DCs were bound by the magnetic beads, immobilized on the magnetic column and flushed out with 2 x 5 mL MACS buffer (positive selection).

Lymph nodes

Inguinal, axial and popliteal lymph nodes were isolated from animals and manually homogenized with 70 µm cell strainers in R10. The lymphocytes were then counted using the Countess™ Automated cell counter (Thermo Fisher).

4.2.2.3. Characterization of CaPs by cell culture methods

CaPs coupled with fluorescently-labeled Env trimers (AlexaFluor®-647-Env-Ald_6/FGE) were characterized via microscopy by Kathrin Kostka. Fluorescent imaging was done with a Keyence Biorevo BZ-9000 fluorescence microscope using both a GFP-B filter (Ex. 470/40 nm, DM 495 nm, BA 535/50 nm) and a TRITC filter (Ex. 540/25 nm, DM 565 nm, BA 605/55 nm). Confocal microscopy was done with a Leica TCS SP8X FALCON (Imaging Center Campus, Essen) using laser wavelengths of 405 nm, 488 nm and 647 nm as well as a pulsed laser WLL (470-670 nm) and an HC PL APO UVIS CS2 63X/1.2 water immersion lens.

Fluorescence microscopy

5 x 10^4 HeLa cells were seeded in 0.5 mL medium per well in 24-well plates and incubated for 12 h to allow cell adhesion to the culture flask. 30 µL CaP NPs coupled with fluorescently-labelled Env were added to the cells and the co-culture was incubated for 7 h in the cell incubator. The cells were then washed three times with DPBS to remove any remaining nanoparticles in the supernatant. Fresh D10 medium was added and the cells were incubated again for 24 h. Afterwards, the uptake of the nanoparticles was evaluated by fluorescence microscopy.

Confocal laser scanning microscopy

5 x 10^4 HeLa cells were seeded in 250 µL D10 per well in 6-well plates with poly-D-lysine-coated glass coverslips and incubated for 24 h, before 30 µL of CaPs coupled with fluorescently-labeled Env trimers were added. The cells were incubated for another 24 h, washed three times with DPBS and fixated with 150 µL PFA per well (3.7 % stock). After 15 min fixation at RT, the cells were washed again and then incubated with 230 µL AlexaFluor®-488 phalloidin (1:40 in DPBS supplemented with 1 % BSA) per well for 20 min at RT for actin staining. The cells were washed two times and further incubated in 230 µL Hoechst 33342 solution (1:10000 in DPBS) for 15 min to stain the cell nuclei. The wells were washed thrice again. The coverslips with the cell samples were fixed on slides using Fluoromount-G™ mounting medium. Finally, actin and nuclear staining as well as nanoparticle-derived fluorescent signals were imaged with a confocal microscope.

4.2.2.4. *In vitro* B cell activation

MACS-purified B cells from both *wt* C57bl/6NRj and BCR-transgenic PGT121 mice were seeded in 96-well U-bottom plates (2 x 10^5 cells per well) in 100 µL R10 medium. Lyophilized CaPs were reconstituted in H_2O, vortexed and ultrasonicated. Dilution series (1:5) of CaPs in R10 were made ranging from 2000 ng/mL to 0.64 ng/mL bulk Env. 100 µL of each dilution were added to the B cells, respectively. Additional cell samples were incubated in the presence of 200 ng/mL soluble Env trimers (negative control) or 1000 ng/mL LPS (positive control). As another positive control, both *wt* and PGT121 B cells were incubated with Env-VLPs (200 ng/mL bulk Env). After overnight incubation, the 96-well plate was centrifuged for 3 min at 300 g and the supernatants were discarded. The cells were washed once with 200 µL FACS buffer, centrifuged again and were then resuspended in FACS buffer containing 1:400-diluted Fixable Viability Dye, either 1:300-diluted anti-CD19-Qdot655 or anti-CD45R/B220-APC (both directed against B cell surface markers) as well as 1:300-diluted early activation marker antibody anti-CD69-PE-Cy7. After 30 min incubation on ice, the cells were washed thrice with 300 µL FACS buffer, respectively. The cells were finally resuspended in 300 µL FACS buffer, transferred into FACS tubes and measured on a benchtop BD™ LSR II flow cytometer. Unstained cells were used as mock control. Analysis of activation in living B cells was done with FlowJo software.

4.2.3. Protein biochemistry

4.2.3.1. Expression and purification of soluble Env trimers

Expression of Env was induced by transient transfection of HEK293F suspension cells with Env-encoding plasmids pBG505-NFL-gp140-His (Env-His_8), pBG505-NFL-gp120-His (Env-His_8-gp120) or pBG505-NFL-gp140-Ald_6 (Env-Ald_6). Alternatively, cells were co-transfected with pBG505-NFL-gp140-Ald_6 and pcDNA3.1-hSUMF1 (Env-Ald_6/FGE) in a ratio of 2:1 to overexpress FGE and optimize Fgly conversion. The supernatant was harvested 2 - 3 d after transfection. Cell debris was removed by centrifugation. The sterile-filtered (0.2 µm) supernatant was then run over an equilibrated affinity column packed with agarose-bound *Galanthus nivalis* lectin (GNL) by gravity flow. The lectin column was washed with three column volumes of Lectin washing buffer. Env was then eluted with two column volumes of Lectin elution buffer and immediately concentrated by Amicon 10 kDa ultrafiltration. Here, the Amicon tube was refilled with PBS/O in consecutive centrifugation steps to re-buffer Env. The lectin column was washed multiple times with elution and washing buffer to remove any remaining protein and to equilibrate the resin. The final Env concentration was defined by UV/Vis spectroscopy using a NanoDrop™ adjusted to a wavelength of 280 nm and an extinction coefficient of 113090 $M^{-1}cm^{-1}$. In order to monitor and quantify the coupling of Env trimers to calcium phosphate nanoparticles, Env-Ald_6 was labeled with AlexaFluor®-647 using protein labeling kits (Thermo Fisher) that target primary amines on the antigen.

4.2.3.2. NativePAGE and silver stain

The analysis of the native conformation of purified Env proteins was done using the NativePAGE™ Novex Bis-Tris Gel System (Thermo Fisher). 2 µg of protein were mixed with 7 µL 4x sample buffer and 0.5 µL 5 % G-250 sample additive. PBS/O was added to a total volume of 28 µL per sample. 4 – 16 % NativePAGE™ Bis-Tris gels were placed in gel running chambers. The combs were removed and the pockets were filled with Light Blue cathode buffer. 15 µL of each sample as well as NativeMark™ Unstained Protein Ladder diluted 1:20 in PBS/O were loaded onto the gels. The chamber was filled in the back of the gel with NativePAGE™ running buffer working as anode buffer. The front was carefully filled

with Light Blue cathode buffer not to disturb the loaded samples. Native gels were run for 2 h under 180 V at RT, since SOSIP NFL Env trimers are stable up to 62.5°C. After the run, the gels were incubated overnight in Gel Fixation Buffer to remove unconjugated coomassie. The separated protein bands were then visualized by gel treatment with silver nitrate using the Pierce Silver Stain Kit following manufacturer's instructions. Gel images were made with an Intas Advanced Fluorescence Imager, while placing the gel on a light table.

4.2.3.3. SDS-PAGE and Western Blot analysis

The molecular size and antigenicity of Env and VLP components as well as the conjugation of Env-Ald_6 with 40 kDa GSL were analyzed by reducing SDS-PAGE and subsequent Western Blot using 12 % polyacrylamide gels. 1 µg soluble Env or 300 ng Env on VLPs were mixed with 8 µL 6x SDS loading buffer and PBS/O in total volumes of 48 µL. The samples were boiled for 15 min at 95°C and 300 rpm. 45 µL of each sample as well as 8 µL PageRuler™ Prestained Protein Ladder were loaded onto the gels, which were then run for 45 min at 130 V in SDS running buffer. Following gel electrophoresis, the proteins were transferred onto 0.45 µm nitrocellulose membranes with a semi-dry technique enclosed by three Whatman papers on both sides using SDS transfer buffer supplemented with 10 % methanol. After transfer for 90 min at 45 mA per 54 cm^2 blotting area, the membranes were blocked by incubation in 5 % skimmed milk in PBS/T for 1 h at RT. Subsequently, the membranes were incubated overnight at 4°C with Acris polyclonal goat-anti gp120 antibody diluted 1:2000 in 2 % skimmed milk in PBS/T, then washed 3x with PBS/T for 10 min and finally incubated with Dianova HRP-coupled anti-goat IgG antibody diluted 1:5000 in 2 % skimmed milk in PBS/T for 1 h at RT. After another three washing cycles, the membranes were developed by incubation in ECL solution followed by imaging with an Intas Advance Fluorescence Imager in the dark. For gel shift analysis, 8 % polyacrylamide gels were used and run for 2 h at 80 V to avoid gel disruption by excessive gel shift linker. In the case of VLP analysis, the membranes were washed and blocked again after imaging. The membranes were then incubated first with a hybridoma mouse anti-p24 (1:2000) and Dianova HRP-coupled anti-mouse IgG as secondary antibody (1:5000) with subsequent imaging following the same protocol as described above.

4.2.3.4. Deglycosylation of Env

Lectin-purified Env samples were deglycosylated using a glycerol-free PNGase F kit (NEB) under denaturing reaction conditions. 20 µL Env (1 mg/mL stock) were mixed with 2.5 µL 10x Denaturing Buffer and 2.5 µL H_2O and incubated for 10 min at 97°C. The reaction was chilled on ice, before 3.3 µL 10x GlycoBuffer2 and 3.3 µL 10 % NP-40 and 1.4 µL glycerol-free PNGase F were added. The mixture was incubated for 1 h at 37°C. Env was then concentrated and re-buffered with PBS/O by Amicon 30 kDa ultrafiltration to remove PNGase F (~ 36 kDa) and retain deglycosylated Env (~ 70 kDa). Deglycosylation was verified by SDS-PAGE and Western Blot.

4.2.3.5. Oxime ligation

The covalent reaction of two reagents, one with a terminal aldehyde group and another with a terminal aminooxy group, forms an oxime molecule. Oxime ligations with aldehyde-tagged Env proteins were performed with different binding partners for analytical and nanoparticle-coupling applications. If not indicated otherwise, standard oxime reactions were composed of 6 µg Env and 10 mM aminooxy-terminated reagent in a total volume of 50 µL 2x oxime binding buffer (pH 4.5) in PBS/O. The samples were incubated for 6 h at 37°C and 300 rpm. Variations in incubation time, pH value and reagent concentration were used for optimization experiments.

Oxime reporter assay with AlexaFluor®-647-hydroxylamine

The specificity of oxime ligations with aldehyde-tagged Env was addressed in a fluorescent reporter assay using aminooxy-terminated AlexaFluor®647-hydroxylamine as binding partner. Control reactions with Env-His_8 in the presence or absence of AlexaFluor®-647-hydroxylamine were additionally done. After incubation, the whole ligation samples were loaded onto 10 % polyacrylamide gels and separated by SDS-PAGE. The gel electrophoresis was performed in the dark and stopped before the lower protein fraction containing unconjugated dye ran out of the gel. This fraction was then cut off. The remaining gel containing the fluorescently labeled Env fraction was washed several times in SDS running buffer and imaged with the Advanced Fluorescence Imager exposing 150 ms with red light in the dark.

Gel Shift

6 µg Env-His_8, Env-Ald_6 or Env-Ald_6/FGE were used for oxime reactions in the presence or absence of 500 µM 40 kDa gel shift linker (GSL, ME-400CA). This linker consists of a long PEG chain with a terminal aminooxy group (AO-$[PEG]_n$). After incubation at oxime ligation conditions, all samples were diluted 1:6 in PBS/O and prepared for SDS-PAGE and subsequent Western Blot.

Ligation with Propargyl-PEG_3-AO linker (Coupling Step-One)

Lypophilized Propargyl-PEG_3-aminooxy was reconstituted in ultrapure water at a concentration of 500 mM, aliquoted and stored at -20°C as stock solutions. Pre-dilutions were made 1:100 in PBS/O and stored for several weeks at 4°C. 500 µM, 250 µM or 125 µM Propargyl-PEG_3-AO were used in oxime ligations with 6 µg Env in total reaction volumes of 50 µL at pH 4.5 for subsequent click reaction reporter assays with AlexaFluor®488-azide. Oxime ligations to prepare linker-bound, aldehyde-tagged Env (lnkr-(Env-Ald_6/FGE)) for subsequent nanoparticle coupling were solely done with 125 µM Propargyl-PEG_3-AO and Env-Ald_6/FGE at pH 4.5 overnight. The total reaction volume was proportionally adapted to the amount of Env. Furthermore, lnkr-(Env-Ald_6/FGE) was concentrated and re-buffered with PBS/O by Amicon 10 kDa ultrafiltration, before Step-Two of the coupling procedure was done. Mock ligations without Propargyl-PEG_3-AO were done as controls. Fluorescently-labeled Env was used in oxime ligations for later tracing of nanoparticles by fluorescence microscopy (4.2.2.3).

4.2.3.6. Copper-catalyzed azide-alkyne cycloaddition (Click reaction)

After the oxime ligation of aldehyde-tagged Env and Propargyl-PEG_3-AO, the resulting linker-bound trimers bear C-terminal alkyne groups that can be harnessed for copper-catalyzed azide-alkyne cycloaddition (Click reaction). This reaction was performed in a reporter assay using AlexaFluor®-488-azide as well as for the final nanoparticle coupling (Step-Two) using calcium phosphate nanoparticles with surface-functionalized azide groups.

Click reaction reporter assay

1 M $CuSO_4$ stock solution was pre-diluted 1:50 in water. 60 µL of this solution were mixed with 120 µl aqueous THPTA (50 mM) to obtain a master mix containing total concentrations of 33.3 mM THPTA and 6.6 mM $CuSO_4$. The master mix was

incubated for at least 10 min at RT. Afterwards, several reagents were added to previously prepared oxime reactions of Env with Propargyl-PEG_3-AO linker (total volume 50 µL) in the following order: 7.5 µL $CuSO_4$/THPTA master mix, 25 µL aminoguanidine hydrochloride (100 mM stock), 25 µL sodium ascorbate (100 mM stock), 2.5 µL AlexaFluor®-488-azide (10 mM stock) and 390 µL potassium phosphate buffer (pH 7.0). The click reactions were incubated for 1 h at 37°C and 300 rpm. Then, 50 µL click reaction mixture were supplemented with 10 µL 6x SDS loading buffer, boiled for 10 min at 95°C and loaded onto 10 % SDS gels. As previously described for the oxime ligation reporter assay, electrophoresis was stopped before unconjugated dye ran out of the gel. The upper and lower gel parts were cut off and the gel fragments containing the Env fractions were washed in SDS running buffer. Fluorescent signals were detected by 150 ms exposure with blue light using an Advanced Fluorescence Imager.

Click reaction of linker-bound Env with CaP/PEI/SiO_2-N_3 (Coupling Step-Two)

The conditions for click reactions of alkyne-terminated reagents to the surface of azide-functionalized were optimized by Rojas-Sánchez *et al.* [119] and applied by Kathrin Kostka. 3.65 µL of an aqueous solution containing 40 µM $CuSO_4$ and 200 µM THPTA were prepared and incubated for 10 min at RT. 38.5 µL aminoguanidine solution (1 mg/mL stock), 36.5 µL sodium ascorbate (100 mM stock) and 0.35 µL NaOH (100 mM stock) as well as 25 µL linker-conjugated Env (1 mg/mL stock) were added. The reagent solution was mixed with 0.5 mL CaP/PEI/SiO_2-N_3 nanoparticle dispersion and stirred for 1 h at RT in the dark.

4.2.3.7. Conformational ELISA

Conformational ELISAs were performed in opaque, white 96-well plates. The wells were coated with 100 µL murine anti-His antibody diluted 1:400 in PBS/O. The plates were sealed with adhesive plastic sheets and incubated overnight at 4°C. Volumes of Env-His_8 solutions were mixed with equal volumes of 2x oxime labeling buffer adjusted to pH 3.0, pH 4.5, pH 5.0 and pH 5.5, respectively, and incubated for 24 h at 37°C and 300 rpm. Env-His_8 was additionally incubated with PBS/O at pH 7.0 as control. All samples were then filled with PBS/O (pH 7.0) to a final Env concentration of 1.5 µg/mL. The neutralization of the former acidic environment was verified using pH indicator paper. The ELISA plates were washed three times with PBS/O, before 300 µL 5 % skimmed milk in PBS/O were added in

each well for blocking. After 2 h incubation at RT, the wells were washed again, 100 µL of the differently treated Env-His_8 samples were added (150 ng Env per well) and the plates were incubated for another 2 h at RT. Meanwhile, serial dilutions of trimer-specific apex antibodies PG9, PG16 and PGT145 as well as of glycan patch antibody 2G12 in PBS/O ranging from 10 – 0.15 µg/mL were prepared. The wells were washed thrice again. The antibody dilutions were added and the plates were incubated for 1 h at RT. After washing, the wells were finally incubated for 1 h at RT in the dark with a 1:5000 dilution of HRP-coupled anti-human IgG secondary antibody. The plates were washed six times with PBS/O. Finally, 60 µL ECL solution were added per well followed by the measurement of the relative light units per second [RLU/s] using an Orion Microplate Luminometer.

4.2.3.8. Mass spectrometry analysis of the formylglycine conversion rate

The relative amount of Fgly residues within the aldehyde-tags at the C-terminus of Env was analyzed by mass spectrometry. Preparation, measurement and bioinformatical analysis were done by PD Dr. Sabrina Gensberger-Reigl. PNGase-treated and untreated Env samples were re-buffered with 100 mM tris(hydroxymethyl)aminomethane hydrochloride buffer (pH 7.8) by Amicon ultrafiltration. Disulfides were reduced with 5 mM DTT. The alkylation of thiols was induced with 18 mM iodoacetamide. The samples were then treated with Glu-C for enzymatic hydrolysis (Glu-C:Env = 1:50) at 37°C overnight. After stopping the reaction by addition of formic acid, the samples were first vacuum-dried and then reconstituted in 2 % acetonitrile containing 0.1 % formic acid to a final concentration of 0.7 µg/µL Env. Peptide analysis was done by reversed phase micro liquid chromatography with an Ultimate 3000 RS system coupled to a timsTOF Pro mass spectrometer equipped with an electrospray ionization source in PASEF mode. Gradient elution (eluent A: 0.1 % formic acid, eluent B: acetonitrile containing 0.1 % formic acid) was applied on a YMC Triart C18 column operated at 35°C and a flow rate of 15 µL/min. The eluent mixture was changed in the course of operation time (time [min] / % eluent B: 0 / 2, 15 / 45, 15.5 / 80, 20 / 80, 20.1 / 2, 30 / 2). Ion spectra were analyzed with PEAKS® XPro software and the AUC of corresponding extracted ion chromatograms were used to calculate the percentage of Fgly conversion (Rabuka *et al.* [286], conversion rate [%] = (AUC Fgly-aldehyde + AUC Fgly-diol) ⁄ (AUC Fgly-aldehyde + AUC Fgly-diol + AUC LC(+57.02)TPSR) x 100).

4.2.4. Nanoparticle preparation and characterization

4.2.4.1. VLP expression, purification and quantification

Virus-like Env-VLP-p30 particles were expressed in HEK293T cells by transient co-transfection with plasmids coding for Env (pBG505-NFL-gp140-G/TMCD) and a Gag-p30 fusion protein (pHgpsyn-TTp30) in a 1:1 ratio. The cell supernatant containing VLPs was harvested 60 – 72 h after transfection and cell debris was removed by centrifugation for 10 min at 1000 g. The supernatant was subsequently 0.45 µm sterile-filtered and carefully layered on 5 mL 35 % sucrose diluted in PBS/O in polypropylene ultracentrifuge tubes. The VLPs were then pelletized by ultracentrifugation for 2.5 h at 28000 g. The supernatant was discarded completely and the VLPs were resuspended in PBS/O and aliquoted. The aliquots were shock-frozen in liquid nitrogen and stored at -80°C. Control VLPs containing only Env and Gag (Env-VLP) were purified equally after co-transfection of cells with pBG505-NFL-gp140-G/TMCD and pHgpsyn.

The amount of Env and Gag in different VLP batches was determined by ELISA. To this end, 1:5 serial dilutions of VLPs as well as 1:2 serial dilutions of both recombinant conS.gp140.CFI.avi and recombinant HIV-1 Gag p24 protein were prepared in ELISA Coating Buffer. In total, the VLP dilution series ranged from 1:20 to 1:12500, while the Env and Gag standard rows contained starting concentrations of 1000 ng/mL and ended with 0.1 ng/mL. Opaque MaxiSorp plates were coated overnight at 4°C with 100 µL VLP or standard dilution per well. On the next day, the plates were washed three times with PBS/T and the wells were blocked with 300 µL 5 % skimmed milk in PBS/T for 2 h at RT. The blocking reagent was discarded and the wells were incubated either with 100 µL human 2G12 antibody (100 ng/well) for Env detection or with 100 µL of a 1:2000 purified hybridoma mouse anti-p24 antibody for Gag detection. Both primary antibodies were diluted in PBS/T supplemented with 2 % skimmed milk. After incubation for 1 h at RT, the wells were washed three times with PBS/T. 100 µL of 1:5000 dilutions of HRP-conjugated anti-human IgG and anti-mouse IgG in 2 % skimmed milk in PBS/T were added to the respective wells. Again, the plates were incubated for 1 h at RT in the dark. The wells were washed six times with PBS/T. 60 µL house-made ECL solution were added in each well. The relative light units per second (RLU/s) were immediately measured by an Orion Microplate Luminometer. Point-to-point curves of the

standard dilutions were created with GraphPad Prism 7 software. Both the Env and Gag concentrations in different VLP batches were calculated from these curves.

4.2.4.2. Synthesis and characterization of calcium phosphate nanoparticles

General information

Calcium phosphate nanoparticles (CaPs) were produced by Dr. Leonardo Rojas-Sanchez and Kathrin Kostka. The particles were centrifuged at RT or ultracentrifuged at -20°C with a 5430/5430 R centrifuge and a Sorvall WX Ultra Series centrifuge, respectively. Sonication was done using a UP50H Sonotrode N7 with a 70 % amplitude and a pulse duration of 0.8 s. A Zetasizer Nano ZS with a laser wavelength of λ = 633 nm was used for DLS and zetapotential measurement with the Smoluchowski approximation. The calcium concentration in particle batches was defined by AAS with an M-Series AA spectrometer after sample aliquots were dissolved in diluted HCl. Assuming a spherical morphology and hydroxyapatite to be the prevalent calcium phosphate component, the particle concentration is calculated from the Ca^{2+} concentration and the hydroxyapatite density. The amount of antigen coupled to the nanoparticle surface was determined by UV-Vis spectroscopy with AlexaFluor®-488-labelled Env. A detailed description of the calculation procedure to obtain these characterization data is described in Rojas-Sanchez *et al.* (2019) [119]. UV-Vis absorption was either measured with a NanoDrop DS-11 FX+ spectrophotometer or with a Varian Cary 300 Bio spectrophotometer using a 400 µL Suprasil® quartz cuvette. The nanoparticles were immobilized on grids with gold/palladium for scanning electron microscopy (SEM) performed either with an ESEM Quanta 400 instrument or with an Apreo S LoVac microscope. Endotoxin levels in different CaP batches were measured with an Endosafe Nexgen-PTS handheld spectrophotometer. Finally, nanoparticle aliquots were shock-frozen in liquid nitrogen and lyophilized (72 h, 0.31 mBar, -10°C) with a Christ Alpha 2-4 LSC device using D-(+)-trehalose dihydrate (20 mg per 1 mL NP dispersion) as anti-freeze protector. The aliquots were reconstituted with H_2O immediately before usage in downstream assays or immunizations. All preparations and analyses were done with ultrapure water at RT if not indicated otherwise. Furthermore, all buffers were sterile-filtered before use.

Cap/PEI/SiO_2-SH and rCaPs

5 mL calcium lactate solution (18 mM stock, pH 10.0), 5 mL diammonium hydrogen phosphate (10.8 mM stock, pH 10.0) and branched PEI (2 g/L stock, Mw = 25 kDa) were simultaneously pumped in the course of 1 min into a vessel containing 20 mL ultrapure water and stirred for 20 min to form CaP/PEI nanoparticles. For the synthesis of adjuvanted (rCaP-CpG) or peptide-containing (rCaP-p30) CaPs, 40 µL CpG solution (1 mg/mL stock) or 60 µL p30 peptide (1 mg/mL stock) were added to 1 mL CaP/PEI nanoparticle dispersion and stirred for 30 min. The CaP/PEI nanoparticles were further stabilized by a silica shell coating. To this end, 1 mL CaP/PEI NP dispersion was mixed with 4 mL ethanol, 5 µL tetraethylorthosilicate and 10 µL ammonia solution. After 16 h incubation at constant stirring, the resulting CaP/PEI/SiO_2 nanoparticles were obtained by ultracentrifugation for 30 min at 66,000 g and resuspension in 1 mL ultrapure water followed by ultrasonication to dissociate aggregates. 1 mL of CaP/PEI/SiO_2 NPs were added to a mixture of 4 mL ethanol and 50 µL (3-mercaptopropyl)-trimethoxysilane and stirred for 8 h to finally modify the particle surface with terminal thiol groups (CaP/PEI/SiO_2-SH). The nanoparticles were purified by ultracentrifugation as described above. Lectin-purified Env-His_8 trimers were coupled to the surface of CaP/PEI/SiO_2-SH NPs in a random manner (rCaPs) by targeting primary amines on Env with sulfo-SMCC crosslinkers that additionally react with the thiol groups on the CaP surface. To this end, 600 µL Env-His_8 were mixed with 300 µL aqueous sulfo-SMCC solution (1.78 mg/mL stock) and were incubated for 2 h at 4°C. After removal of unconjugated crosslinker by 3 kDa Amicon ultrafiltration, 330 µL sulfo-SMCC-bound Env-His_8 (1 mg/mL stock) were mixed with 4 mL CaP/PEI/SiO_2-SH NPs and incubated overnight at 4°C for final rCaP formation. The nanoparticles were centrifuged for 30 min at 21,000 g and 8°C. They were resuspended once with 1 mL H_2O, centrifuged again and were finally reconstituted in 4 mL H_2O and subsequently ultrasonicated.

CaP/PEI/SIO_2-N_3 and oCaPs

First, CaP/PEI/SiO_2 nanoparticles were produced as described above. As requirement for subsequent orthogonal Env coupling, the nanoparticle surface was functionalized with terminal azide groups. To this end, 1 mL CaP/PEI/SiO_2 NP dispersion was mixed with 4 mL ethanol and 15 µL (3-azidopropyl)triethoxysilane and 5 µL aqueous ammonia solution and incubated for 8 h at RT under constant

stirring. As previously described, the resulting CaP/PEI/SiO_2-N_3 nanoparticles were purified by ultracentrifugation (66,000 g, 30 min) and reconstitution in 0.5 mL H_2O. Linker-bound Env (lnkr-(Env-Ald_6) or lnkr-(Env-Ald_6/FGE)) was then orthogonally conjugated to the particle surface (oCaPs) by copper-catalyzed azide-alkyne cycloaddition as described in 4.2.3.6. The oCaPs were purified by centrifugation for 30 min at 5,000 rpm and 8°C. The supernatant was discarded and the oCaPs were redispersed and ultrasonicated in 0.5 mL ultrapure water. Coupling controls were done either with Env-His_8 or with aldehyde-tagged Env in the absence of propargyl-PEG_3-AO linker.

4.2.4.3. Nanoparticle characterization by flow cytometry

Lyophilized rCaPs and oCaPs were reconstituted with PBS/O up to the initial aliquot volume. 30 µL nanoparticle solution were mixed with 30 µL primary antibody solution (2 µg/mL stock) and incubated for 30 min at 4°C. The used antibody panel comprised both trimer-specific apex antibodies (PG9, PGT145) and a CD4 binding site antibody (b12) as well as a SARS-CoV-2-specific antibody (TRES567hu) as isotype control. 240 µL secondary, AlexaFluor®-647-coupled anti-human-IgG (0.25 µg/mL stock) were added to each sample. After 15 min incubation at 4°C in the dark, the nanoparticles were measured for antibody binding with a benchtop BD™ LSR II flow cytometer and evaluated using the FlowJo software. Unstained CaPs were used as mock control.

4.2.5. Immunology

4.2.5.1. Ethical statement

All animal experiments were approved by an external ethics committee of the North Rhine-Westphalian Ministry for Nature, Environment and Consumer Protection (license AZ 84-02.04.2014. A191), additionally acknowledged by the Government of Lower Franconia (license 55.2-2532-2-96) and were carried out in accordance with the EU Directive 2010/63/EU. The mice were housed in the Franz-Penzoldt-Center (Faculty of Medicine, Friedrich-Alexander-Universität Erlangen, Germany) under specifications of the national law and were handled following guidelines of the Federation of European Laboratory Animal Science Associations. Wildtype (*wt*) C57bl/6NRj mice were obtained from Janvier. PGT121 mice [287] were provided by Dr. Michel Nussenzweig (The Rockefeller University, New York City, USA) and bred in the Franz-Penzoldt-Center. All immunized *wt* mice were female, while PGT121 B cells from both male and female mice were used.

4.2.5.2. Mouse immunizations and collection of blood

Mice were 6 – 10 weeks old at the time of the first immunization. All animals were immunized by intramuscular injections in both hind legs using Micro-Fine™ Insulin syringes. The injection volume per leg did not exceed 30 mL. 100 – 150 µL of blood were collected from the retrobulbar venous plexus using non-heparinized glass capillaries (minicaps®) prior to the start of the experiment (naïve blood) and 2 – 3 weeks after each immunization. Blood was collected in BD Microtainer® tubes and the serum fraction was isolated by centrifugation for 5 min at 5000 rpm. Sera were stored at -20°C. Both immunizations and blood collection were performed under constant isoflurane anesthesia.

Induction of intrastructural help

Mice were immunized with the licensed vaccine Tetanol®pur diluted 1:10 in sterile DPBS for the induction of Tetanus-specific CD4+ T cell responses (ISH group) or with DPBS alone (control group) in week 0 and week 4. The mice were then boosted either with rCaP, rCaP-p30, rCaP-CpG or Env-VLP-p30 diluted in sterile DPBS in week 8, 12 and 16. The vaccine doses were normalized to the amount of Env. Thus, one mouse received a total of 10 µg Env on CaPs or 300 ng Env on VLPs, respectively.

Comparison between rCaPs and oCaPs

Mice were vaccinated in week 0 with CpG-adjuvanted rCaPs or oCaPs diluted in sterile DPBS and normalized to a total of 3 µg Env on CaPs per mouse.

4.2.5.3. Analysis of humoral immune responses

Opaque, white 96-well MaxiSorp plates were coated overnight at 4°C with 100 µL per well of 1 ng/µL Env-His_8 in ELISA Coating Buffer. To prevent evaporation, the plates were sealed with sticky plastic cover slides during incubation. The wells were washed thrice with 300 µL PBS/T and were blocked with 300 µL 5 % skimmed milk in PBS/T for 2 h at RT. The blocking suspension was then replaced with 100 µL mice sera diluted 1:100 – 1:1000 in 2 % skimmed milk in PBS/T. After 1 h incubation at RT, the wells were washed thrice with PBS/T. 100 µL per well of HRP-coupled secondary anti-mouse IgG antibody diluted 1:4000 in 2 % skimmed milk in PBS/T were added to evaluate the total Env-specific immune response. HRP-coupled anti-mouse IgG1 or IgG2c antibodies were added to address the IgG subtype responses in immunized mice. The wells were incubated in the presence of secondary antibodies for 1 h at RT. The plates were finally washed six times with PBS/T. 60 µL house-made ECL solution were added per well and the plates were immediately measured with an Orion microplate luminometer evaluating the relative light units per second (RLU/s) in each well. Background RLU/s levels were evaluated in wells that were coated with Env and only incubated with secondary antibodies, but not with sera (secondary antibody controls).

4.2.5.4. Analysis of cellular immune responses

The mice participating in the intrastructural help immunization trial were sacrificed in week 18. The spleens were isolated and the splenocytes were purified as described above. The cellular immune responses against both p30 and Env were analyzed by cytokine profiling with two different assays: intracellular cytokine staining (ICS) and cytokine ELISA. For both assays 1 x 10^6 purified splenocytes were seeded in U-bottom 96-well plates in a total volume of 100 µL R10 medium. At least six wells were seeded with the splenocytes from each mouse (mock-stimulation, p30-stimulation, Env-stimulation for both ICS and cytokine ELISA, respectively). 100 µL of different stimulation solutions were added to the wells. All stimulation mixtures contained 4 µg/mL anti-CD28 superagonistic, T cell-activating

antibody. For subsequent ICS, 6 µg/mL intracellular protein trafficking inhibitor Brefeldin A was additionally added to the mix. For stimulation of Tetanus-specific T helper cells, 10 µg/mL p30 peptide was included and the equal volume of DMSO in the mock-stimulation solution. Since there are no immunodominant MHC-II-restricted Env peptides identified for restimulation of C57bl/6 splenocytes, an alternative restimulation approach was established. PGT121 B cells were purified from B cell receptor-transgenic mice. 1 x 10^6 B cells per mL were incubated for 3 h at 37°C and 5 % CO_2 atmosphere with Env-VLPs at a bulk Env concentration of 0.2 µg/mL. As control, PGT121 B cells were incubated with the equal amount of ΔEnv-VLPs normalized to the Gag concentration. During this incubation time the Env-VLPs are taken up by the Env-specific B cells in a B cell receptor-dependent manner. The nanoparticles are processed within the cells and both Gag- as well as Env-derived peptides are presented by MHC-II molecules on the cell surface. After the incubation time, the B cells were centrifuged and washed twice in R10 to remove any remaining VLPs. The cells were finally resuspended in 330 µL R10 and mixed with 330 µL of a Master mix containing 8 µg/mL anti-CD28 and optionally 12 µg/mL Brefeldin A in R10 to finally obtain the Env-stimulation solution. 100 µL of this Env-stimulation solution containing 1.5 x 10^5 B cells were added to the splenocytes.

Intracellular cytokine staining (ICS)

The induction of Th1-associated cytokines interferon gamma (IFN-γ), tumor necrosis factor alpha (TNF-α) and interleukin-2 (IL-2) was analyzed by ICS. To this end, splenocytes were stimulated for 6 h with stimulation solutions including Brefeldin A in order to block any cellular release of produced cytokines. The cells were pelletized and resuspended in 70 µL FACS Buffer supplemented with 1:50 diluted anti-CD16/CD32 antibody to block any Fc receptor molecules on the cell surface. After incubation for 15 min at 4°C, the wells were filled with 180 µL FACS Buffer. The plate was centrifuged and the cells were washed with 200 µL FACS Buffer. After another centrifugation cycle, the cells were resuspended in 70 µL FACS Buffer supplemented with anti-mouse CD4 BV650 (1:300 dilution) and Fixable Viability Dye eFluor450 (1:400 dilution) antibodies and incubated on ice for 30 min in the dark. 130 µL FACS Buffer were added, the cells were centrifuged and resuspended in Fixation Buffer. After 20 min incubation at RT in the dark, the fixed cells were washed twice with FACS Buffer. Subsequently, the cells were

resuspended in Permeabilization Buffer and incubated for 10 min at RT in the dark. After another centrifugation step, the cells were resuspended in 70 µL Permeabilization Buffer supplemented with the antibodies anti-mouse IL-2 APC, anti-mouse IFN-y PE and anti-mouse TNF-α PE-Cy7 (all 1:300 diluted) and incubated for 30 min on ice protected from light. The cells were then washed twice with Permeabilization Buffer and once with FACS Buffer, before they were finally resuspended in 250 µL FACS Buffer and transferred into FACS tubes. The accumulation of Th1 cytokines in CD4 T cells was analyzed by flow cytometry using a benchtop BD™ LSR II device. For data evaluation, the background values (mock for p30, ΔEnv-VLPs for Env-VLPs) were subtracted for each mouse.

Cytokine ELISA

Th2-associated interleukin-4 (IL-4) and interleukin-5 (IL-5) secretion was evaluated by colorimetric cytokine ELISAs using the Mouse IL-4 / IL-5 Uncoated ELISA kits according to the manufacturer's instructions. Splenocytes were stimulated in the absence of Brefeldin A for 60 h. The cells were pelletized and 100 – 150 µL of the conditioned supernatant containing the released Th2 cytokines IL-4 and IL-5 were harvested. Briefly, transparent MaxiSorp plates were coated with anti-mouse IL-4 or anti-mouse IL-5 capture antibodies overnight at 4°C. After washing, the wells were blocked with the kit's ELISA/ELISPOT diluent. Two-fold dilutions of recombinant mouse IL-4 and IL-5 standards were prepared. The wells were washed and both the standard rows as well as the harvested supernatants were added (100 µL/well) and incubated for 2 h. After thorough washing, biotin-conjugated anti-mouse IL-4 and IL-5 detection antibodies were added. Following incubation and washing, the wells were finally incubated with streptavidin-HRP for 30 min and thoroughly washed afterwards. Colorimetric signals were elicited by the addition of 100 µL TMB substrate and the reaction was stopped with 50 µL sulfuric acid (H_2SO_4). The signal intensity was detected using a Victor X4.

4.2.5.5. Data evaluation and statistical analyses

Analysis of data and generation of the corresponding graphs were done either with GraphPad Prism 7 or FlowJo software. Statistics were performed using GraphPad Prism 7 software as indicated in the Figure Legends.

5. Bibliography

1. Roychoudhury, S. *et al.* Viral Pandemics of the Last Four Decades : Pathophysiology, Health Impacts and Perspectives. *Int. J. Environ. Res. Public Health* **17**, 1–39 (2020).
2. Karcher, D. From HIV to Coronavirus Disease 2019 (COVID-19). *Arch Pathol Lab Med* **146**, 433–439 (2022).
3. Barré-Sinoussi, F. *et al.* Isolation of a T-Lymphotropic Retrovirus from a Patient at Risk for Acquired Immune Deficiency Syndrome (AIDS). *Science (80-.).* **220**, 868–871 (1983).
4. Barré-Sinoussi, F., Ross, A. L. & Delfraissy, J. Past, present and future: 30 years of HIV research. *Nat. Rev. Microbiol.* **11**, 877–883 (2013).
5. Popovic, M., Sarngadharan, M., Read, E. & Gallo, R. C. Detection, Isolation, and Continuous Production of Cytopathic Retroviruses (HTLV-III) from Patients with AIDS and Pre-AIDS. *Science (80-.).* **224**, 497–500 (1984).
6. Zhu, T. *et al.* An African HIV-1 sequence from 1959 and implications for the origin of the epidemic. *Nature* **391**, 10–13 (1998).
7. Sharp, P. M. & Hahn, B. H. Origins of HIV and the AIDS Pandemic. *Cold Spring Harb. Perspect. Med.* (2011).
8. Worobey, M. *et al.* Early HIV / AIDS history in North America. *Nat. Publ. Gr.* **539**, 98–101 (2016).
9. Sharp, P. M. *et al.* The origins of acquired immunodeficiency syndrome viruses : where and when ? *Philos Trans R Soc L. B Biol Sci* **356**, 867–876 (2001).
10. UNAIDS. Global HIV statistics. *UNAIDS Fact Sheet 2022* 1–6 (2022).
11. Reid, S. & Juma, O. A. Minimum infective dose of HIV for parenteral dosimetry. *Int. J. STD AIDS* **20**, 828–833 (2009).
12. McIntyre, J. Strategies to prevent mother-to-child transmission of HIV. *Curr. Opin. Infect. Dis.* **19**, 33–38 (2006).
13. Frankel, A. D. & Young, J. A. T. HIV-1: Fifteen proteins and an RNA. *Annu. Rev. Biochem.* **67**, 1–25 (1998).
14. Costin, J. M. Cytopathic mechanisms of HIV-1. *Virol. J.* **4**, 1–22 (2007).
15. Goonetilleke, N. *et al.* The first T cell response to transmitted/founder virus contributes to the control of acute viremia in HIV-1 infection. *J. Exp. Med.* **206**, 1253–1272 (2009).
16. Wilson, J. D. K. *et al.* Direct visualization of HIV-1-specific cytotoxic T lymphocytes during primary infection. *Aids* **14**, 225–233 (2000).
17. Tomaras, G. D. *et al.* Initial B-Cell Responses to Transmitted Human Immunodeficiency Virus Type 1: Virion-Binding Immunoglobulin M (IgM) and IgG Antibodies Followed by Plasma Anti-gp41 Antibodies with Ineffective Control of Initial Viremia. *J. Virol.* **82**, 12449–12463 (2008).
18. Decroly, E. *et al.* The convertases furin and PC1 can both cleave the human immunodeficiency virus (HIV)-1 envelope glycoprotein gp160 into gp120 (HIV-I SU) and gp41 (HIV-I TM). *J. Biol. Chem.* **269**, 12240–12247 (1994).
19. Checkley, M. A., Luttge, B. G. & Freed, E. O. HIV-1 Envelope Glycoprotein Biosynthesis, Trafficking, and Incorporation. *J. Mol. Biol.* **410**, 582–608 (2011).
20. Zhu, P. *et al.* Distribution and three-dimensional structure of AIDS virus envelope spikes. *Nature* **441**, 847–852 (2006).
21. Zanetti, G., Briggs, J. A. G., Grünewald, K., Sattentau, Q. J. & Fuller, S. D. Cryo-electron tomographic structure of an immunodeficiency virus envelope complex in situ. *PLoS Pathog.* **2**, 790–797 (2006).

22. Kwong, P. D. *et al.* Structure of an HIV gp120 envelope glycoprotein in complex with the CD4 receptor and a neutralizing human antibody. *Nature* **393**, 648–659 (1998).

23. Buzon, V. *et al.* Crystal structure of HIV-1 gp41 including both fusion peptide and membrane proximal external regions. *PLoS Pathog.* **6**, 1–7 (2010).

24. Wyatt, R. & Sodroski, J. The HIV-1 Envelope Glycoproteins: Fusogens, Antigens, and Immunogens. *Science (80-.).* **283**, 1148–1150 (1998).

25. Preston, B. D., Poiesz, B. J. & Loeb, L. A. Fidelity of HIV-1 reverse transcriptase. *Science (80-.).* **242**, 1168–1171 (1988).

26. Li, H. *et al.* Identification of an N-Linked Glycosylation in the C4 Region of HIV-1 Envelope gp120 That is Critical for Recognition of Neighboring CD4 T Cell Epitopes. *J. Immunol.* **180**, 4011–4021 (2008).

27. Leonard, C. K. *et al.* Assignment of intrachain disulfide bonds and characterization of potential glycosylation sites of the type 1 recombinant human immunodeficiency virus envelope glycoprotein (gp120) expressed in Chinese hamster ovary cells. *J. Biol. Chem.* **265**, 10373–10382 (1990).

28. Lyumkis, D. *et al.* Cryo-EM Structure of a Fully Glycosylated Soluble Cleaved HIV-1 Envelope Trimer. *Science (80-.).* **342**, 1484–1490 (2013).

29. McCoy, L. E. *et al.* Holes in the Glycan Shield of the Native HIV Envelope Are a Target of Trimer-Elicited Neutralizing Antibodies. *Cell Rep.* **16**, 2327–2338 (2016).

30. Wong, M. E., Jaworowski, A. & Hearps, A. C. The HIV reservoir in monocytes and macrophages. *Front. Immunol.* **10**, 1–16 (2019).

31. Chauveau, L. *et al.* HIV Fusion in Dendritic Cells Occurs Mainly at the Surface and is Limited by Low CD4 Levels. *J. Virol.* **91**, (2017).

32. Bruner, K. M. & Cohn, L. B. HIV-1 reservoir dynamics in CD4+ T cells. *Curr. Opin. HIV AIDS* **14**, 108–114 (2019).

33. Weissenhorn, W., Hinz, A. & Gaudin, Y. Virus membrane fusion. *FEBS Lett.* **581**, 2150–2155 (2007).

34. Thali, M. *et al.* Characterization of Conserved Human Immunodeficiency Virus Type 1 gp120 Neutralization Epitopes Exposed upon gp120-CD4 Binding. *J. Virol.* **67**, 3978–3988 (1993).

35. Alkhatib, G. *et al.* CC chemokine receptor 5-mediated signaling and HIV-1 co-receptor activity share common structural determinants. Critical residues in the third extracellular loop support HIV-1 fusion. *J. Biol. Chem.* **272**, 19771–19776 (1997).

36. Bieniasz, P. D. *et al.* HIV-1-induced cell fusion is mediated by multiple regions within both the viral envelope and the CCR-5 co-receptor. *EMBO J.* **16**, 2599–2609 (1997).

37. Wilen, C. B., Tilton, J. C. & Doms, R. W. HIV: Cell Binding and Entry. *Cold Spring Harb. Perspect. Med.* **2**, 6866–6866 (2012).

38. Lu, M. *et al.* Associating HIV-1 envelope glycoprotein structures with states on the virus observed by smFRET. *Nature* **568**, 415–419 (2019).

39. Pancera, M. *et al.* Structure and immune recognition of trimeric pre-fusion HIV-1 Env. *Nature* **514**, 455–461 (2014).

40. Munro, J. B. *et al.* Conformational dynamics of single HIV-1 envelope trimers on the surface of native virions. *Science (80-.).* **346**, 759–763 (2014).

41. Schiffner, T. *et al.* Chemical Cross-Linking Stabilizes Native-Like HIV-1 Envelope Glycoprotein Trimer Antigens. *J. Virol.* **90**, 813–828 (2016).

42. Sattentau, Q. Envelope Glycoprotein Trimers as HIV-1 Vaccine Immunogens. *Vaccines* **1**, 497–512 (2013).

43. Shi, B. *et al.* Comparative analysis of human and mouse immunoglobulin variable heavy

regions from IMGT/LIGM-DB with IMGT/HighV-QUEST. *Theor. Biol. Med. Model.* **11**, (2014).

44. Sanders, R. W. *et al.* HIV-1 neutralizing antibodies induced by native-like envelope trimers. *Science (80-.).* **349**, 154–165 (2015).

45. Gaschen, B. *et al.* Diversity Considerations in HIV-1 Vaccine Selection. *Science (80-.).* **296**, 2254–2360 (2002).

46. Wyatt R. *et al.* The antigenic structure of the HIV gp120 envelope glycoprotein. *Nature* **393**, 705–711 (1998).

47. Munro, J. B. & Mothes, W. Structure and Dynamics of the Native HIV-1 Env Trimer. *J. Virol.* **89**, 5752–5755 (2015).

48. Hu, J. K. *et al.* Murine Antibody Responses to Cleaved Soluble HIV-1 Envelope Trimers Are Highly Restricted in Specificity. *J. Virol.* **89**, 10383–10398 (2015).

49. Sheppard, H. W. Inactivated- or killed-virus HIV/AIDS vaccines. *Curr. Drug Targets - Infect. Disord.* **5**, 131–141 (2005).

50. Whitney, J. B. & Ruprecht, R. M. Live attenuated HIV vaccines: Pitfalls and prospects. *Curr. Opin. Infect. Dis.* **17**, 17–26 (2004).

51. Sanders, R. W. *et al.* Variable-Loop-Deleted Variants of the Human Immunodeficiency Virus Type 1 Envelope Glycoprotein Can Be Stabilized by an Intermolecular Disulfide Bond between the gp120 and gp41 Subunits. *J. Virol.* **74**, 5091–5100 (2000).

52. Binley, J. M. *et al.* A Recombinant Human Immunodeficiency Virus Type 1 Envelope Glycoprotein Complex Stabilized by an Intermolecular Disulfide Bond between the gp120 and gp41 Subunits is an Antigenic Mimic of the Trimeric Virion-Associated Structure. *J. Virol.* **74**, 627–643 (2000).

53. Sanders, R. *et al.* Stabilization of the Soluble, Cleaved, Trimeric Form of the Envelope Glycoprotein Complex of Human Immunodeficiency Virus Type 1. *J. Virol.* **76**, 8875–8889 (2002).

54. Khayat, R. *et al.* Structural Characterization of Cleaved, Soluble HIV-1 Envelope Glycoprotein Trimers. *J. Virol.* **87**, 9865–9872 (2013).

55. Sanders, R. W. *et al.* A Next-Generation Cleaved, Soluble HIV-1 Env Trimer, BG505 SOSIP.664 gp140, Expresses Multiple Epitopes for Broadly Neutralizing but Not Non-Neutralizing Antibodies. *PLos Pathog.* **9**, (2013).

56. Wu, X. *et al.* Neutralization Escape Variants of Human Immunodeficiency Virus Type 1 Are Transmitted from Mother to Infant. *J. Virol.* **80**, 835–844 (2006).

57. Rawi, R. *et al.* Automated Design by Structure-Based Stabilization and Consensus Repair to Achieve Prefusion-Closed Envelope Trimers in a Wide Variety of HIV Strains. *Cell Rep.* **33**, (2020).

58. Binley, J. M. *et al.* Enhancing the Proteolytic Maturation of Human Immunodeficiency Virus Type 1 Envelope Glycoproteins. *J. Virol.* **76**, 2606–2616 (2002).

59. Sharma, S. K. *et al.* Cleavage-Independent HIV-1 Env Trimers Engineered as Soluble Native Spike Mimetics for Vaccine Design. *CellReports* **11**, 539–550 (2015).

60. Bale, S. *et al.* Cleavage-independent HIV-1 trimers from CHO cell lines elicit robust autologous tier 2 neutralizing antibodies. *Front. Immunol.* **9**, 1–15 (2018).

61. Aldon, Y. *et al.* Rational Design of DNA-Expressed Stabilized Native-Like HIV-1 Envelope Trimers. *Cell Rep.* **24**, 3324–3338 (2018).

62. Cheng, C. *et al.* Immunogenicity of a Prefusion HIV-1 Envelope Trimer in Complex with a Quaternary-Structure-Specific Antibody. *J. Virol.* **90**, 2740–2755 (2016).

63. Van Schooten, J. *et al.* Antibody responses induced by SHIV infection are more focused than those induced by soluble native HIV-1 envelope trimers in nonhuman primates. *PLoS*

Pathog. **17**, 1–22 (2021).

64. Wagner, R. *et al.* Rev-independent expression of synthetic gag-pol genes of human immunodeficiency virus type 1 and simian immunodeficiency virus: Implications for the safety of lentiviral vectors. *Hum. Gene Ther.* **11**, 2403–2413 (2000).

65. Kang, C. Y., Luo, L., Wainberg, M. A. & Li, Y. Development of HIV/AIDS vaccine using chimeric gag-env virus-like particles. *Biol. Chem.* **380**, 353–364 (1999).

66. McBurney, S. P., Young, K. R. & Ross, T. M. Membrane embedded HIV-1 envelope on the surface of a virus-like particle elicits broader immune responses than soluble envelopes. *Virology* **358**, 334–346 (2007).

67. Deml, L., Speth, C., Dierich, M. P., Wolf, H. & Wagner, R. Recombinant HIV-1 Pr55gag virus-like particles: Potent stimulators of innate and acquired immune responses. *Mol. Immunol.* **42**, 259–277 (2004).

68. Deml, L., Wild, J. & Wagner, R. Virus-like Particles: A Novel Tool for the Induction and Monitoring of Both T-Helper and Cytotoxic T-Lymphocyte Activity. *Methods Mol. Med.* **94**, 133–157 (2004).

69. Wells, D. E. & Compans, R. W. Expression and characterization of a functional human immunodeficiency virus envelope glycoprotein in insect cells. *Virology* **176**, 575–586 (1990).

70. Deml, L. *et al.* Increased incorporation of chimeric human immunodeficiency virus type 1 gp120 proteins into Pr55(gag) virus-like particles by an Epstein-Barr virus gp220/350-derived transmembrane domain. *Virology* **235**, 10–25 (1997).

71. Yao, Q., Kuhlmann, F. M., Eller, R. O. N., Compans, R. W. & Chen, C. Production and Characterization of Simian-Human Immunodeficiency Virus-Like Particles. *AIDS Res. Hum. Retroviruses* **16**, 227–236 (2000).

72. Kuate, S. *et al.* Immunogenicity and efficacy of immunodeficiency virus-like particles pseudotyped with the G protein of vesicular stomatitis virus. *Virology* **351**, 133–144 (2006).

73. Haglund, K., Forman, J., Kräusslich, H. G. & Rose, J. K. Expression of human immunodeficiency virus type 1 gag protein precursor and envelope proteins from a vesicular stomatitis virus recombinant: High-level production of virus-like particles containing HIV envelope. *Virology* **268**, 112–121 (2000).

74. Reuter, N. *et al.* Cell Fusion Induced by a Fusion-Active Form of Human Cytomegalovirus Glycoprotein B (gB) Is Inhibited by Antibodies Directed at Antigenic Domain 5 in the Ectodomain of gB. *J. Virol.* **94**, (2020).

75. Kim, G. N. *et al.* A vesicular stomatitis virus-based prime-boost vaccination strategy induces potent and protective neutralizing antibodies against SARS-CoV-2. *PLoS Pathogens* **17**, (2021).

76. Sharma, S. K. *et al.* Cleavage-Independent HIV-1 Env Trimers Engineered as Soluble Native Spike Mimetics for Vaccine Design. *Cell Rep.* **11**, 539–550 (2015).

77. McMichael, A. J., Borrow, P., Tomaras, G. D., Goonetilleke, N. & Haynes, B. F. The immune response during acute HIV-1 infection: Clues for vaccine development. *Nat. Rev. Immunol.* **10**, 11–23 (2010).

78. Smith, R. L., de Boer, R., Brul, S., Budovskaya, Y. & van der Spek, H. Premature and accelerated aging: HIV or HAART? *Front. Genet.* **3**, 1–10 (2013).

79. Lykins, W. R., Luecke, E., Johengen, D., van der Straten, A. & Desai, T. A. Long acting systemic HIV pre-exposure prophylaxis: an examination of the field. *Drug Deliv. Transl. Res.* **7**, 805–816 (2017).

80. McGowan, J. P. *et al.* PEP to Prevent HIV Infection. *Clin. Guidel. Progr.* (2022).

81. McKinnon, L. R. & Card, C. M. HIV vaccine efficacy trials: A brief history and options for going forward. *AIDS Rev.* **12**, 209–217 (2010).

82. Buchbinder, S. P. *et al.* Efficacy assessment of a cell-mediated immunity HIV-1 vaccine (the Step Study): a double-blind, randomised, placebo-controlled, test-of-concept trial. *Lancet* **372**, 1881–1893 (2008).

83. Russell, N. D. *et al.* Phase 2 study of an HIV-1 canarypox vaccine (vCP1452) alone and in combination with rgp120: Negative results fail to trigger a phase 3 correlates trial. *J. Acquir. Immune Defic. Syndr.* **44**, 203–212 (2007).

84. Rerks-Ngarm, S. *et al.* Vaccination with ALVAC and AIDSVAX to Prevent HIV-1 Infection in Thailand. *N. Engl. J. Med.* **365**, 687–696 (2009).

85. Sokolova, V., Westendorf, A., Buer, J., Überla, K. & Epple, M. The potential of nanoparticles for the immunization against viral infections. *J. Mater. Chem.* **3**, 4767–4779 (2015).

86. Kim, B., Rutka, J. & Warren, C. Nanomedicine. *N. Engl. J. Med.* **17**, 121–130 (2010).

87. Jennings, G. T. & Bachmann, M. F. The coming of age of virus-like particle vaccines. *Biol. Chem.* **389**, 521–536 (2008).

88. Harper, D. M. Currently approved prophylactic HPV vaccines. *Expert Rev. Vaccines* **8**, 1663–1679 (2009).

89. Thompson, C. M. *et al.* Critical assessment of influenza VLP production in Sf9 and HEK293 expression systems. *BMC Biotechnol.* **15**, 1–12 (2015).

90. Young, K. R., McBurney, S. P., Karkhanis, L. U. & Ross, T. M. Virus-like particles: Designing an effective AIDS vaccine. *Methods* **40**, 98–117 (2006).

91. Sahay, G., Alakhova, D. Y. & Kabanov, A. V. Endocytosis of nanomedicines. *J. Control. Release* **145**, 182–195 (2010).

92. Sardar, R., Funston, A. M., Mulvaney, P. & Murray, R. W. Gold nanoparticles: Past, present, and future. *Langmuir* **25**, 13840–13851 (2009).

93. Maitra, A. Calcium phosphate nanoparticles: Second-generation nonviral vectors in gene therapy. *Expert Rev. Mol. Diagn.* **5**, 893–905 (2005).

94. Henriksen-Lacey, M., Korsholm, K. S., Andersen, P., Perrie, Y. & Christensen, D. Liposomal vaccine delivery systems. *Expert Opin. Drug Deliv.* **8**, 505–519 (2011).

95. Prabha, S., Zhou, W. Z., Panyam, J. & Labhasetwar, V. Size-dependency of nanoparticle-mediated gene transfection: Studies with fractionated nanoparticles. *Int. J. Pharm.* **244**, 105–115 (2002).

96. Giljohann, D. A. *et al.* Gold nanoparticles for biology and medicine. *Angew. Chemie - Int. Ed.* **49**, 3280–3294 (2010).

97. Lai, S. K. *et al.* Privileged delivery of polymer nanoparticles to the perinuclear region of live cells via a non-clathrin, non-degradative pathway. *Biomaterials* **28**, 2876–2884 (2007).

98. Treuel, L., Jiang, X. & Nienhaus, G. U. New views on cellular uptake and trafficking of manufactured nanoparticles. *J. R. Soc. Interface* **10**, 1–13 (2013).

99. Foged, C., Brodin, B., Frokjaer, S. & Sundblad, A. Particle size and surface charge affect particle uptake by human dendritic cells in an in vitro model. *Int. J. Pharm.* **298**, 315–322 (2005).

100. Oussoren, C., Zuidema, J., Crommelin, D. J. A. & Storm, G. Lymphatic uptake and biodistribution of liposomes after subcutaneous injection. II. Influence of liposomal size, lipid composition and lipid dose. *Biochim. Biophys. Acta - Biomembr.* **1328**, 261–272 (1997).

101. Kozlova, D. *et al.* Cell targeting by antibody-functionalized calcium phosphate nanoparticles. *J. Mater. Chem.* **22**, 396–404 (2012).

102. Saupe, A., McBurney, W., Rades, T. & Hook, S. Immunostimulatory colloidal delivery systems for cancer vaccines. *Expert Opin. Drug Deliv.* **3**, 345–354 (2006).

103. Sokolova, V., Knuschke, T., Buer, J., Westendorf, A. M. & Epple, M. Quantitative

determination of the composition of multi-shell calcium phosphate – oligonucleotide nanoparticles and their application for the activation of dendritic cells. *Acta Biomater.* **7**, 4029–4036 (2011).

104. Zilker, C. *et al.* Nanoparticle-based B-cell targeting vaccines: Tailoring of humoral immune responses by functionalization with different TLR-ligands. *Nanomedicine Nanotechnology, Biol. Med.* **13**, 173–182 (2017).

105. Kozlova, D. & Epple, M. Biological targeting with nanoparticles: State of the art. *BioNanoMaterials* **14**, 161–170 (2013).

106. Temchura, V. V, Kozlova, D., Sokolova, V., Überla, K. & Epple, M. Targeting and activation of antigen-specific B-cells by calcium phosphate nanoparticles loaded with protein antigen. *Biomaterials* **35**, 6098–6105 (2014).

107. Saroja, C., Lakshmi, P. & Bhaskaran, S. Recent trends in vaccine delivery systems: A review. *Int. J. Pharm. Investig.* **1**, 64–74 (2011).

108. Irvine, D. J., Swartz, M. A. & Szeto, G. L. Engineering synthetic vaccines using cues from natural immunity. *Nat. Mater.* **12**, 978–990 (2013).

109. Bale, S. *et al.* Covalent Linkage of HIV-1 Trimers to Synthetic Liposomes Elicits Improved B Cell and Antibody Responses. *J. Virol.* **91**, (2017).

110. Stano, A. *et al.* Dense Array of Spikes on HIV-1 Virion Particles. *J. Virol.* (2017). doi:10.1128/JVI.00415-17

111. Suleiman, E. *et al.* Conjugation of native-like HIV-1 envelope trimers onto liposomes using EDC/Sulfo-NHS chemistry: Requirements and limitations. *Pharmaceutics* **12**, (2020).

112. Damm, D. *et al.* Design and Functional Characterization of HIV-1 Envelope Protein-Coupled T Helper Liposomes. *Pharmaceutics* **14**, 1–19 (2022).

113. Ingale, J. *et al.* High-Density Array of Well-Ordered HIV-1 Spikes on Synthetic Liposomal Nanoparticles Efficiently Activate B Cells. *Cell Rep.* **15**, 1986–1999 (2016).

114. Sokolova, V. *et al.* Mechanism of the uptake of cationic and anionic calcium phosphate nanoparticles by cells. *Acta Biomater.* **9**, 7527–7535 (2013).

115. Bhattacharya, R. *et al.* Gold nanoparticles inhibit the proliferation of multiple myeloma cells. *Adv. Mater.* **19**, 711–716 (2007).

116. Baptista, P. *et al.* Gold nanoparticles for the development of clinical diagnosis methods. *Anal. Bioanal. Chem.* **391**, 943–950 (2008).

117. Nguyen, K. *et al.* Superparamagnetic iron oxide nanoparticles carrying chemotherapeutics improve drug efficacy in monolayer and spheroid cell culture by enabling active accumulation. *Nanomaterials* **10**, 1–21 (2020).

118. Verbeke, R., Lentacker, I., De Smedt, S. C. & Dewitte, H. The dawn of mRNA vaccines: The COVID-19 case. *J. Control. Release* **333**, 511–520 (2021).

119. Rojas-Sanchez, L., Sokolova, V., Steffen, R., Voskuhl, J. & Epple, M. Covalent Surface Functionalization of Calcium Phosphate Nanoparticles with Fluorescent Dyes by Copper-Catalysed and by Strain-Promoted Azide-Alkyne Click Chemistry. *Chem Nano Mat* **5**, 436–446 (2018).

120. Ingale, J. *et al.* High-Density Array of Well-Ordered HIV-1 Spikes on Synthetic Liposomal Nanoparticles Efficiently Activate B Cells. *CellReports* 1–14 (2016). doi:10.1016/j.celrep.2016.04.078

121. Sokolova, V. & Epple, M. Biological and Medical Applications of Calcium Phosphate Nanoparticles. *Chem. - A Eur. J.* **27**, 7471–7488 (2021).

122. Hagmeyer, D. *et al.* Self-assembly of calcium phosphate nanoparticles into hollow spheres induced by dissolved amino acids. *J. Mater. Chem.* **21**, 9219–9223 (2011).

123. Leskiv, M. *et al.* Energetics of Calcium Phosphate Nanoparticle Formation by the Reaction of Ca(NO3)2 with (NH4)2HPO4. *J. Phys. Chem.* **113**, 5478–5484 (2009).

124. Sokolova, V. V, Radtke, I., Heumann, R. & Epple, M. Effective transfection of cells with multi-shell calcium phosphate-DNA nanoparticles. *Biomaterials* **27**, 3147–3153 (2006).

125. Temchura, V. V, Kozlova, D., Sokolova, V., Überla, K. & Epple, M. Biomaterials Targeting and activation of antigen-speci fi c B-cells by calcium phosphate nanoparticles loaded with protein antigen. *Biomaterials* **35**, 6098–6105 (2014).

126. Sokolova, V. *et al.* The use of calcium phosphate nanoparticles encapsulating Toll-like receptor ligands and the antigen hemagglutinin to induce dendritic cell maturation and T cell activation. *Biomaterials* **31**, 5627–5633 (2010).

127. Knuschke, T. *et al.* Immunization with Biodegradable Nanoparticles Efficiently Induces Cellular Immunity and Protects against Influenza Virus Infection. *J. Immunol.* **190**, 6221–6229 (2013).

128. Knuschke, T. *et al.* Prophylactic and Therapeutic Vaccination with a Nanoparticle-based Peptide Vaccine Induces Efficient Protective Immunity during Acute and Chronic Retroviral Infection. *Nanomedicine* **10**, 1787–1798 (2014).

129. Rojas-Sánchez, L. *et al.* Genetic immunization against hepatitis B virus with calcium phosphate nanoparticles in vitro and in vivo. *Acta Biomater.* **110**, 254–265 (2020).

130. Presolski, S. I., Hong, V. P. & Finn, M. G. Copper-Catalyzed Azide–Alkyne Click Chemistry for Bioconjugation. *Curr. Protoc. Chem. Biol.* **3**, 153–162 (2011).

131. Behzadi, S. *et al.* Cellular Uptake of Nanoparticles: Journey Inside the Cell. *Chem Soc Rev* **46**, 4218–4244 (2018).

132. Sokolova, V., Rojas-Sanchez, L. & Epple, M. Calcium phosphate nanoparticle-mediated transfection in 2D and 3D mono- and co-culture cell models. *Acta Biomater.* **84**, 391–401 (2019).

133. Ganesan, K., Jansen, M., Kovtun, A., Neumann, S. & Epple, M. Calcium phosphate nanoparticles : colloidally stabilized and made fluorescent by a phosphate-functionalized porphyrin. *J. Mater. Chem.* **18**, 3617–3724 (2008).

134. Kollenda, S. A. *et al.* In vivo biodistribution of calcium phosphate nanoparticles after intravascular, intramuscular, intratumoral, and soft tissue administration in mice investigated by small animal PET / CT. *Acta Biomater.* **109**, 244–253 (2020).

135. Gao, P. *et al.* Biocompatible and colloidally stabilized mPEG-PE / calcium phosphate hybrid nanoparticles loaded with siRNAs targeting tumors. *Oncotarget* **7**, 2855–2866 (2015).

136. Sokolova, V. & Epple, M. Biological and Medical Applications of Calcium Phosphate Nanoparticles. *Chem. Eur. J.* **27**, 7471–7488 (2021).

137. Thalhauser, S., Peterhoff, D., Wagner, R. & Breunig, M. Presentation of HIV-1 Envelope Trimers on the Surface of Silica Nanoparticles. *J. Pharm. Sci.* **109**, 911–921 (2020).

138. Sliepen, K. *et al.* Presenting native-like HIV-1 envelope trimers on ferritin nanoparticles improves their immunogenicity. *Retrovirology* **12**, (2015).

139. Sliepen, K. *et al.* Structure and immunogenicity of a stabilized HIV-1 envelope trimer based on a group-M consensus sequence. *Nat. Commun.* **10**, 2355–2367 (2019).

140. Brouwer, P. J. M. *et al.* Enhancing and shaping the immunogenicity of native-like HIV-1 envelope trimers with a two-component protein nanoparticle. *Nat. Commun.* **10**, (2019).

141. Brouwer, P. J. M. *et al.* Immunofocusing and enhancing autologous Tier-2 HIV-1 neutralization by displaying Env trimers on two-component protein nanoparticles. *npj Vaccines* **6**, (2021).

142. Brouwer, P. J. M. *et al.* Two-component spike nanoparticle vaccine protects macaques from SARS-CoV-2 infection. *Cell* **184**, 1188–1200 (2021).

143. Tokatlian, T. *et al.* Enhancing Humoral Responses Against HIV Envelope Trimers via Nanoparticle Delivery with Stabilized Synthetic Liposomes. *Sci. Rep.* **8**, (2018).

144. Chen, Z., Moon, J. J. & Cheng, W. Quantitation and Stability of Protein Conjugation on Liposomes for Controlled Density of Surface Epitopes. *Bioconjug. Chem.* **29**, 1251–1260 (2018).

145. Shao, S. *et al.* Functionalization of cobalt porphyrin-phospholipid bilayers with His-tagged ligands and antigens. *Nat. Chem.* **7**, 438–446 (2015).

146. Dubrovskaya, V. *et al.* Vaccination with Glycan-Modified HIV NFL Envelope Trimer-Liposomes Elicits Broadly Neutralizing Antibodies to Multiple Sites of Vulnerability. *Immunity* **51**, 915–929 (2019).

147. Pejawar-Gaddy, S., Kovacs, J. M., Barouch, D. H., Chen, B. & Irvine, D. J. Design of lipid nanocapsule delivery vehicles for multivalent display of recombinant Env trimers in HIV vaccination. *Bioconjug. Chem.* **25**, 1470–1478 (2014).

148. Suleiman, E. *et al.* Electrostatically driven encapsulation of hydrophilic, non-conformational peptide epitopes into liposomes. *Pharmaceutics* **11**, (2019).

149. Thalhauser, S. *et al.* Augmenting the immune response against a stabilized HIV-1 clade C envelope trimer by silica nanoparticle delivery. *Vaccines* **9**, 1–24 (2021).

150. Saito, M. *et al.* Molecular mechanisms of nickel allergy. *Int. J. Mol. Sci.* **17**, 1–8 (2016).

151. Oswald, M., Geissler, S. & Goepferich, A. Determination of the activity of maleimide-functionalized phospholipids during preparation of liposomes. *Int. J. Pharm.* **514**, 93–102 (2016).

152. Kirchhof, S. *et al.* New insights into the cross-linking and degradation mechanism of Diels-Alder hydrogels. *J. Mater. Chem. B* **3**, 449–457 (2015).

153. Luchansky, S. J., Argade, S., Hayes, B. K. & Bertozzi, C. R. Metabolic functionalization of recombinant glycoproteins. *Biochemistry* **43**, 12358–12366 (2004).

154. Sletten, E. M. & Bertozzi, C. R. Bioorthogonal chemistry: Fishing for selectivity in a sea of functionality. *Angew. Chemie - Int. Ed.* **48**, 6974–6998 (2009).

155. Mahal, L. K. & Bertozzi, C. R. Engineered cell surfaces: Fertile ground for molecular landscaping. *Chem. Biol.* **4**, 415–422 (1997).

156. Wang, M., Xu, P. & Lei, B. Engineering multifunctional bioactive citrate-based biomaterials for tissue engineering. *Bioact. Mater.* **19**, 511–537 (2022).

157. Schmidt, B., Selmer, T., Ingendoh, A. & Figurat, K. von. A novel amino acid modification in sulfatases that is defective in multiple sulfatase deficiency. *Cell* **82**, 271–278 (1995).

158. Cosma, M. P. *et al.* The Multiple Sulfatase Deficiency Gene Encodes an Essential and Limiting Factor for the Activity of Sulfatases. *Cell* **113**, 445–456 (2003).

159. Dierks, T. *et al.* Multiple sulfatase deficiency is caused by mutations in the gene encoding the human Cα-formylglycine generating enzyme. *Cell* **113**, 435–444 (2003).

160. Landgrebe, J., Dierks, T., Schmidt, B. & Figura, K. Von. The human SUMF1 gene, required for posttranslational sulfatase modification, defines a new gene family which is conserved from pro- to eukaryotes. *Gene* **316**, 47–56 (2003).

161. Carrico, I. S., Carlson, B. L. & Bertozzi, C. R. Introducing genetically encoded aldehydes into proteins. *Nat. Chem. Biol.* **3**, 321–322 (2007).

162. Yin, J., Liu, F., Li, X. & Walsh, C. T. Labeling Proteins with Small Molecules by Site-Specific Posttranslational Modification. *J. Am. Chem. Soc.* **126**, 7754–7755 (2004).

163. Wang, L., Xie, J. & Schultz, P. G. Expanding the Genetic Code. *Annu. Rev. Biophys. Biomol. Struct.* **35**, 225–249 (2006).

164. Link, A. J., Mock, M. L. & Tirrell, D. Non-canonical amino acids in protein engineering. *Curr.*

Opin. Biotechnol. **14**, 603–609 (2003).

165. Frese, M. & Dierks, T. Formylglycine Aldehyde Tag — Protein Engineering through a Novel Post-translational Modification. *ChemBioChem* **10**, 425–427 (2009).

166. Wu, P. *et al.* Site-specific chemical modification of recombinant proteins produced in mammalian cells by using the genetically encoded aldehyde tag. *Proc. Natl. Acad. Sci. U. S. A.* **106**, 3000–3005 (2009).

167. Rabuka, D., Rush, J. S., Dehart, G. W., Wu, P. & Bertozzi, C. R. Site-specific chemical protein conjugation using genetically encoded aldehyde tags. *Nat. Protoc.* (2012). doi:10.1038/nprot.2012.045

168. Hudak, J. E. *et al.* Synthesis of Heterobifunctional Protein Fusions Using Copper-Free Click Chemistry and the Aldehyde Tag. *Angew. Chemie - Int. Ed.* 4161–4165 (2012). doi:10.1002/anie.201108130

169. Heß, R. *et al.* Glycosylation of HIV Env Impacts IgG Subtype Responses to Vaccination. *Viruses* **11**, 153–170 (2019).

170. Li, Z., Feng, S., Zhang, H., Chao, Z. & Shi, S. Immunogenicity and protective efficacy of a DNA vaccine inducing optimal expression of the SARS-CoV-2 S gene in hACE2 mice. *Arch. Virol.* 1–10 (2022). doi:10.1007/s00705-022-05562-z

171. Coutelier, J.-P., van der Logt, J., Heessen, F., Warnier, G. & van Snick, J. IgG2a restriction of murine antibodies elicited by viral infections. *J. Exp. Med.* **165**, 64–69 (1987).

172. Nimmerjahn, F. & Ravetch, J. V. Divergent Immunoglobulin G Subclass Activity through Selective Fc Receptor Binding. *Science (80-.).* **310**, 1510–1512 (2005).

173. Nimmerjahn, F., Gordan, S. & Lux, A. FcγR dependent mechanisms of cytotoxic, agonistic, and neutralizing antibody activities. *Trends Immunol.* **36**, 325–336 (2015).

174. Nimmerjahn, F. *et al.* FcγRIV deletion reveals its central role for IgG2a and IgG2b activity in vivo. *Proc. Natl. Acad. Sci. U. S. A.* **107**, 19396–19401 (2010).

175. Lu, L. L., Suscovich, T. J., Fortune, S. M. & Alter, G. Beyond binding: antibody effector functions in infectious diseases. *Nat Rev Immunol* **18**, 46–61 (2018).

176. Isakson, P. C. & Vitetta, E. S. T cell-derived B cell differentiation factor(s). Effect on the isotype switch of murine B cells. *J. Exp. Med.* **155**, 734–748 (1982).

177. Spensieri, F. *et al.* Early rise of blood T follicular helper cell subsets and baseline immunity as predictors of persisting late functional antibody responses to vaccination in humans. *PLoS One* **11**, 1–16 (2016).

178. Jeger-Madiot, R., Heredia, M. & Graff-Dubois, S. Germinal centers B-cell reaction and T follicular helper cells in response to HIV-1 infection. *Curr. Opin. HIV AIDS* **14**, 246–252 (2019).

179. Pallikkuth, S., de Armas, L., Rinaldi, S. & Pahwa, S. T follicular helper cells and B cell dysfunction in aging and HIV-1 infection. *Front. Immunol.* **8**, 1–8 (2017).

180. Snapper, C. M. & Paul, W. E. Interferon-γ and B cell stimulatory factor-1 reciprocally regulate Ig isotype production. *Science (80-.).* **236**, 944–947 (1987).

181. Mosmann, T. R., Cherwinski, H., Bond, M. W., Giedlin, M. A. & Coffman, R. L. Two types of murine helper T cell clone. I. Definition according to profiles of lymphokine activities and secreted proteins. *J. Immunol.* **136**, 2348–2357 (1986).

182. Yu, S., Kuan, W., Wong, C., Li, E. K. & Tam, L. Immunopathological Roles of Cytokines, Chemokines, Signaling Molecules, and Pattern-Recognition Receptors in Systemic Lupus Erythematosus. *Clin. Dev. Immunol.* **2012**, (2012).

183. Zhu, J. T helper 2 (Th2) cell differentiation, type 2 innate lymphoid cell (ILC2) development and regulation of interleukin-4 (IL-4) and IL-13 production. *Cytokine* **75**, 14–24 (2015).

184. Zhu, J., Yamane, H., Cote-sierra, J., Guo, L. & Paul, W. E. GATA-3 promotes Th2 responses through three different mechanisms : induction of Th2 cytokine production , selective growth of Th2 cells and inhibition of Th1 cell-specific factors. *Cell Res.* **16**, 3–10 (2006).

185. Raphael, I., Nalawade, S., Eagar, T. N. & Forsthuber, T. G. T cell subsets and their signature cytokines in autoimmune and inflammatory diseases. *Cytokine* **74**, 5–14 (2015).

186. Martinez-Sanchez, M. E., Huerta, L. & Alvarez-buylla, E. R. Role of Cytokine Combinations on CD4 + T Cell Differentiation, Partial Polarization, and Plasticity : Continuous Network Modeling Approach. *Front. Physiol.* **9**, 1–14 (2018).

187. Zhou, L., Chong, M. M. W. & Littman, D. R. Plasticity of CD4+ T Cell Lineage Differentiation. *Immunity* **30**, 646–655 (2009).

188. Seif, F., Khoshmirsafa, M., Aazami, H., Mohsenzadegan, M. & Sedighi, G. The role of JAK-STAT signaling pathway and its regulators in the fate of T helper cells. *Cell Commun. Signal.* **15**, 1–13 (2017).

189. Manetti, R. *et al.* Natural killer cell stimulatory factor (Interleukin 12 [IL-12]) induces T helper type 1 (Th1)-specific immune responses and inhibits the development of IL-4-producing Th cells. *J. Exp. Med.* **177**, 1199–1204 (1993).

190. Murphy, K. M., Reiner, S. L. & Medical, H. H. The Lineage Decisions of Helper T Cells. *Immunology* **2**, 933–944 (2002).

191. Margaret A. Liu. DNA vaccines: an historical perspective and view to the future. *Immunol. Rev.* **239**, 62–84 (2011).

192. Kim, J. J. *et al.* Coadministration of IL-12 or IL-10 expression cassettes drives immune responses toward a Th1 phenotype. *J. Interf. Cytokine Res.* **18**, 537–547 (1998).

193. Kim, J. J. *et al.* Cytokine molecular adjuvants modulate immune responses induced by DNA vaccine constructs for HIV-1 and SIV. *J. Interf. Cytokine Res.* **19**, 77–84 (1999).

194. Moore, A. C., Kong, W., Chakrabarti, B. K. & Nabel, G. J. Effects of Antigen and Genetic Adjuvants on Immune Responses to Human Immunodeficiency Virus DNA Vaccines in Mice. *J. Virol.* **76**, 243–250 (2002).

195. Akache, B., Stark, F., Agbayani, G., Renner, T. & McCluskie, M. Adjuvants: Engineering Protective Immune Responses in Human and Veterinary Vaccines. 179–231 (2022).

196. Podda, A. The adjuvanted influenza vaccines with novel adjuvants: Experience with the MF59-adjuvanted vaccine. *Vaccine* **19**, 2673–2680 (2001).

197. Leroux-Roels, G. Prepandemic H5N1 influenza vaccine adjuvanted with AS03: A review of the pre-clinical and clinical data. *Expert Opin. Biol. Ther.* **9**, 1057–1071 (2009).

198. HogenEsch, H. Mechanisms of stimulation of the immune response by aluminum adjuvants. *Vaccine* **20**, 34–39 (2002).

199. Marrack, P., McKee, A. S. & Munks, M. W. Towards an understanding of the adjuvant action of aluminium. *Nat. Rev. Immunol.* **9**, 287–293 (2009).

200. Sun, H. X., Xie, Y. & Ye, Y. P. Advances in saponin-based adjuvants. *Vaccine* **27**, 1787–1796 (2009).

201. Bode, C., Zhao, G., Steinhagen, F., Kinjo, T. & Klinman, D. CpG DNA as a vaccine adjuvant. *Expert Rev. Vaccines* **10**, 499–511 (2011).

202. Klinman, D. M., Klaschik, S., Sato, T. & Tross, D. CpG oligonucleotides as adjuvants for vaccines targeting infectious diseases. *Adv. Drug Deliv. Rev.* **61**, 248–255 (2009).

203. Honko, A. N. & Mizel, S. B. Effects of flagellin on innate and adaptive immunity. *Immunol. Res.* **33**, 83–101 (2005).

204. Mata-Haro, V. *et al.* The Vaccine Adjuvant Monophosphoryl Lipid A as a TRIF-Biased Agonist of TLR4. *Science (80-.).* **316**, 1628–1633 (2007).

205. Didierlaurent, A. M. *et al.* AS04, an Aluminum Salt- and TLR4 Agonist-Based Adjuvant System, Induces a Transient Localized Innate Immune Response Leading to Enhanced Adaptive Immunity. *J. Immunol.* **183**, 6186–6197 (2009).

206. Hafner, A. M., Corthésy, B. & Merkle, H. P. Particulate formulations for the delivery of poly(I: C) as vaccine adjuvant. *Adv. Drug Deliv. Rev.* **65**, 1386–1399 (2013).

207. Apostólico, J. D. S. *et al.* Adjuvants: Classification, Modus Operandi, and Licensing. *J. Immunol. Res.* (2016).

208. Vitetta, E. S., Bossie, A. & Fernandez-botran-, R. Interaction and Activation of Antigen-Specific T and B Cells. *Immunol. Rev.* 193–239 (1987).

209. Lanzavecchia, A. Antigen-specific interaction between T and B cells. *Nature* **314**, 537–539 (1985).

210. Singer, A. & Hodes, R. J. Mechanisms of T cell - B cell interaction. *Annu. Rev. Immunol.* 211–241 (1983).

211. Nabi, G. *et al.* T cell independent secondary antibody responses to the envelope protein of simian immunodeficiency virus. 1–11 (2012).

212. Koh, W. H. *et al.* HIV-Captured DCs Regulate T Cell Migration and Cell-Cell Contact Dynamics to Enhance Viral Spread. *iScience* **23**, (2020).

213. Fouts, T. R. *et al.* Balance of cellular and humoral immunity determines the level of protection by HIV vaccines in rhesus macaque models of HIV infection. *Proc. Natl. Acad. Sci. U. S. A.* **112**, 992–999 (2015).

214. Tenbusch, M. *et al.* Risk of Immunodeficiency Virus Infection May Increase with Vaccine-Induced Immune Response. *J. Virol.* **86**, 10533–10539 (2012).

215. Staprans, S. I. *et al.* Enhanced SIV replication and accelerated progression to AIDS in macaques primed to mount a CD4 T cell response to the SIV envelope protein. *Proc. Natl. Acad. Sci. U. S. A.* **101**, 4–9 (2004).

216. Temchura, V. & Tenbusch, M. The two faces of vaccine-induced immune response: Protection or increased risk of HIV infection?! *Virol. Sin.* **29**, 7–9 (2014).

217. Russell, S. M. & Liew, F. Y. T cells primed by influenza virion internal components can cooperate in the antibody response to haemagglutinin. *Nature* **280**, 147–148 (1979).

218. Milich, D. R., McLachlan, A., Thornton, G. B. & Hughes, J. L. Antibody production to the nucleocapsid and envelope of the hepatitis B virus primed by a single synthetic T cell site. *Nature* **329**, 547–549 (1987).

219. Crotty, S. A brief history of T cell help to B cells. *Immunology* **15**, 185–189 (2015).

220. Temchura, V. & Überla, K. Intrastructural help : Improving the HIV-1 envelope antibody response induced by virus-like particle vaccines. *Curr. Opin. HIV AIDS* **12**, 272–277 (2017).

221. Nabi, G. *et al.* GagPol-specific CD4+ T-cells increase the antibody response to Env by intrastructural help. *Retrovirology* **10**, 1–10 (2013).

222. Storcksdieck, M. *et al.* Enhancing the Quality of Antibodies to HIV-1 Envelope by GagPol-Specific Th Cells. *J. Immunol.* **195**, 4861–4872 (2015).

223. Grun, J. L. & Maurer, P. H. Different T helper cell subsets elicited in mice utilizing two different adjuvant vehicles: The role of endogenous interleukin 1 in proliferative responses. *Cell. Immunol.* **121**, 134–145 (1989).

224. Elsayed, H. *et al.* Intrastructural Help: Harnessing T Helper Cells Induced by Licensed Vaccines for Improvement of HIV Env Antibody Responses to Virus-Like Particle Vaccines. *J. Virol.* **92**, 1–15 (2018).

225. Klessing, S. *et al.* CD4+ T cells induced by tuberculosis subunit vaccine H1 can improve the HIV-1 Env humoral response by intrastructural help. *Vaccines* **8**, 1–20 (2020).

226. van Dissel, J. T. *et al.* A novel liposomal adjuvant system, CAF01, promotes long-lived Mycobacterium tuberculosis-specific T-cell responses in human. *Vaccine* **32**, 7098–7107 (2014).

227. Hills, T. *et al.* A rapid-response humoral vaccine platform exploiting pre-existing non-cognate populations of anti-vaccine or anti-viral CD4+ T helper cells to confirm B cell activation. *PLoS One* **11**, 1–20 (2016).

228. Damm, D. *et al.* Calcium phosphate nanoparticle-based vaccines as a platform for improvement of HIV-1 Env antibody responses by intrastructural help. *Nanomaterials* **9**, 1–17 (2019).

229. Damm, D. *et al.* Covalent coupling of HIV-1 glycoprotein trimers to biodegradable calcium phosphate nanoparticles via genetically encoded aldehyde-tags. *Acta Biomater.* **140**, 586–600 (2022).

230. Finzi, A. *et al.* Conformational characterization of aberrant disulfide-linked HIV-1 gp120 dimers secreted from overexpressing cells. *J. Virol. Methods* **168**, 155–161 (2010).

231. Ota, T. *et al.* B Cells from Knock-in Mice Expressing Broadly Neutralizing HIV Antibody b12 Carry an Innocuous B Cell Receptor Responsive to HIV Vaccine Candidates. *J. Immunol.* **191**, 3179–3185 (2013).

232. Escolano, A. *et al.* Sequential Immunization Elicits Broadly Neutralizing Anti-HIV-1 Antibodies in Ig Knockin Mice. *Cell* **166**, 1445–1458 (2016).

233. Huang, D., Abbott, R. K., Havenar-Daughton, C., Skog, P. D. & Al-Kolla, R. B cells expressing authentic naive human VRC01-class BCRs can be recruited to germinal centers and affinity mature in multiple independent mouse models. *PNAS* **117**, 22920–22931 (2020).

234. Campbell, J. D. Development of the CpG adjuvant 1018: A case study. *Methods Mol. Biol.* **1494**, 15–27 (2017).

235. Sethi, S., Ebner, S., Hinske, C. & Kretzschmar, H. Multiple administrations of oligodeoxynucleotides containing CpG motifs influence Ig isotype production. *Immunopharmacol. Immunotoxicol.* **27**, 447–460 (2005).

236. Shirai, S. *et al.* Lipid Nanoparticles Potentiate CpG-Oligodeoxynucleotide-Based Vaccine for Influenza Virus. *Front. Immunol.* **10**, (2020).

237. Kolenbrander, A., Grewe, B., Nemazee, D., Überla, K. & Temchura, V. Generation of T-follicular helper cells in vitro: requirement for BCR cross-linking and cognate B- and T-cell interaction. *Immunology* (2017). doi:10.1111/imm.12834

238. Sliepen, K. *et al.* Engineering and Characterization of a Fluorescent Native-Like HIV-1 Envelope Glycoprotein Trimer. *Biomolecules* **5**, 2919–2934 (2015).

239. Peter, A. S. *et al.* A pair of noncompeting neutralizing human monoclonal antibodies protecting from disease in a SARS-CoV-2 infection model. *Eur. J. Immunol.* **52**, 770–783 (2022).

240. Kozlova, D. *et al.* Calcium phosphate nanoparticles show an effective activation of the innate immune response in vitro and in vivo after functionalization with flagellin. *Virol. Sin.* **29**, 33–39 (2014).

241. Huang, Y. *et al.* Silica nanoparticles: Biomedical applications and toxicity. *Biomed. Pharmacother.* **151**, (2022).

242. Brunot, C. *et al.* Cytotoxicity of polyethyleneimine (PEI), precursor base layer of polyelectrolyte multilayer films. *Biomaterials* **28**, 632–640 (2007).

243. Koniev, O. & Wagner, A. Developments and recent advancements in the field of endogenous amino acid selective bond forming reactions for bioconjugation. *Chem. Soc. Rev.* **44**, 5495–5551 (2015).

244. Klausen, M. S. *et al.* NetSurfP-2.0: Improved prediction of protein structural features by integrated deep learning. *Proteins Struct. Funct. Bioinforma.* **87**, 520–527 (2019).

245. Gardt, O., Grewe, B., Tippler, B. G., Überla, K. & Temchura, V. V. HIV-derived lentiviral particles promote T-cell independent activation and differentiation of naïve cognate conventional B2-cells in vitro. *Vaccine* **31**, 5088–5098 (2013).

246. Sveen, K. & Skaug, N. Comparative mitogenicity and polyclonal B cell activation capacity of eight oral or nonoral bacterial lipopolysaccharides in cultures of spleen cells from athymic (nu/nu-Balb/c) and thymic (Balb/c) mice. *Oral Microbiol Immunol* **7**, 71–77 (1992).

247. Barnowski, C., Kadzioch, N., Damm, D., Yan, H. & Temchura, V. Advantages and Limitations of Integrated Flagellin Adjuvants for HIV-Based Nanoparticle B-Cell Vaccines. *Pharmaceutics* **11**, (2019).

248. Nabi, G. *et al.* T cell independent secondary antibody responses to the envelope protein of simian immunodeficiency virus. *Retrovirology* **9**, 1–11 (2012).

249. Oscherwitz, J., Yu, F. & Cease, K. B. A Heterologous Helper T-Cell Epitope Enhances the Immunogenicity of a Multiple-Antigenic-Peptide Vaccine Targeting the Cryptic Loop-Neutralizing Determinant of Bacillus anthracis Protective Antigen . **77**, 5509–5518 (2009).

250. Hu, J. K. *et al.* Murine Antibody Responses to Cleaved Soluble HIV-1 Envelope Trimers Are Highly Restricted in Specificity. *J. Virol.* **89**, 10383–10398 (2015).

251. Mosmann, T. R. & Coffman, R. L. TH1 and TH2 cells: Different patterns of lymphokine secretion lead to different functional properties. *Annu. Rev. Immunol.* **7**, 145–173 (1989).

252. Sekaly, R. P. The failed HIV Merck vaccine study: A step back or a launching point for future vaccine development? *J. Exp. Med.* **205**, 7–12 (2008).

253. Turner, M. D., Nedjai, B., Hurst, T. & Pennington, D. J. Cytokines and chemokines: At the crossroads of cell signalling and inflammatory disease. *Biochim. Biophys. Acta - Mol. Cell Res.* **1843**, 2563–2582 (2014).

254. Knuschke, T. *et al.* Immunization with Biodegradable Nanoparticles Efficiently Induces Cellular Immunity and Protects against Influenza Virus Infection. *J. Immunol.* **190**, 6221–6229 (2013).

255. Starsich, F. H. L., Herrmann, I. K. & Pratsinis, S. E. Nanoparticles for Biomedicine: Coagulation During Synthesis and Applications. *Annu. Rev. Chem. Biomol. Eng.* **10**, 155–176 (2019).

256. Sanità, G., Carrese, B. & Lamberti, A. Nanoparticle Surface Functionalization: How to Improve Biocompatibility and Cellular Internalization. *Front. Mol. Biosci.* **7**, (2020).

257. Brinkkemper, M. & Sliepen, K. Nanoparticle Vaccines for Inducing HIV-1 Neutralizing Antibodies. *Vaccines* **7**, 1–14 (2019).

258. Hu, J. K. *et al.* Murine Antibody Responses to Cleaved Soluble HIV-1 Envelope Trimers Are Highly Restricted in Specificity. *J. Virol.* **89**, 10383–10398 (2015).

259. Ulrich, S., Boturyn, D., Marra, A., Renaudet, O. & Dumy, P. Oxime Ligation: A Chemoselective Click-Type Reaction for Accessing Multifunctional Biomolecular Constructs. *Chem. - A Eur. J.* **20**, 34–41 (2014).

260. Torrents de la Pena, A. *et al.* Improving the Immunogenicity of Native-like HIV-1 Envelope Trimers by Hyperstabilization Article Improving the Immunogenicity of Native-like HIV-1 Envelope Trimers by Hyperstabilization. *Cell Rep.* **20**, 1805–1817 (2018).

261. Suleiman, E. *et al.* Electrostatically driven encapsulation of hydrophilic, non-conformational peptide epitopes into liposomes. *Pharmaceutics* **11**, (2019).

262. Laezza, A. *et al.* Protecting Group Free Synthesis of Glyconanoparticles Using Amino-Oxy-Terminated Polymer Ligands. *Bioconjug. Chem.* **31**, 2392–2403 (2020).

263. Nagahori, N., Abe, M. & Nishimura, S.-I. Structural and Functional Glycosphingolipidomics by Glycoblotting with an Aminooxy-Functionalized Gold Nanoparticle. *Biochemistry* **48**, 583–594 (2009).

264. Thygesen, M. B., Sørensen, K. K., Clo, E. & Jensen, K. J. Direct chemoselective synthesis of glyconanoparticles from unprotected reducing glycans and glycopeptide aldehydes. *Chem. Commun.* 6367–6369 (2009). doi:10.1039/b911676a

265. Jan, M., Pertejo, A., Hioe, C. E. & Upadhyay, C. Heterogeneity in glycan composition on the surface of HIV-1 envelope determines virus sensitivity to lectins. *PLoS One* **13**, 1–21 (2018).

266. Behrens, A., Struwe, W. B., Crispin, M. & Crispin, M. Glycosylation profiling to evaluate glycoprotein immunogens against HIV-1. *Expert Rev. Proteomics* **14**, 881–890 (2017).

267. Coulibaly, F. S., Thomas, D. N. & Youan, B. C. Anti-HIV lectins and current delivery strategies. *Mol. Sci.* **5**, 96–116 (2018).

268. Cao, L. *et al.* Global site-specific N-glycosylation analysis of HIV envelope glycoprotein. *Nat. Commun.* **8**, (2017).

269. Mizuochi, T., Matthewsv, T. J. & Solomon, J. Diversity of Oligosaccharide Structures on the Envelope Glycoprotein gp120 of Human Immunodeficiency Virus 1 from the Lymphoblastoid Cell Line H9. *J. Biol. Chem.* **265**, 8519–8524 (1990).

270. Silver, Z. *et al.* Discovery of O-Linked Carbohydrate on HIV-1 Envelope and Its Role in Shielding against One Category of Broadly Neutralizing Antibodies. *Cell Rep.* **30**, 1862–1869 (2021).

271. Dey, A. K. *et al.* cGMP production and analysis of BG505 SOSIP.664, an extensively glycosylated, trimeric HIV-1 envelope glycoprotein vaccine candidate. *Biotechnol. Bioeng.* **115**, 885–899 (2017).

272. Ozorowski, G. *et al.* Effects of Adjuvants on HIV-1 Envelope Glycoprotein SOSIP Trimers In Vitro. *J. Virol.* **92**, 381–399 (2018).

273. Sok, D., Gils, M. J. Van, Pauthner, M., Julien, J. & Saye-francisco, K. L. Recombinant HIV envelope trimer selects for quaternary-dependent antibodies targeting the trimer apex. *Proc. Natl. Acad. Sci. U. S. A.* **111**, 17624–17629 (2014).

274. Pape, K. A., Catron, D. M., Itano, A. A. & Jenkins, M. K. The Humoral Immune Response is Initiated in Lymph Nodes by B Cells that Acquire Soluble Antigen Directly in the Follicles. *Immunity* **26**, 491–502 (2007).

275. Costantini, L. M. *et al.* Engineering and exploitation of a fluorescent HIV-1 gp120 for live cell CD4 binding assays. *Virology* **476**, 240–248 (2015).

276. Maity, P. C. *et al.* B cell antigen receptors of the IgM and IgD classes are clustered in different protein islands that are altered during B cell activation. *Immunology* **8**, 1–16 (2015).

277. Hobeika, E., Maity, P. C. & Jumaa, H. Control of B Cell Responsiveness by Isotype and Structural Elements of the Antigen Receptor. *Trends Immunol.* **37**, 310–320 (2016).

278. Munro, J. B. *et al.* Conformational dynamics of single HIV-1 envelope trimers on the surface of native virions. *Science (80-.).* **346**, 759–764 (2014).

279. Schiller, J. & Chackerian, B. Why HIV Virions Have Low Numbers of Envelope Spikes: Implications for Vaccine Development. *PLos Pathog.* **10**, 8–11 (2014).

280. Veneziano, R. *et al.* Role of nanoscale antigen organization on B-cell activation probed using DNA origami. *Nat. Nanotechnol.* **15**, 716–723 (2020).

281. Saunders, K. O. *et al.* Vaccine Induction of Heterologous Tier 2 HIV-1 Neutralizing Antibodies in Animal Models. *CellReports* **21**, 3681–3690 (2017).

282. Sok, D. *et al.* Priming HIV-1 broadly neutralizing antibody precursors in human Ig loci transgenic mice. *Science (80-.).* **353**, 1557–1560 (2016).

283. Hsieh, C. *et al.* Structure-based design of prefusion-stabilized SARS-CoV-2 spikes. *Science (80-.).* **1505**, 1501–1505 (2020).

284. Rutten, L. *et al.* Structure-Based Design of Prefusion-Stabilized Filovirus Glycoprotein

Trimers. *CellReports* **30**, 4540–4550 (2020).

285. Metz, S. W. *et al.* In Vitro Assembly and Stabilization of Dengue and Zika Virus Envelope Protein Homo-Dimers. *Sci. Rep.* **7**, 4524–4533 (2017).

286. Rabuka, D., Rush, J. S., Gregory, W., Wu, P. & Bertozzi, C. R. Site-specific chemical protein conjugation using genetically encoded aldehyde tags. *Nat. Protoc.* **7**, 1052–1067 (2012).

287. Escolano, A. *et al.* Sequential Immunization Elicits Broadly Neutralizing Anti-HIV-1 Antibodies in Ig Knockin Mice Article Sequential Immunization Elicits Broadly Neutralizing Anti-HIV-1 Antibodies in Ig Knockin Mice. *Cell* **166**, 1445-1458.e12 (2016).

6. Publications and Presentations

6.1. Publications

6.1.1. First-Author

Design and Functional Characterization of HIV-1 Envelope Protein-Coupled T Helper Liposomes.

Damm D, Suleiman E, Theobald H, Wagner JT, Batzoni M, Ahlfeld B, Walkenfort B, Albrecht JC, Ingale J, Yang L, Hasenberg M, Wyatt RT, Vorauer-Uhl K, Überla K, Temchura V.

Pharmaceutics. 2022 Jun 14, 1385. https://doi.org/10.3390/pharmaceutics14071385. PMID: 35890282

Covalent coupling of HIV-1 glycoprotein trimers to biodegradable calcium phosphate nanoparticles via genetically encoded aldehyde-tags.

Damm D, Kostka K, Weingärtner C, Wagner JT, Rojas-Sánchez L, Gensberger-Reigl S, Sokolova V, Überla K, Epple M, Temchura V.

Acta Biomater. 2022 Mar 1; 140:586-600. doi: 10.1016/j.actbio.2021.12.022. PMID: 34968725

Calcium Phosphate Nanoparticle-Based Vaccines as a Platform for Improvement of HIV-1 Env Antibody Responses by Intrastructural Help.

Damm D, Rojas-Sánchez L, Theobald H, Sokolova V, Wyatt RT, Überla K, Epple M, Temchura V.

Nanomaterials (Basel). 2019 Sep 27;9(10):1389. doi: 10.3390/nano9101389. PMID: 31569763

6.1.2. Co-Author

A pair of noncompeting neutralizing human monoclonal antibodies protecting from disease in a SARS-CoV-2 infection model.

Peter AS, Roth E, Schulz SR, Fraedrich K, Steinmetz T, **Damm D**, Hauke M, Richel E, Mueller-Schmucker S, Habenicht K, Eberlein V, Issmail L, Uhlig N, Dolles S, Grüner E, Peterhoff D, Ciesek S, Hoffmann M, Pöhlmann S, McKay PF, Shattock RJ, Wölfel R, Socher E, Wagner R, Eichler J, Sticht H, Schuh W, Neipel F, Ensser A, Mielenz D, Tenbusch M, Winkler TH, Grunwald T, Überla K, Jäck HM.

Eur J Immunol. 2022 May;52(5):770-783. doi: 10.1002/eji.202149374. PMID: 34355795

Conjugation of Native-Like HIV-1 Envelope Trimers onto Liposomes Using EDC/Sulfo-NHS Chemistry: Requirements and Limitations.

Suleiman E, Mayer J, Lehner E, Kohlhauser B, Katholnig A, Batzoni M, **Damm D**, Temchura V, Wagner A, Überla K, Vorauer-Uhl K.

Pharmaceutics. 2020 Oct 16;12(10):979. doi: 10.3390/pharmaceutics12100979. PMID: 33081278

Genetic Co-Administration of Soluble PD-1 Ectodomains Modifies Immune Responses against Influenza A Virus Induced by DNA Vaccination.
Tannig P, Peter AS, Lapuente D, Klessing S, **Damm D**, Tenbusch M, Überla K, Temchura V.
Vaccines (Basel). 2020 Oct 1;8(4):570. doi: 10.3390/vaccines8040570. PMID: 33019546

Modulation of Vaccine-Induced HIV-1-Specific Immune Responses by Co-Electroporation of PD-L1 Encoding DNA.
Tannig P, Peter AS, Lapuente D, Klessing S, **Damm D**, Tenbusch M, Überla K, Temchura V.
Vaccines (Basel). 2020 Jan 14;8(1):27. doi: 10.3390/vaccines8010027. PMID: 31947643

Electrostatically Driven Encapsulation of Hydrophilic, Non-Conformational Peptide Epitopes into Liposomes.
Suleiman E, **Damm D**, Batzoni M, Temchura V, Wagner A, Überla K, Vorauer-Uhl K.
Pharmaceutics. 2019 Nov 18;11(11):619. doi: 10.3390/pharmaceutics11110619. PMID: 31752070

Advantages and Limitations of Integrated Flagellin Adjuvants for HIV-Based Nanoparticle B-Cell Vaccines.
Barnowski C, Kadzioch N, **Damm D**, Yan H, Temchura V.
Pharmaceutics. 2019 May 1;11(5):204. doi: 10.3390/pharmaceutics11050204. PMID: 31052410

Peptide Paratope Mimics of the Broadly Neutralizing HIV-1 Antibody b12.
Haußner C, **Damm D**, Nirschl S, Rohrhofer A, Schmidt B, Eichler J.
Chembiochem. 2017 Apr 4;18(7):647-653. doi: 10.1002/cbic.201600621. PMID: 28125767

Ligand selectivity of a synthetic CXCR4 mimetic peptide.
Groß A, Brox R, **Damm D**, Tschammer N, Schmidt B, Eichler J.
Bioorg Med Chem. 2015 Jul 15;23(14):4050-5. doi: 10.1016/j.bmc.2015.03.003. PMID: 25801155

6.2. Presentations

Characterization of T Helper Liposomes for the Modulation of Env-Specific Antibody Responses

(Oral presentation)

7th Annual Meeting of the European AIDS Vaccine Initiative (Brussels, April 2022)

Functional Characterization of HIV-1 Env-Coupled T Helper Liposomes for Future Vaccine Applications

(Oral presentation)

31th Annual Meeting of the Society for Virology (Munich, March 2022)

Calcium Phosphate Nanoparticle-Based Vaccines as a Platform for Improvement of HIV-1 Env Antibody Responses by Intrastructural Help.

(Poster Presentation)

Damm D, Kostka K, Weingärtner C, Theobald H, Wagner JT, Rojas-Sánchez L, Sokolova V, Überla K, Epple M, Temchura V.

31th Annual Meeting of the Society for Virology (Munich, March 2022)

Design and characterization of polyfunctional liposomes for the modulation of HIV-1 Env-specific antibody responses

(Oral presentation)

Research Call of the European AIDS Vaccine Initiative (digital, February 2022)

Intrastructural Help with Synthetic Nanoparticles

(Oral presentation)

Research Call of the European AIDS Vaccine Initiative (digital, November 2018)

Intrastructural Help with Synthetic Nanoparticles

(Oral presentation)

Guest speaker at the Academisch-Medisch Centrum (AMC), Amsterdam (October 2018)

Activation of transgenic T and B cells by liposomal vaccines encapsulating heterologous T helper cell epitopes

(Poster presentation)

Damm D, Suleiman E, Elsayed H, Kolenbrander A, Ingale J, Wyatt RT, Temchura V, Überla K

28th Annual Meeting of the Society for Virology (Würzburg, March 2018)

Activation of antigen-specific T and B cells by liposomal vaccines encapsidating heterologous T helper cell epitopes

(Oral presentation)

2nd Annual Meeting of the European AIDS Vaccine Initiative (Barcelona, October 2017)

Improving Env antibody responses induced by nanoparticle vaccines through intrastructural help

(Poster presentation)

Temchura V, Ingale J, **Damm D**, Wyatt RT, Überla K

1st Annual Meeting of the European AIDS Vaccine Initiative (Barcelona, October 2016)

Peptide paratope mimics of the broadly neutralizing HIV-1 antibody b12

(Poster presentation)

Haussner C, **Damm D**, Rohrhofer A, Schmidt B, Eichler J

Frontiers of Retrovirology Conference (Erlangen, September 2016)

Inhibitory activity of a paratope-mimetic peptide on HIV-1 infection of target cells.

(Oral presentation)

13th Workshop “Immunobiology of Viral Infections” (Bad Dürkheim, October 2014)